Issue no. 2/2005
MEDICA Edition

MAGNETOM FLASH

www.siemens.com/magnetom-world

Price 10,- EUR

Content

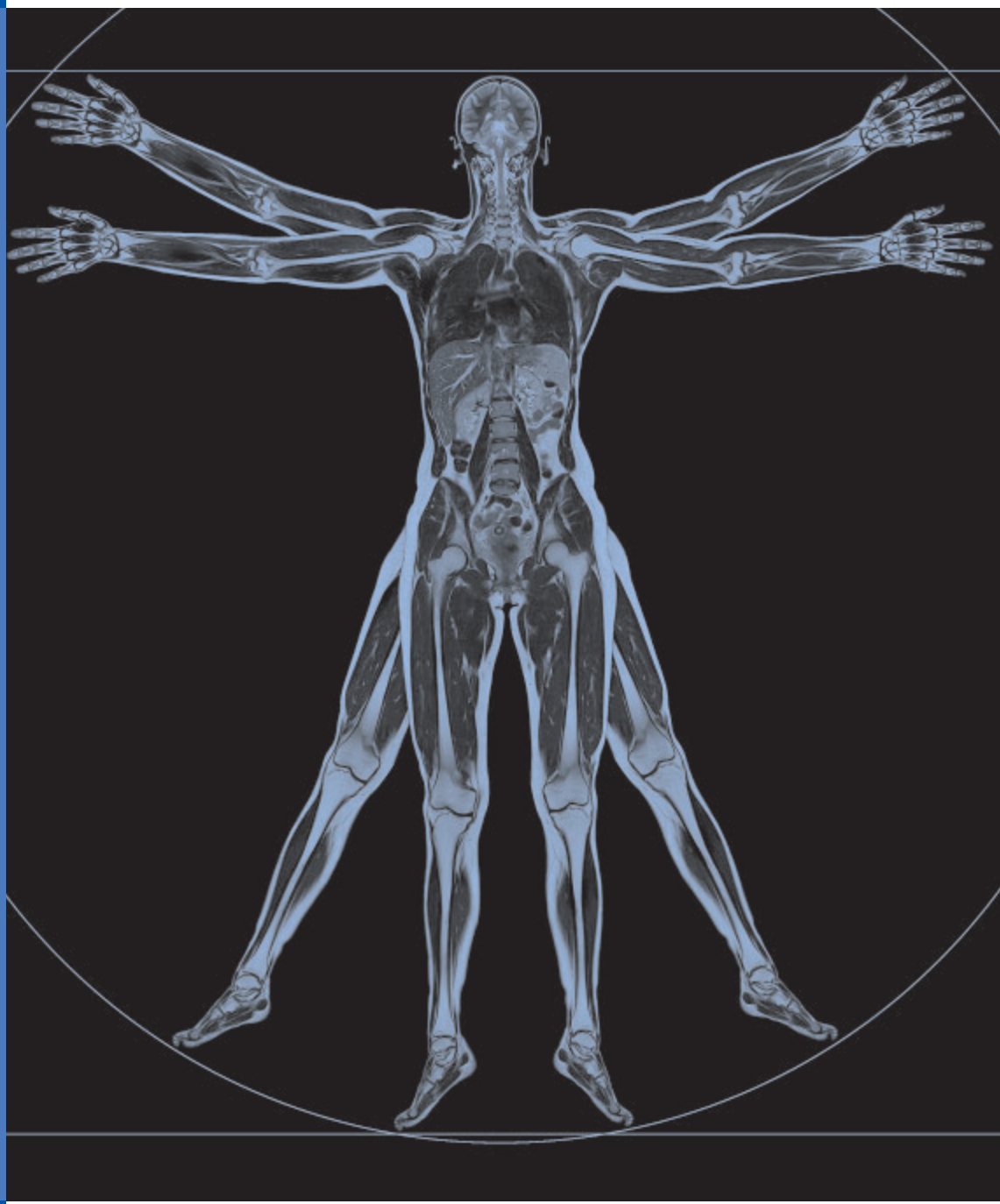

3T

SIEMENS
medical

Dear MAGNETOM User,

At Siemens MR our constant goal is to provide you with better, earlier, faster, easier and more comprehensive medical diagnoses. This requires the development and implementation of the most advanced medical imaging technology. One such development is the availability of Tim (Total Imaging Matrix) – our revolutionary MR technology – at 3T. Siemens' constantly growing range of Tim products now includes MAGNETOM Trio.

3T MR systems – initially of interest mainly in research areas due to their higher image resolution – have enjoyed steadily increasing popularity in clinical routine over the last few years, and industry analysts predict that by 2008, 3T MRI will emerge as a mainstream investment for a majority of hospitals of all specializations. Siemens is the only manufacturer offering receiver coils for all applications in the 3T range, from abdominal, cardiological or orthopedic applications, whole-body scans or examinations of the whole spine. Thanks to its revolutionary acquisition ability to breakthrough applications, Tim has opened up new possibilities for 3T MRI.

The core of Tim technology is the revolutionary matrix coil concept. Up to 102 coil elements can be combined with up to 32 independent radio-frequency channels – providing much higher image quality. Tim allows parallel image acquisition along all three axes over the entire body up to a length of 182 cm (6 ft). The physician can choose any area relevant to the clinical question at hand – from individual sub-areas of the body to the entire anatomy – without having to limit the number of coils that can be connected.

iPAT (integrated Parallel Acquisition Techniques) technology makes the Trio the only 3T system on the market to perform parallel high-speed imaging with up to 16 PAT factors. Massive iPAT improves acquisition speed and image quality even further – a particular advantage for examining moving organs, such as the heart or the intestines, or for improved patient throughput.

MAGNETOM Trio and Tim have turned pioneering medical research into daily clinical routine. Examples include:

- Virtual bone biopsy for the early diagnosis of osteoporosis with down to 0.3 mm^3 image resolution. Early detection of osteoporosis could help by enabling early treatment that will delay the onset of symptoms, such as fractions.
- Potential early diagnosis of Alzheimer's disease as well as mental diseases (schizophrenia, depression, epilepsy etc). Accurate and early diagnosis will enable preventive treat ment that could help very large numbers of patients.

Ioannis Panagiotelis, Ph.D Ultra High Field Segment Manager

- Potential prostate cancer diagnosis without endorectal coil (differentiation of benign and malignant tumours in the prostate without biopsy). This spares the patient from an invasive and painful examination.
- Resolution similar to digital mammography (image resolution 0.2 mm) for breast MR without radiation. This will help reduce repetitive breast scans with higher capability to differentiate between tumours and cysts.
- Accurate diagnosis of microscopic joint injuries, e.g. finger/toe joint injuries of football/basketball players, musicians, golfers and climbers. Imaging at this resolution could make the use of invasive diagnostic approaches like arthroscopy unnecessary.

Other articles cover a summary of 3T MRI's main clinical applications, highlight their benefits and limitations, analyze trends in 3T MRI utilization and outline future directions in MRI technology.

We hope you will enjoy this special edition of MAGNETOM FLASH, dedicated to 3T.

Ioannis Panagiotelis, Ph.D
Ultra High Field Segment Manager

The Editorial Team

We appreciate your comments.
Please contact us at magnetomworld.med@siemens.com

Lisa Reid,
US Installed Base Manager,
Malvern, PA

Dagmar Thomsik-Schröpfer, Ph.D.
MR Marketing-Products, Erlangen

Antje Hellwich
Associate Editor

A. Nejat Bengi, M.D.
Editor in Chief

Heike Weh,
Clinical Data Manager,
Erlangen

Bernhard Baden,
Clinical Data Manager,
Erlangen

Tony Enright, Ph.D.
Asia Pacific Collaborations,
Australia

Milind Dhamankar, M.D.
Manager Clinical MR
Research Collaborations,
Siemens Medical
Solutions USA

Peter Kreisler, Ph.D.
Collaborations & Applications,
Erlangen

Gary R. McNeal, MS (BME)
Advanced Application Specialist,
Cardiovascular MR Imaging
Siemens Medical Solutions USA

Cécile Mohr, Ph.D
Head of Market Segment
Management, Erlangen

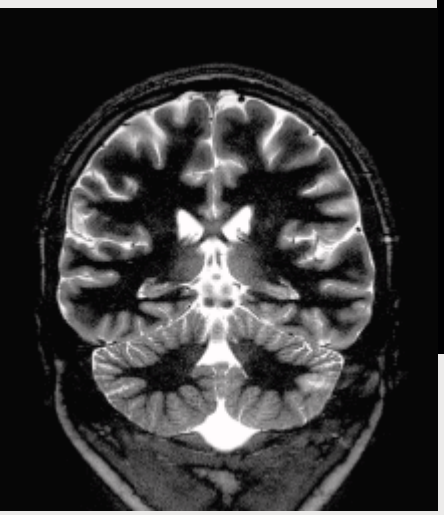

High Resolution T2 weighted 3T head imaging. ***Page 54***

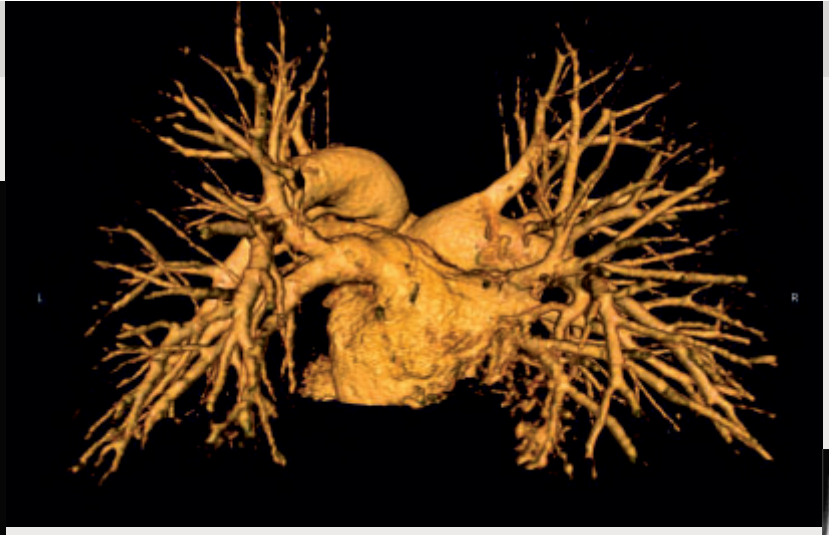

3D Volume rendered image of pulmonary venous anatomy at 3T. ***Page 43***

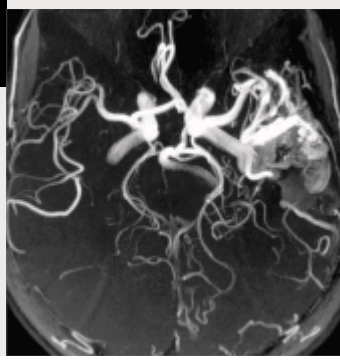

Left temporal AVM with superior small vessel delineation at 3T. ***Page 39***

CLINICAL

3D Neuro taskcard showing functional activation. ***Page 58***

The new Peripheral Angiography Coil of MAGNETOM Trio a Tim System. ***Page 98***

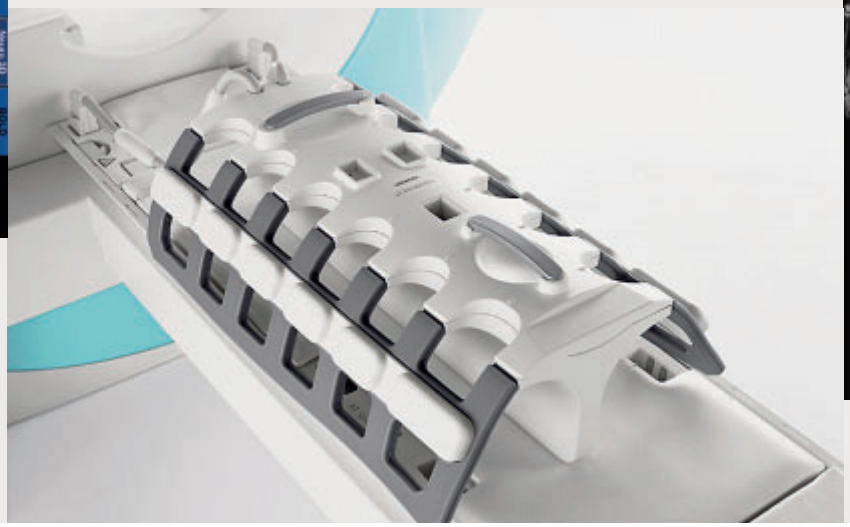

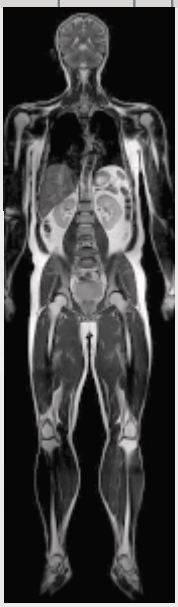

Whole Body Imaging at 3T
Page 100

TECHNOLOGY

LIFE

M-Z934-1-7600

Proven Outcomes with Tim (Total imaging matrix technology). In hundreds and hundreds of installations around the world, Tim® is proving that a new era in MRI is here. With Tim's unmatched 32 independent RF channels and up to 102 Matrix coil elements, you can combine coils in any way, for multi-organ exams, all in a single patient set-up. Offering incredible flexibility and accuracy.

Ensuring no detail is lost — from the smallest lesions to a large organ or extended anatomical region. And with iPAT in all directions, you can actually reduce image time, yet scan at a higher resolution. Visit us at www.siemens.com/Tim and let Tim prove it to you.

Siemens **Medical Solutions** that help

SIEMENS
medical

Abdomen and Pelvis

MAGNETOM Trio, A Tim System enables for the first time comprehensive clinical abdominal imaging at 3T. The use of parallel imaging in combination with the Matrix coil technology helps overcome 3T related technical challenges like SAR limitations as well as physiological motion artefacts. In addition, the largest Field of View (FoV) and the best magnet homogeneity at 3T delivered with the system enable abdominal imaging with excellent fat saturation capable of delineating the finest abdominal structures.

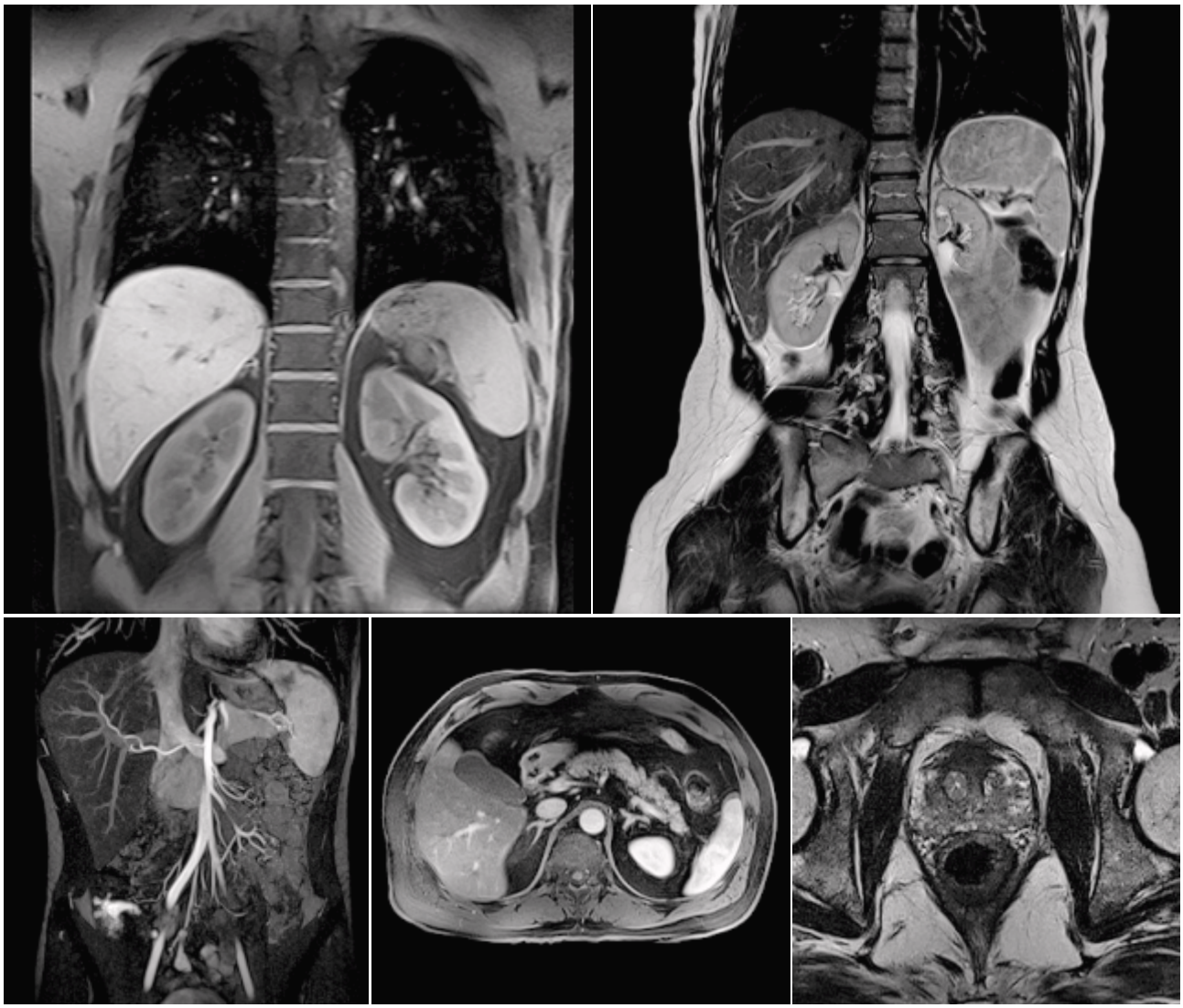

MR Cholangiopancreatography at 3.0 Tesla – Initial Experience and Future Outlook

Elmar M. Merkle, M.D.[1] and Brian M. Dale, Ph.D.[2]

[1] *Duke University Medical Center, Department of Radiology, Durham, NC, USA*
[2] *Siemens Medical Solutions, Cary, NC, USA*

Introduction

Since its original description in 1991 by Wallner et al. [1], magnetic resonance cholangiopancreatography (MRCP) has gained general acceptance along with transabdominal ultrasound as the non-invasive imaging method of choice for diseases of the biliary system. It has replaced endoscopic retrograde cholangiography (ERC), particularly in those cases in which an endoscopic intervention seems unlikely at the outset [2]. While transabdominal ultrasound seems to be superior for gallbladder imaging, MRC is favored for evaluation of extrahepatic biliary ductal disease [3]. Unfortunately, both imaging modalities are of limited use for evaluating the intrahepatic biliary anatomy, particularly if the biliary system is not dilated. The underlying reasons are mainly limitations in spatial resolution and/or signal-to-noise. However, a detailed anatomical depiction of the 'non-distended' intrahepatic biliary ductal system is occasionally needed, e.g. for the preoperative evaluation of potential living liver donors.
The introduction of whole body 3.0-Tesla MR systems in combination with a dedicated receive-only torso coil array is an appealing concept with the potential to overcome these limitations.

State-of-the-art MRCP imaging protocol

A current MRCP protocol at ultra-high field MR imaging is very similar to a standard 1.5 Tesla MRCP protocol and includes several steps. Following the acquisition of a multiplanar localizer, a HASTE sequence in coronal orientation and a Gradient Echo in and opposed phase sequence in axial orientation through the liver and pancreas are performed. These imaging data sets are primarily used to optimize the positioning of the subsequent 'dedicated' MRCP sequences. In particular the opposed phase imaging data set has been shown to be helpful as it allows the identification of the pancreas with a high level of confidence even for inexperienced MR technologists due to the chemical shift artifact of the second kind (also known as India ink artifact). The dedicated MRCP sequences include single-slice breath hold RARE* (Rapid Acquisition with Relaxation Enhancement) in various angulations, multi-slice breath hold HASTE (Half Fourier Acquisition Single-Shot Turbo Spin Echo), and a respiratory triggered 3D Turbo Spin Echo sequence. A more detailed description is provided as follows:

Sequence 1: *Triplanar localizer*
TR/TE/FA/NSA = 15/5/40/1, 96 x 192 matrix, ST 10 mm
Sequence 2: *Coronal T2-weighted HASTE*
TR/TE/FA/NSA = 1000/83/136/1, 256 x 256 matrix, 17 slices, ST 8 mm

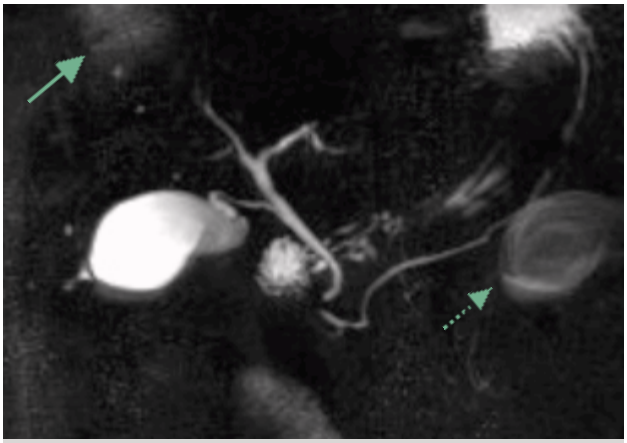

[Figure 1] *Maximum intensity projection of a respiratory triggered coronal 3D T2-weighted TSE dataset showing a normal biliary and pancreatic ductal anatomy. Note ghosting artifacts from the stomach (solid arrow) and gallbladder (dashed arrow).*

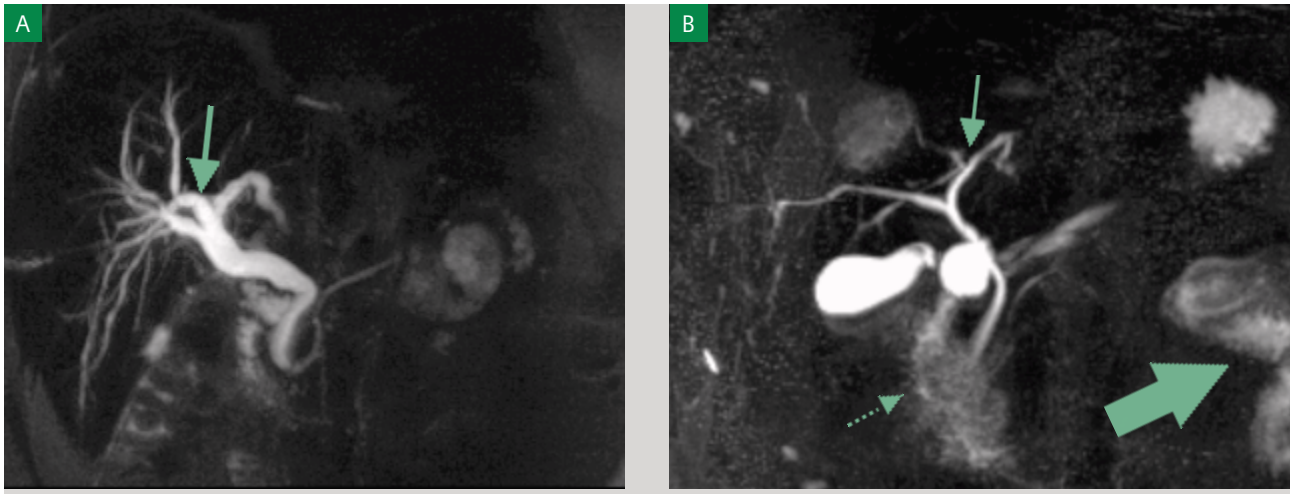

[Figure 2] *Maximum intensity projections of a SPACE (A) and a respiratory triggered coronal 3D T2-weighted TSE (B) dataset showing two normal variants of the biliary ductal anatomy. (A), Trifurcation variant where the right posterior segmental branch (arrow), the right anterior segmental branch and left hepatic duct join at the same point. (B), Cross-over variant where the right posterior segmental branch (arrow) drains into the left hepatic duct. Note ghosting artifacts (dashed arrow) from fluid filled small bowel loops (large arrow) obscuring the area of the papilla of Vater.*

Sequence 3: *Axial T1-weighted gradient recalled echo in- and opposed phase TR/TE1/TE2/FA/NSA = 216/1.52/4.9/71/1, iPAT 2, 192 x 256 matrix, 2 x 19 slices, ST 8 mm*
Sequence 4–6: *Coronal single slice T2-weighted RARE with fat saturation, coronal and ± 20 oblique coronal TR/TE/FA/NSA = 2120/964/150/1, 256 x2 56 matrix, ST 50 mm, 30 x 30 cm^2 FoV, TA 2 s*
Sequence 7: *Coronal T2-weighted HASTE with fat saturation TR/TE/FA/NSA = 3000/106/123/1, 256 x 256 matrix, 16 slices, ST 3 mm, 35 x 35 cm^2 FoV, 2 concatenations , TA 2 x 24 s*
Sequence 8: *Respiratory triggered coronal 3D T2-weighted TSE with fat saturation utilizing a navigator technique for detection of the diaphragm position TR/TE/FA/NSA = 1 x respiratory cycle/645/180/1, 240 x 256 matrix, 60 slices, ST 1 mm, 30 x 30 cm^2 FoV, TA 3 – 6 min depending on the respiratory frequency*

Normal biliary anatomy

Accurate preoperative radiological imaging with a high level of confidence is essential in order to assess the vascular and biliary anatomy of patients prior to liver resection or potential living related liver donors. It is the unique ability of MR imaging to delineate the biliary system without the need for biliary excreted contrast agents. This allows a fast preoperative workup using a single imaging approach. Visualization and classification of the intrahepatic biliary variants represent the most challenging part of the preoperative evaluation with variants in as many as 45% of cases [4]. A correct understanding of the biliary anatomy is crucial in order to achieve safe hepatic resections and to minimize biliary complications [5].

The 'classic' biliary anatomy is known as a left hepatic duct and a short right hepatic duct which together form the common hepatic duct. The right hepatic duct itself is formed by the anterior and posterior right hepatic segmental branches (Figure 1). Unfortunately, this classic anatomy is seen in only two-thirds of all cases. The most common variants are so-called cross-over anomalies where the right posterior segmental branch either joins together with the right anterior segmental branch the left hepatic duct or the right posterior segmental branch crosses over to drain into the left hepatic duct. These cross-over variants are seen in approximately 30% of cases (Figure 2). Depiction of these variants is important for the hepatic surgeon to optimize patient outcome. Preliminary data suggest that MRCP at 3.0 Tesla offers improved CNR and a higher level of confidence for depicting intrahepatic variants compared to MRCP at 1.5 Tesla [6].

Remaining challenges at ultra-high field MRCP

The RARE and HASTE sequences are very robust and reliable. However, they are orientation-dependent and have a relatively coarse through-plane resolution. The respiratory triggered sequence, on the other hand, is a nearly isotropic 3D

high resolution sequence. It can be used to generate a high resolution MIP in any orientation and detect small structures with a high degree of confidence [6], but it is less robust and occasionally suffers from certain artifacts. In particular, it is common to see a FoV/2 ghost (Figure 1 arrows and Figure 2B dashed and large arrows) because each partition is acquired over two separate respiratory cycles. Additionally, this sequence is quite long, requiring 3 – 6 minutes depending on the respiratory cycle of the patient.

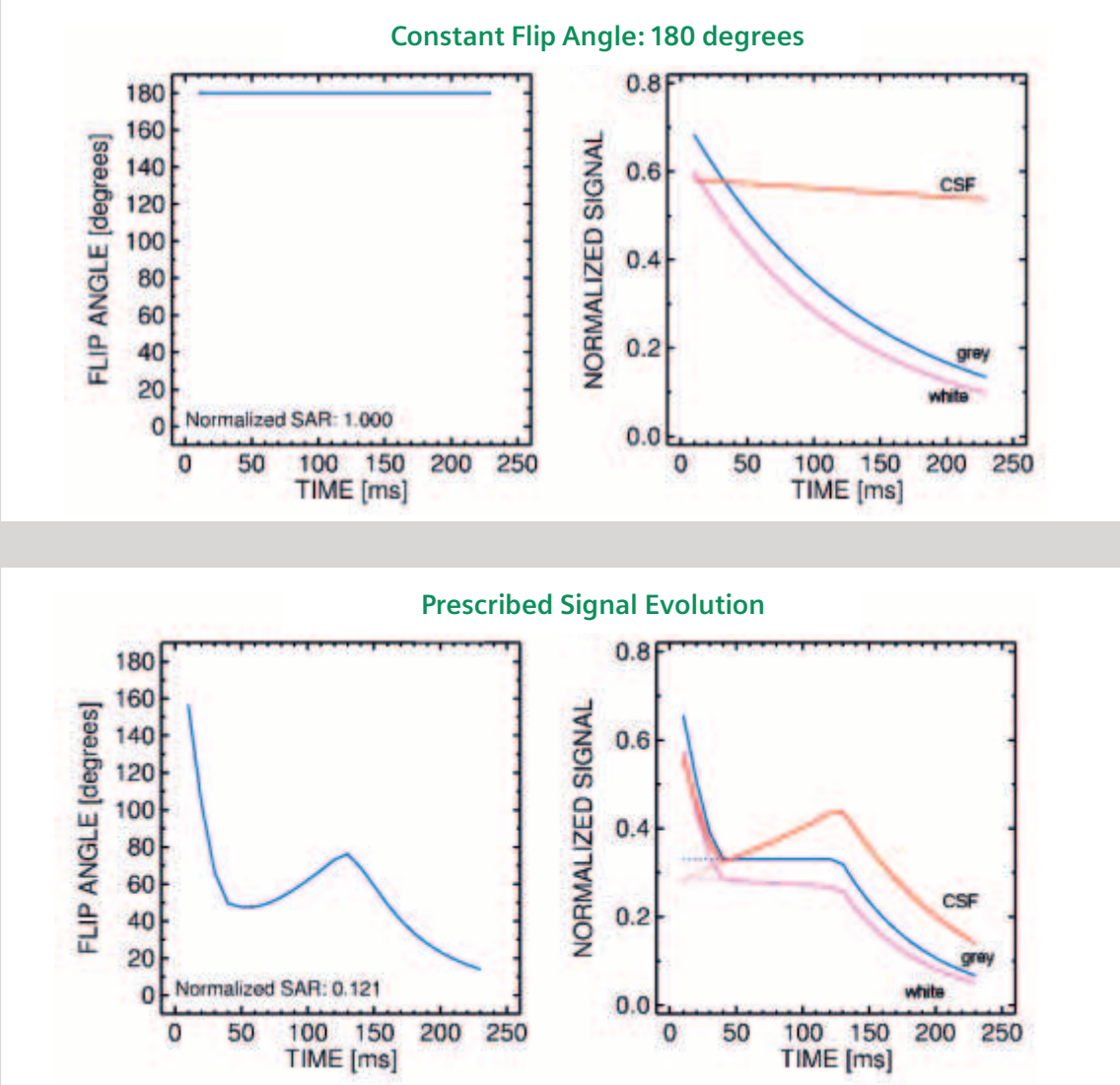

[Figure 3] *Plots of signal evolution during the echo train with a standard TSE sequence (top) and the SPACE sequence (bottom). In each case the flip angles used during the echo train are shown (left), as well as the resulting MR signal during the echo train (right). The standard TSE sequence uses a constant train of 180° pulses while the SPACE sequence varies the flip angle during the echo train. Due to SAR restrictions, the 180° train is oftentimes not possible at 3.0T leading to degraded contrast and signal properties. With the SPACE sequence SAR is dramatically reduced and the desirable signal properties, especially late in the train, are maintained. Because longer echo trains can be used, an entire partition is acquired in a single TR with SPACE, which effectively eliminates the FoV/2 ghosts present with the standard sequence.*

Potential solutions and further outlook

One potential solution to the ghosting is to use the SPACE sequence. Instead of using a constant train of 180° refocusing pulses, the SPACE sequence uses a varying train. These carefully designed refocusing pulse trains allow the use of very large Turbo-factors while maintaining desired contrast and even reducing SAR (Figure 3) [7]. With these large Turbo-factors an entire partition may be acquired in a single respiratory cycle, thereby eliminating the FoV/2 ghost artifacts and improving resolution (Figure 4 and Figure 2A). Image quality with this sequence is generally high with high resolution isotropic 3D datasets allowing a high-resolution MIP (Maximum Intensity Projection) in any direction.

The SPACE sequence is a respiratory-triggered sequence, which therefore requires a substantial amount of time for acquisition, just like the original respiratory-triggered TSE sequence suggested above. Whilst it is possible that the higher SNR and iPAT factors available on the MAGNETOM Trio, A Tim System will allow for a more rapid acquisition with similarly high image quality, this possibility, however, remains to be validated clinically.

Summary

MRCP is an important and effective imaging technique that benefits significantly from the additional SNR available at 3.0T. A state of the art protocol is presented including RARE, HASTE, and respiratory triggered 3D T2-weighted TSE. The new SPACE sequence can eliminate some of the artifacts encountered with the suggested TSE sequence without compromising resolution or contrast.

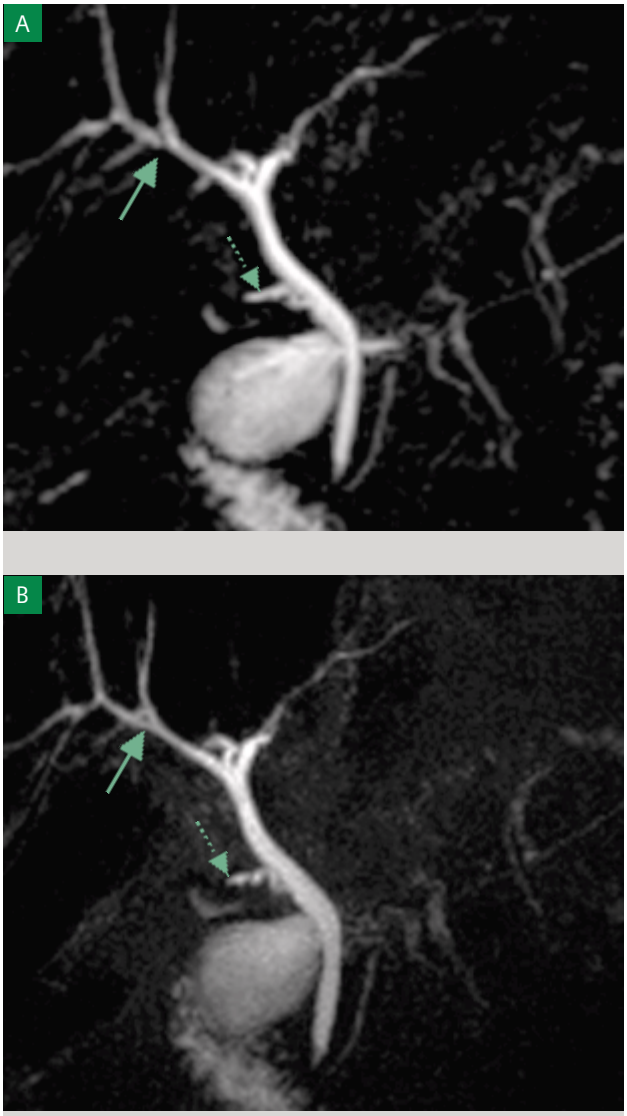

[Figure 4] *Maximum intensity projections from the T2-weighted respiratory navigated standard TSE (A) and abdominal SPACE (B) sequences. Patient is status post cholecystectomy. Note the generally sharper edges and better detail with the SPACE sequence (B). The SPACE sequence does not show a pseudo obstruction (solid arrow) and the remnant of the cystic duct (dashed arrow) is more clearly defined for the SPACE sequence.*

Literature

[1] Wallner BK, Schumacher KA, Weidenmaier W, Friedrich JM. Dilated biliary tract: evaluation with MR cholangiography with a T2-weighted contrast-enhanced fast sequence. Radiology 1991;181:805–8.

[2] Barish MA, Yucel EK, Ferrucci JT. Magnetic resonance cholangiopancreatography. N Engl J Med 1999;341:258–264.

[3] Varghese JC, Liddell RP, Farrell MA, Murray FE, Osborne H, Lee MJ. The diagnostic accuracy of magnetic resonance cholangiopancreatography and ultrasound compared with direct cholangiography in the detection of choledocholithiasis. Clin Radiol 1999;54:604–14.

[4] Gazelle GS, Lee MJ, Mueller PR. Cholangiographic segmental anatomy of the liver. Radiographics 1994;14:1005–13.

[5] Goldman J, Florman S, Varotti G, et al. Noninvasive preoperative evaluation of biliary anatomy in right-lobe living donors with mangafodipir trisodium-enhanced MR cholangiography. Transplant Proc 2003;35:1421–2.

[6] Merkle EM, Haugan PA, Thomas J, Jaffe TA, Gullotto C. MR Cholangiography: 3.0 Tesla versus 1.5 Tesla – A Pilot Study. Am J Roentgenol, in press.

[7] Mugler, JP. Variable-Flip-Angle Strategies for T2-Weighted 2D TSE: A Preliminary Theoretical Comparison. Radiology and Biomedical Engineering, University of Virginia, presented at Siemens Medical Solutions, Erlangen. 2002.

*The information about this product is preliminary. The product is under developement and is not commercially available in the US. and its future availability cannot be assured.

New Perspectives and Challenges in Abdominal Imaging with the MAGNETOM Trio, A Tim System

Christoph J. Zech[1] , M.D., Stefan O. Schoenberg[1], M.D., Olaf Dietrich[1], Ph.D, Wilhelm Horger[3], Gerhard Laub, Ph.D[3], Ioannis Panagiotelis Ph.D[3], Paul J. Finn[2], M.D., Maximilian F. Reiser, M.D.[1]

[1]*Institute of Clinical Radiology, University Hospitals-Grosshadern, Ludwig-Maximilians-University Munich*
[2]*Cardiovascular Research, Department of Radiology, University of California at Los Angeles, USA*
[3]*Siemens Medical Solutions, Malvern PA, USA*

Introduction

In general, the challenges for abdominal magnetic resonance imaging (MRI) are confined to the three-fold issues of spatial resolution, signal-to-noise ratio, and artifacts from respiratory motion or vascular pulsation. Within the last few years, a number of strategies have been developed to overcome these limitations. The use of parallel acquisition techniques on MRI systems with multiple receiver channels now allows the increase of the spatial resolution at almost no cost in scan time [Heidemann RM et al., 2003; Zech et al., JMRI 2004]. Motion artifacts can be successfully avoided by the application of navigator-based correction techniques thereby synchronizing the image acquisition with the position of the diaphragm [Zech et al., JMRI 2004; Pauleit et al., 2001]. Lastly, signal-to-noise constraints can now be effectively overcome by the introduction of 3 Tesla (T) MRI systems into the clinical routine. To truly assess the additional value of 3T systems for abdominal MR imaging one has to ensure that a fair comparison is made to current state-of-the-art 1.5T MRI systems, in order to evaluate the benefit of 3T in view of the higher hardware costs .

At the present time, state-of-the-art 1.5T MRI scanners are equipped with between 8 and 32 independent receiver channels allowing the use of parallel acquisition techniques (PAT) in all three directions with acceleration factors of up to 16. For PAT, essentially two different algorithms are applied, which perform the reconstruction either in the image domain (SENSE-based algorithms) [Pruessmann et al., 1999] or k-space domain (SMASH-based algorithms) [Sodickson et Manning, 1997; Jakob et al., 1998; Griswold et al., 2000; Griswold et al., 2002]. Dependent on the vendor-specific implementation, the information of the coil sensitivity profiles is either acquired within a separate breath-hold-scan (SENSE) or by acquisition of additional reference lines within the same scan (mSENSE, GRAPPA) [Griswold et al., 2004]. The latter implementation is known as integrated parallel acquisition techniques (iPAT).

Current state-of-the-art imaging at 1.5 Tesla

With 1.5T state-of-the-art scanners, a slice thickness for abdominal imaging of 4 to 6 mm can be routinely applied with 2D-sequences and 2 to 4 mm with 3D-sequences. Acquisition of a $(320)^2$ matrix at a $(350\ mm)^2$ field-of-view allows the routine obtaining of an in-plane resolution of approximately 1 mm^2. By the combination of parallel acquisition techniques with prospective navigator correction e.g. in T2-weighted (w) turbo-spin-echo (TSE) sequences, the image acquisition of larger organs such as the liver is feasible in three breath-holds with a breath-hold time of only 13 seconds [Zech et al., JMRI 2004]. For free-breathing acquisitions, the total acquisition time can be effectively reduced by parallel acquisition techniques to around 4 minutes. Studies have shown that the use of PAT does not result in a substantially larger number of artifacts from aliasing, while at the same time motion artifacts are decreased due to the shorter overall scan times [Zech et al., JMRI 2004]. With these techniques liver lesions can now be reliably detected with T2-w sequences at a size of 4 to 5 mm or less after administration of superparamagnetic iron oxides (SPIO). It has been shown that the combination of dynamic gadolinium-enhanced imaging using thin-slice 3D T1-w gradient-echo (GRE) sequences with SPIO-imaging further improves the detection of small lesions < 10 mm [Kwak et al, 2004].

In sequence types that have an intrinsically high signal-to-noise ratio (SNR), such as steady-state free precession techniques (TrueFISP, balanced FFE, FIESTA), higher PAT acceleration factors can be applied. These techniques are particularly

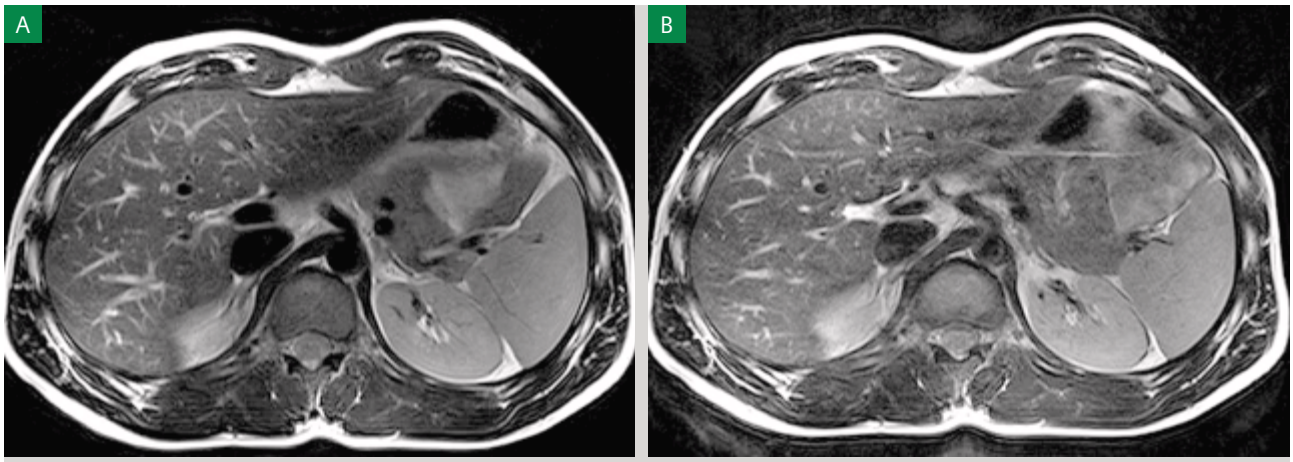

[Figure A-1] *Comparison of a navigator-triggered T2-weighted TSE sequence of the liver on a 3T system (MAGNETOM Trio, Siemens Medical Solutions). The time of acquisition is decreased from 1:52 min without (A) parallel imaging to 1:11 min with (B) parallel imaging with an acceleration factor of 2. Same parameter settings were used for both sequences: TR: > 1900 ms, depending on the respiratory cycle; TE: 109 ms; 27 slices with 6 mm thickness; $(384)^2$ matrix with a rectangular field of view (360 x 270 mm^2).*

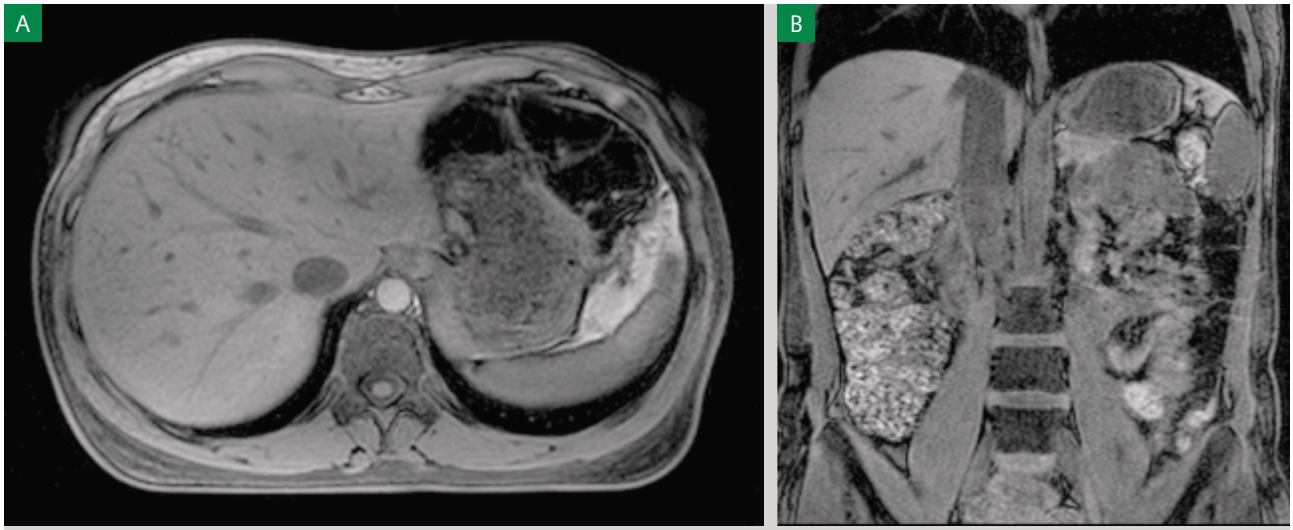

[Figure A-2] *Transversal (A) and coronal (B) VIBE fat-sat T1-weighted 3D GRE images acquired on a 3T system (MAGNETOM Trio, Siemens Medical Solutions) with a novel whole-body coil concept (total imaging matrix) and parallel imaging with an acceleration factor of 2 for the transversal study and 3 for the coronal study. Note the excellent image homogeneity and fat suppression. The whole liver can be covered with 2 mm slices within a single breath-hold of 18 s.*

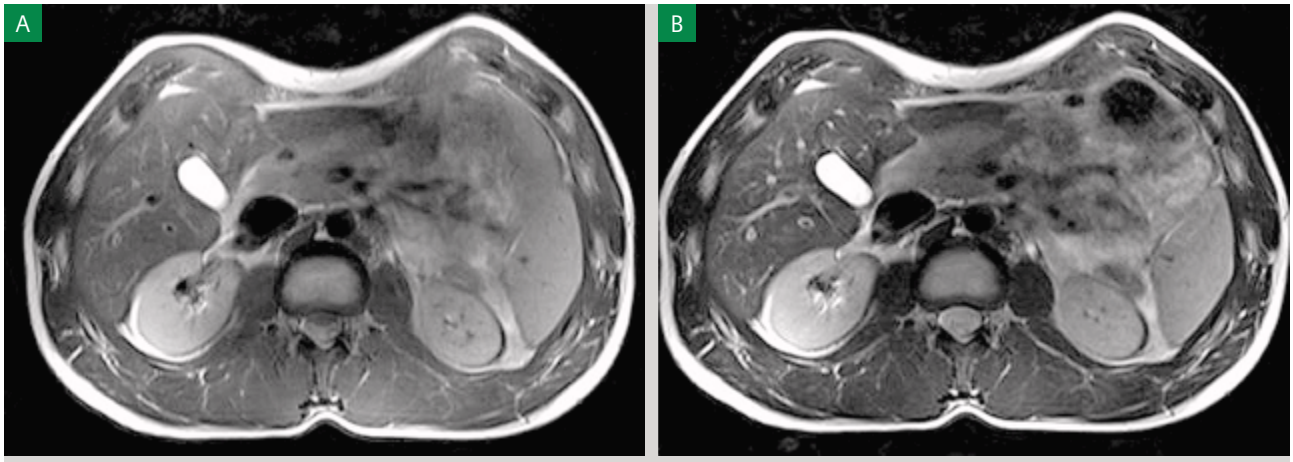

[Figure B] *Comparison of a navigator-triggered T2-weighted TSE sequence of the liver on a 3T system using the hyper-echo technique (MAGNETOM Trio, Siemens Medical Solutions). Each two sections at different levels with a flip angle of 60° (A) and 120° (B). The other parameter settings were the same for both sequences: TR: > 1900 ms, depending on the respiratory cycle; TE: 109 ms; 27 slices with 6 mm thickness; $(384)^2$ matrix with a rectangular field of view (360 x 270 mm^2).*

favorable for single-breath-hold 3D imaging of the small and large bowel after intra-luminal water distension with acceleration in two phase-encoding directions. A total PAT factor of six allows the acquisition of an entire data set with 1.5 mm isotropic voxel length in a single breath-hold of less than 20 seconds. This data can be individually reformatted to show the exact extent of small or large bowel pathology. Imaging of the pancreas can nowadays also be done at very high resolution by the use of PAT, $(320)^2$ to $(384)^2$ matrix size and a slice thickness of 4 mm after administration of manganese-containing contrast agents such as Teslascan™ (Amersham Health, Ismaning, Germany) [Schima et al., 2002]. Similarly, the advent of PAT has revolutionized the use of contrast-enhanced 3D MR-angiography (MRA) in the abdomen. Voxel sizes of less than 1 mm^3 are now achievable within a single breath-hold [Schoenberg et al., SemUltrasCTMR 2003; Schoenberg et al., NDT 2003; Schoenberg et al., Radiology 2005]. These isotropic data sets can also be reformatted in any plane, which offers the possibility of assessing the area stenosis rather than only the diameter stenosis. These area stenosis measurements have shown good correlation to intravascular ultrasound in preliminary studies on renal arteries and appear to be significantly more accurate in terms of the measurement of the true degree of stenosis [Schoenberg et al., Radiology 2005].

Capabilities at 3 Tesla

As already outlined, the current achievements at 1.5T apply a high standard in abdominal MRI. Thus, the initial step at 3T was to reproduce similar image parameters to those at 1.5T. The problem is that there are a number of challenges for abdominal MRI at 3T despite the obvious advantage of a higher SNR. First, the specific absorption rate (SAR) increases quadratically with field strength, resulting in a major limitation particularly for turbo-spin-echo sequences [Kangarlu et al, 1999]. The shorter wavelength at 3T results in substantial dielectric resonance-effects, causing significant signal inhomogeneities due to eddy currents in the tissue with the result of focal field cancellation [Kangarlu et al, 1999]. Relaxation times are substantially longer, which necessitates the adjustment of several imaging parameters (e.g. TR, TE).

The second step for abdominal imaging at 3T has therefore been to effectively address these limitations by new technical strategies. The signal inhomogeneities due to the dielectric resonance effects can be substantially reduced by the application of external gel pads placed on the surface of the patient. These RF homogenisation pads are not visible in the images, but nevertheless alter the dielectric properties of the imaging volume, improving signal homogeneity [Schmitt M et al., 2004]. The SAR can be effectively reduced by new techniques such as the hyper-echo technique and the variable flip angle technique [Mugler JP et al., 1992; Hennig et Scheffler, 2001; Hennig et al., 2003], or parallel imaging [Pruessmann, 2004]. In the third step, these new techniques have been effectively implemented on clinical scanners to extend the limits even further. Currently, matrix sizes of $(512)^2$ and slice thicknesses of less than 4 mm appear feasible, while at the same time breath-hold scans of less than 12 seconds or total scan times for free-breathing acquisitions of less than 2 minutes can be achieved using PAT.

Image optimization

In the following, the individual steps for the optimization of image acquisition for abdominal MRI at 3T are discussed:

- **Optimization of image contrast:** As the T1 relaxation time increases with the field strength B_0 (with a typical increase of 30% to 50% of T1 at 3T compared to 1.5T), the sequence parameters, particularly the repetition time (TR) has to be adapted [de Bazelaire et al, 2004]. The effects on the T2 relaxation are less prominent; T2 is effectively unchanged at 3T, but T2* is shortened [Norris DG, 2003]. The adjustment of the TR strongly depends on the flip angle. Therefore, GRE sequences with small flip angles might require only minor changes in TR compared to sequences with a full 90° flip angle [de Bazelaire et al, 2004].
- **Changes of echo times for in-phase/opposed-phase imaging at 3 Tesla:** Due to the change of the resonance frequency the echo times for in-phase and opposed-phase conditions at 3T have to be adjusted accordingly. The values are almost inverted compared to the conditions at 1.5T. In-phase conditions are found at echo times of 2.3 ms and 4.6 ms, while opposed-phase conditions are present at 1.1 ms, 3.5 ms and 5.75 ms. Therefore, dual echo sequences are problematic, since the echo spacing between the initial opposed-phase echo at 1.1 ms and the following in-phase echo of 2.3 ms are too close for acquisition within a single read-out.
- **Optimization of fat suppression at 3 Tesla:** There are opposite effects at 3T that improve as well as deteriorate the quality of fat suppression. The different resonance frequency at 3T produces a stronger chemical shift between fat and water, thus facilitating the use of spectral fat suppression. At the same time B1 homogeneity decreases with B0 field strength, which results in a more pronounced variation of the flip angle over the field-of-view. This might result in a less optimal fat suppression, which is particularly problematic for TSE sequences, while this effect is less problematic with GRE techniques. In addition, as the field increases stronger eddy currents are generated, that further reduce the quality of fat suppression. Solutions for these limitations are improved gradient-coil design (generating less eddy currents) as well as an alternative, non-radiofrequency-dependent type of fat suppression. This includes, for example, the Dixon method, using several in-phase and opposed-phase images or inversion recovery-type techniques [Wang Y et al, 1998].
- **Increased chemical shift at 3 Tesla:** As mentioned above, the different resonance frequency at 3T produces a stronger chemical shift between fat and water. This can be advantageous for the use of spectral fat suppression and for MR spectroscopy or chemical shift imaging; however, chemical-shift artifacts are also more pronounced at fat/water interfaces. This increase of chemical-shift artifacts can be addressed by using a higher receiver bandwidth with the consequence of losing some of the SNR advantages gained by 3T.
- **Reduction of specific absorption rate (SAR):** As mentioned earlier the three most important techniques for reduction of SAR are new pulse sequences applying the variable flip angle-technique (VFA) or the hyper-echo technique, which is a modification of the former, and parallel imaging that is discussed below. The VFA technique was initially described by Mugler et al. [Mugler JP et al, 1992] and is particularly used for SSFP sequences that offer high SNR efficiency, if large flip angles are applied (α= 60°). However, the SAR also increases quadratically with the flip angle. Since the image contrast is mainly affected by the center of k-space, the flip angle is varied along the phase-encoding direction ensuring a large flip angle in the central parts of k-space, while for the other segments of k-space the flip angle is continuously decreased. This results in a reduction of SAR by at least 50%. The main disadvantage of this technique is that SNR is also reduced by approximately 30%, thus limiting the benefit of the normally two-fold SNR gain at 3T compared to 1.5T. A further refinement of the VFA technique is the so-called hyper-echo technique, which is used for multi-echo sequences such as TSE sequences with long echo trains or single-shot acquisitions (HASTE, RARE). In this technique magnetization can be completely rewound after any arbitrary sequence of RF pulses [Henning et Scheffler, 2001; Henning et al, 2003]. Only the echoes encoding for the center of k-space are refocused by 180° RF pulses. Due to a series of RF pulses with low flip angles stimulated echoes are also obtained, which are used for the image reconstruction together with the conventional echoes as long as they are in-phase with the latter. This technique results in the reduction of SAR by 60% to 80%, while the reduction of SNR is virtually negligible. Simpler techniques to reduce the SAR include the global decrease of the refocusing flip angle in TSE sequences from 180° to a value between 120° and 160°; however, compared to the hyper-echo approach, a larger SNR decrease must be accepted. In fast GRE sequences, the SAR can be reduced by choosing a longer RF pulse, since the RF pulse power scales inversely with the square of the pulse length.
- **Reduction of dielectric resonance effects:** Dielectric resonance effects are caused by local eddy currents because

of the increased conductivity of the tissue. These effects are more enhanced at 3T, since the radio-frequency waves have a shorter length as compared to 1.5T. This causes local inhomogeneities particularly in larger anatomic areas such as the abdomen, where the wavelength is approximately only half the diameter of the body, particularly for patients with low fat content. In the MR images dielectric effects are predominantly noticeable in the ventral aspects of the abdomen as focal areas of varied signal intensity. They can be effectively reduced by placement of an external dielectric gel pad (see above) on the anterior body surface, which increases the resistance for focal eddy currents [Schmitt M et al., 2004]. For standard abdominal imaging this improvement is usually sufficient; however there are certain conditions, in which substantial artifacts with non-diagnostic image quality are virtually unavoidable. These include physiologic or pathologic conditions with large amounts of intraabdominal or intrapelvic fluid, such as pregnancy with a large amount of amniotic fluid or intraabdominal ascites. In those cases, images can be almost non-diagnostic due to focal signal intensity drop-outs [von Falkenhausen et al, 2004].

- **Parallel acquisition techniques:** With PAT, the SNR is reduced by the square root of the acceleration factor times the so-called g-factor, which represents a measure of the local noise amplification, mostly related to array coil design characteristics [Pruessmann et al., 1999; Griswold et al., 2000 and 2002]. Thus with higher acceleration factors of e.g. three, the SNR is reduced to at least 58% of the original value. This causes a visible increase of image noise in the images at 1.5T. Due to the higher SNR at 3T, image noise at comparable acceleration factors is barely visible in the images. Further development can be expected from dedicated multi-channel MR systems such as the MAGNETOM TRIO, A Tim System (Siemens Medical Solutions, Erlangen). Initial results with new multi element array (matrix) coils allow to apply acceleration factors of up to four without noticeable loss of image quality from increased image noise [Pruessmann, 2004].

With all these optimization strategies at 3T, a robust image quality can be obtained in the majority of patients with slice thickness between 4 and 6 mm, matrix sizes between $(320)^2$ and $(384)^2$ and PAT acceleration factors between 2 and 3. With multi-breath-hold imaging the larger abdominal organs, such as the liver, can be covered in 3 breath-holds each lasting 11 seconds using PAT. For single-shot TSE techniques such as HASTE the effective reduction of SAR by the hyper-echo technique allows to acquire 15 to 20 slices in a single breath-hold with a $(384)^2$ matrix without exceeding the SAR limitations. Slice thicknesses of down to 4 mm are feasible even when PAT is used. **The overall results for high-resolution images with a decreased amount of blurring is better with the hyper-echo technique, as it allows the use of higher flip angles compared to the standard VFA technique with reduced flip angles (down to 60°) for the refocusing pulse and, therefore, alternated image contrast (Figure B). For free-breathing techniques, the use of PAT for high resolution images with matrix sizes of $(384)^2$ allows for total acquisition times of less than 1.5 minutes (Figure A).**

The combination of several of these described techniques can be used to optimize dedicated techniques for abdominal imaging such as 3D-TSE MRCP. For this type of sequence a free-breathing acquisition is performed with navigator correction. To effectively reduce SAR in view of the long echo trains, a variable flip angle technique is applied. For maintaining high SNR, the remaining magnetization after the read-out is restored into the longitudinal direction by a dedicated 90° restore pulse. The SNR gain from those restore-pulses in combination with the higher field-strengths allows to apply PAT factors of up to 4. Thus three-dimensional data-sets with an isotropic voxel size of $(0.9\ mm)^3$ can be acquired in only 2 minutes, allowing 3D-assessment of the entire biliary tree by a variety of post-processing possibilities such as multi-planar reformats (MPR), maximum intensity projections (MIP), surface-shading techniques (SSD) or volume-rendering techniques (VRT).

For high-resolution MRA at 3T, voxel sizes of $0.7x0.7x0.7\ mm^3$ are now feasible with a PAT acceleration factor of 3 within a breath-hold of less than 20 seconds. Despite the small voxel sizes and the use of PAT, sufficient SNR is still present due to the higher field strength [Leiner et al, 2003]. The problems for MRA at 3T are two-fold: first the typically short TRs of less than 4 ms result in a high RF power deposition, which easily exceeds the SAR limits. One approach is to lengthen the RF pulse and the TR and to use PAT to compensate for the consecutive increase in scan time; however, this changes the contrast of the image since a longer repetition time increases the background signal. An increased background signal might limit the use of MIPs for the diagnostic evaluation of the MRA. A second problem is the decrease of the flip angle, which is necessary to stay within the SAR limits, which also increases the background signal. Nevertheless in the clinical routine a compromise can usually be found by carefully adjusting these parameters, such that high resolution sub-millimeter MRA is feasible with good image quality [Leiner et al, 2003].

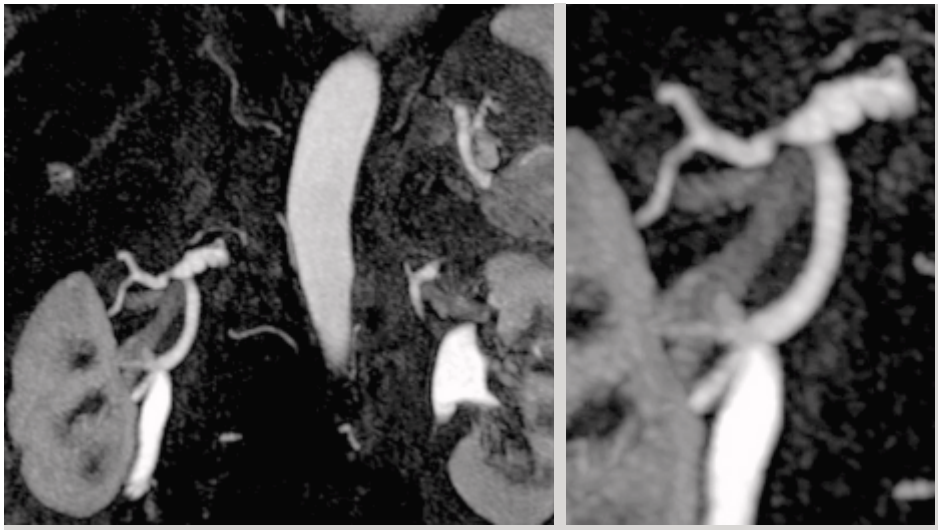

[Figure C-1] *Female patient with fibromuscular dysplasia. MR angiography on MAGNETOM Trio with submillimeter spatial resolution (0.8 x 0.8 x 0.8 mm³) clearly demonstrating the string-of-beads appearance of the FMD lesions. The sequence can be acquired in 18 s with help of parallel imaging (GRAPPA; acceleration factor 3).*

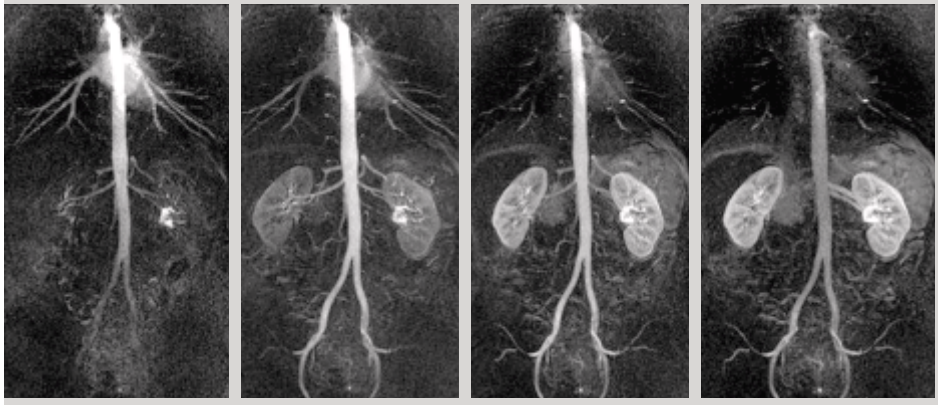

[Figure C-2] *Time-resolved MR angiography on a 3T system (MAGNETOM Trio) with a novel whole-body coil concept (total imaging matrix). At a voxel size of 2 x 2 x 2 mm³, one 3D data set is acquired every 2 susing parallel imaging (GRAPPA; acceleration factor 2).*

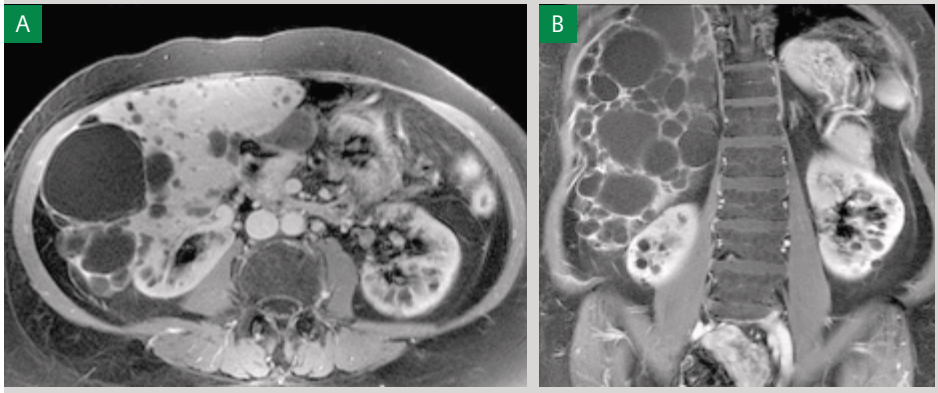

[Figure D] *T1-weighted FLASH 2D sequence on a MAGNETOM Trio, 120 s after injection of Gadolinium in a 54-year-old female patient with polycystic kidney disease. Excellent depiction of the innumerous small cysts, which have to be differentiated from cystic renal cell carcinoma. Although a high spatial resolution is maintained with a (384)² matrix, 23 slices can be acquired in 18 s.*

Clinical value of 3 Tesla for abdominal MRI

In general, those applications for abdominal MRI seem to profit from the higher field strength that critically depend on spatial resolution. One promising application appears to be the assessment of multi-cystic abdominal masses, in which the delineation of enhancing septa is important for the detection of malignancy [Israel et al; 2004]. This includes multi-cystic masses of the kidney and ovaries, in which small nodular thickening of the septa with increased enhancement after gadolinium administration is indicative of early malignancy [Israel et al; 2004]. With an optimal spatial resolution the differentiation between cysts and renal cell carcinoma in von-Hippel-Lindau disease, differentiation between cystadenoma and cystadeno-carcinoma in cystic ovarian lesions as well as early detection of renal cell carcinoma in acquired polycystic disease can be facilitated [Israel et al, 2004; Granata et al, 2004; Mosetti et al, 2004] (Figure D).

For the assessment of focal liver lesions there is still no consensus on whether the high resolution truly converts into a better detection of small lesions of less than 1 cm. However, it has been already demonstrated in small non-controlled studies that a high spatial resolution, e.g. with 3D-GRE sequences, helps to improve the detection of small lesions and the characterization of lesions in terms of better delineation of morphological features such as the vascular architecture or a central scar [Burrel et al, 2003; Heim et al, 2003].

As high-field MRI with a high spatial resolution is not limited by a decreased liver-to-lesion contrast, such as computer tomography, it can be expected that the high resolution should improve overall lesion detection [Mc Kenzie et al, 2004; Zech et al, Radiologe 2004]. The dilemma at this point, however, is that due to the reduced availability of 3T in the clinical routine, no larger systematic studies with comparison between 1.5 and 3T in correlation to an invasive gold standard such as biopsy or surgery have been performed.

An area that holds great promise is the staging of malignant lesions of the uterine cervix and the rectum [Morakkabati-Spitz et al; 2004]. MRI at 1.5T has been notoriously weak in differentiation between stage IIa cervical carcinoma and stage Ib with an accuracy of only around 80% [Sheu et al, 2001]. This question is highly relevant, since differentiation between those two stages affects the decision for either radical hysterectomy or primary radiation therapy. Since extension of the tumor beyond the cervical stroma, which is sometimes less than 1 mm in width, is the discriminator between those two stages, one might expect an improved staging with matrix sizes higher than 512^2. Similar improved performance could be expected for staging of rectal carcinoma, where MRI is known to over-stage lesions of TNM-stage T1 in T2, since reliable differentiation between the submucosa and muscularis propria layers is difficult at current maximum

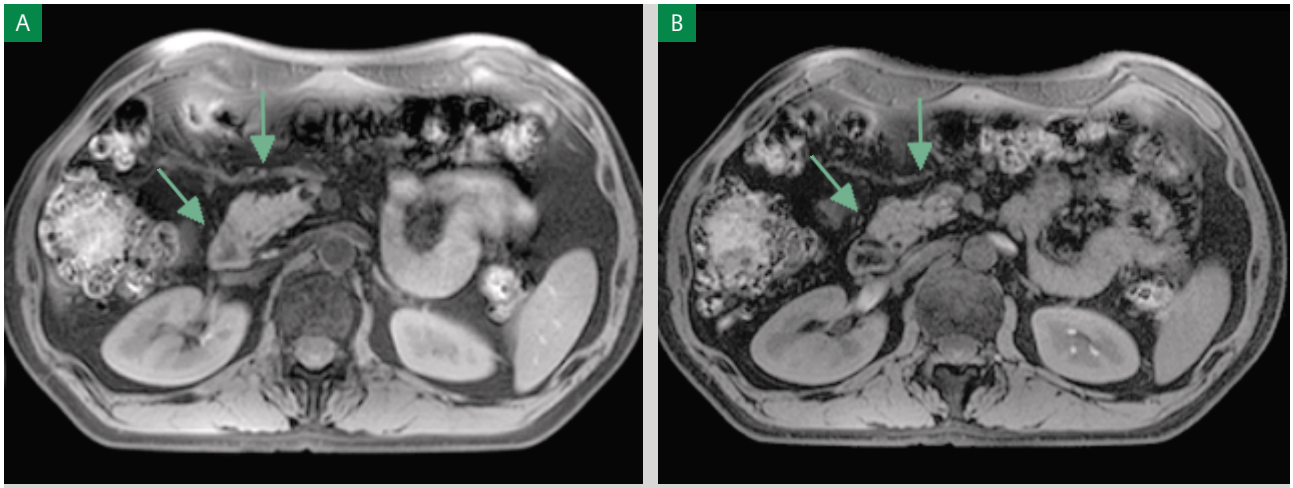

[Figure E] *T1-weighted FLASH 2D sequence with fat-saturation on a 3T system (MAGNETOM Trio, Siemens Medical Solutions) in a healthy volunteer. The sequence with 5 mm slice thickness and a 320 x 256 matrix shows already a very good visualization of the anatomical area of the pancreatic head. However, on the 3T system a substantial increase in spatial resolution with 3 mm slice thickness and a 384 x 320 matrix is still possible without a visible loss of signal (B). Note the superior visualization of the pancreatic head in (B).*

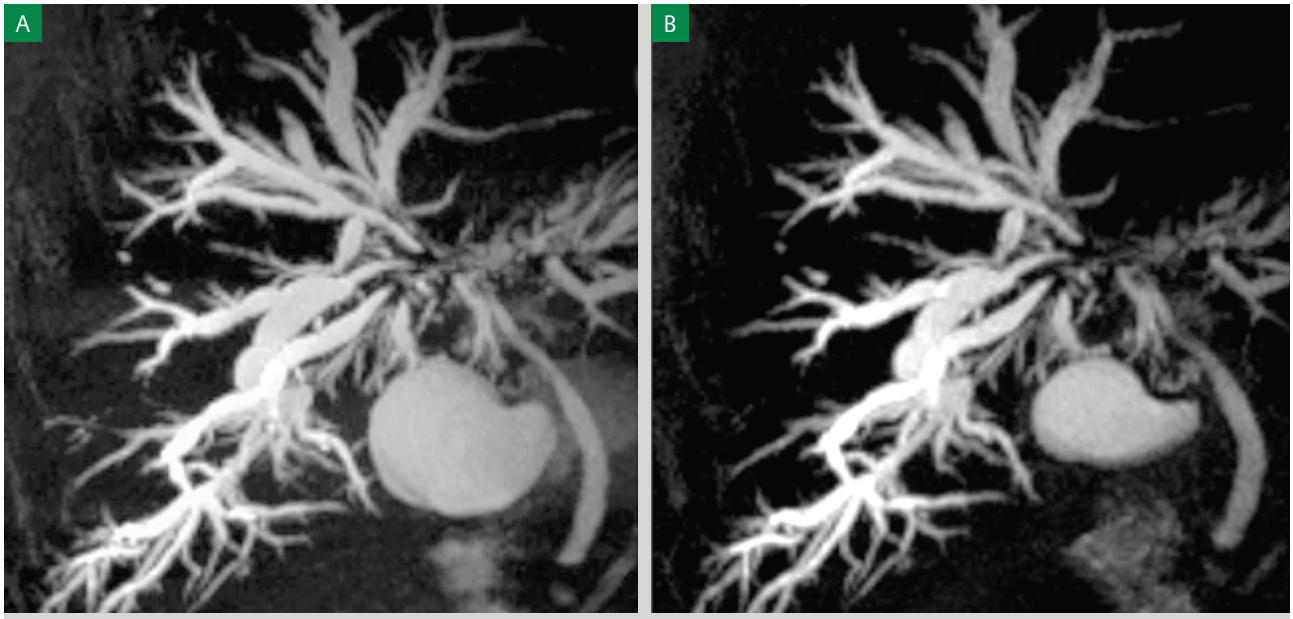

[Figure F] *Submillimeter (0.9 x 0.9 x 0.9 mm^3) T2-weighted 3D TSE sequence with variable flip angle technique on a MAGNETOM Trio in a patient with PSC (Primary Sclerosing Cholangitis), suffering from a severe stenosis at the confluence of the left and right hepatic duct. Due to the high SNR at 3T there is no significant difference of image quality between A (parallel imaging; acceleration factor 2) and B (parallel imaging; acceleration factor 4), although the time of acquisition of the respiratory triggered sequence in free-breathing is decreased from around four (A) to two (B) minutes.*

matrix size of 512^2 [Branagan et al, 2004; Beets-Tan et al, 2001]. Recent publications do also report that increased spatial resolution is helpful for the evaluation of the nodal staging in colorectal cancer, because of the better visualization of morphologic features that help to distinguish malignant from benign lymph-nodes [Kim et al, 2004].

Probably one of the most promising applications is high-resolution 3D MRCP for diseases of the biliary tree that predominantly manifest in the high-order branches in their early stages, such as primary sclerosing cholangitis (PSC) [Schmitz S et al., 2004]. Reliable visualization of the biliary tree with MRCP at 1.5T is only possible up to the second order branches with current techniques [Fulcher et al., 2000]. Therefore, despite proven cost effectiveness of MRCP compared to ERCP due to its lack of any side effects and complete non-invasiveness, it has not established its role for the initial detection of PSC disease manifestation [Talwalkar et al, 2004]. However this patient group particularly benefits from the non-invasive techniques, since they are frequently young patients and early treatment can substantially affect the course of their disease. Untreated patients may experience severe complications such as multiple strictures of the intra- and extrahepatic bile ducts, which ultimately may progress to cirrhosis and liver failure [Porayko et al, 1990]. Moreover, in these patients, ERCP for initial diagnosis can lead to substantial side effects such as pancreatitis or common bile duct perforation, which is observed more frequently than in other patients undergoing ERCP [Beuers et al, 1992]. With voxel sizes of 0.9x0.9x0.9 mm^3 spatial resolution and images free of motion artifacts with scan times of about 2 minutes, 3D MRCP at 3T now allows the detection of high-order branches of the biliary tree already in volunteers without biliary disease. Preliminary results show that focal dilatations and stenoses of third and fourth-order branches, which are often the early manifestation of PSC, can be well detected with good correlation to ERCP [own preliminary data]. The acceleration of the acquisition by a PAT factor up to 4 makes this an easily feasible technique for these patients (Figure F). MRCP can be also combined with high-resolution liver imaging at 3T with a slice thickness of only 3 mm, which may hold out the promise of earlier detection of malignant tumors of the bile duct such as cholangiocarcinoma.

Ultrahigh-resolution contrast-enhanced breath-hold MRA with 0.7 to 0.8 mm isotropic resolution might eliminate the need for diagnostic DSA of the mesenteric and renal arteries (Figure C). A recent publication in the Annals of Internal

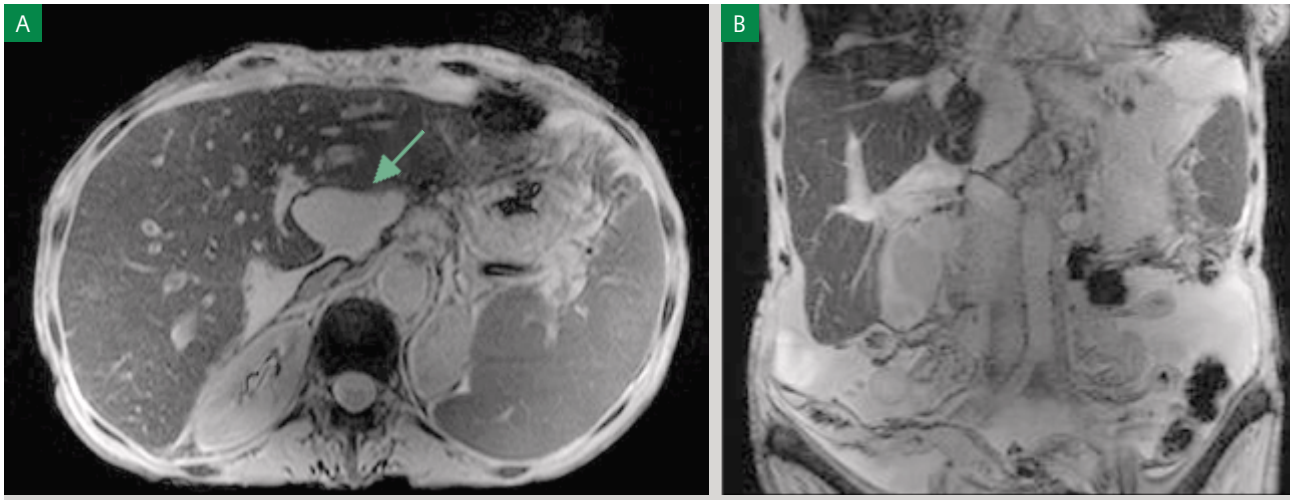

[Figure G] *T2*-weighted 2D GRE sequence in the liver-specific phase after injection of ferucarbotran (Resovist®, Schering Germany, Berlin) in a 68-year-old female patient after liver transplantation. The examination was able to rule out a focal liver lesion (e.g. a hepatocellular carcinoma) with high confidence due to the excellent signal loss in the normal liver parenchyma after injection of the SPIO-contrast agent and due to the high spatial resolution. Sequence parameters are TR/TE/α 132/7.32/30 with 5 mm slice thickness and a 320 x 256 matrix. The whole liver with 37 slices was covered in 4 x 17 seconds breathhold.*

Medicine has shown that MRA at 1.5T with a current spatial resolution of only 1.5 mm or even worse is not sufficient to accurately diagnose and stage the degree of renal artery stenosis [Vasbinder et al., 2004]. Initial results at 1.5T with submillimeter (0.8 x 0.8 x 0.9 mm^3) isotropic spatial resolution and reformats of the vessel area perpendicular to the vessel axis show that assessment of the area stenosis is a much more reliable parameter for exact grading of the degree of stenosis than grading the diameter stenosis in-plane [Schoenberg et al, 2005]. It is expected that this improvement will further increase at 3T.

Conclusion

One has to accept that imaging of the abdomen at 1.5T on a state-of-the-art-system with parallel imaging, navigator correction, and an advanced sequence design is a tough competitor for the evolving field of 3T. Nevertheless, it is now clearly feasible to acquire single-shot TSE images with PAT and hyper-echo technique at a very high resolution with minimal blurring and within the SAR limits. Those images appear to be superior to those currently acquired at 1.5T. PAT is generally applicable without major SNR constraints allowing the use of higher acceleration factors for shorter breathholds. The fat suppression appears acceptable despite problematic dielectric resonance effects. For techniques such as 3D-TSE MRCP, ultra high-resolution submillimeter studies with minimal acquisition times are feasible and may also eliminate the use of diagnostic ERCP for diseases such as primary sclerosing cholangitis in the future. No larger systematic studies have been yet performed for the detection and characterization of small focal liver lesions. It appears, however, that there is improvement at 3T, since in MRI the lesion delineation is primarily limited by the spatial resolution rather than by the liver-to-lesion contrast because of the excellent soft-tissue contrast. The resolution of contrast-enhanced 3D MRA approximates that of DSA for the first time, which should eliminate the use of diagnostic renal or mesenteric DSA other than for rare diseases such as small vessel vasculitis. In the pelvis ultra high-resolution imaging with SE and TSE sequences might further improve the staging of early T1 and T2 tumors of the cervix, uterus and rectum. However, it needs to be pointed out the true gain in clinical value is still speculative at the present time, since no large comparative studies have yet been performed or published.

References

[1] Heidemann RM, Ozsarlak O, Parizel PM, et al. A brief review of parallel magnetic resonance imaging. Eur Radiol. 2003;13:2323–2337.
[2] Zech CJ, Herrmann KA, Huber A, Dietrich O, Stemmer A, Herzog P, Reiser MF, Schoenberg SO. High-resolution MR-imaging of the liver with T2-weighted sequences using integrated parallel imaging: Comparison of prospective motion correction and respiratory triggering. J Magn Reson Imaging 2004;20:443–450.
[3] Pauleit D, Textor J, Bachmann R, et al. Improving the detectability of focal liver lesions on T2-weighted MR images: ultrafast breath-hold or respiratory-triggered thin-section MRI? J Magn Reson Imaging 2001;14:128–133.
[4] Pruessmann KP, Weiger M, Scheidegger MB, Boesiger P. SENSE: sensitivity encoding for fast MRI. Magn Reson Med 1999;42:952–962.
[5] Sodickson DK, Manning WJ. Simultaneous acquisition of spatial harmonics (SMASH): fast imaging with radiofrequency coil arrays. Magn Reson Med. 1997;38:591-603.
[6] Jakob PM, Griswold MA, Edelman RR, et al. AUTO-SMASH: a self-calibrating technique for SMASH imaging. MAGMA 1998;7:42–54.
[7] Griswold MA, Jakob PM, Nittka M, et al. Partially parallel imaging with localized sensitivities (PILS). Magn Reson Med 2000;44:602–609.
[8] Griswold MA, Jakob PM, Heidemann RM, et al. Generalized auto-calibrating partially parallel acquisitions (GRAPPA). Magn Reson Med 2002;47:1202–1210.
[9] Griswold MA, Kannengiesser S, Heidemann RM, Wang J, Jakob PM. Field-of-view limitations in parallel imaging. Magn Reson Med. 2004;52:1118–1126.
[10] Kwak HS, Lee JM, Kim CS. Preoperative detection of hepatocellular carcinoma: comparison of combined contrast-enhanced MR imaging and combined CT during arterial portography and CT hepatic arteriography. Eur Radiol 2004;14:447–457.
[11] Schima W, Fugger R. Evaluation of focal pancreatic masses: comparison of mangafodipir-enhanced MR imaging and contrast-enhanced helical CT. Eur Radiol. 2002;12:2998–3008.
[12] Schoenberg SO, Rieger J, Nittka M, Dietrich O, Johannson LO, Reiser MF. Renal MR angiography: current debates and developments in imaging of renal artery stenosis. Semin Ultrasound CT MR. 2003;24:255–267.
[13] Schoenberg SO, Rieger J, Johannson LO, Dietrich O, Bock M, Prince MR, Reiser MF. Diagnosis of renal artery stenosis with magnetic resonance angiography: update 2003. Nephrol Dial Transplant. 2003;18:1252–1256.
[14] Schoenberg SO, Rieger J, Weber C, Michaely HJ, Waggershauser T, Dietrich O, Reiser MF. High-resolution MR-angiography of the renal arteries using Integrated Parallel Acquisition Techniques (iPAT): value of isotropic cross-sectional reformats compared to digital subtraction angiography and intravascular ultrasound. Radiology. 2005 (in press).
[15] Kangarlu A, Baertlein BA, Lee R, et al. Dielectric resonance phenomena in ultra high field MRI. J Comput Assist Tomogr. 1999;23:821–831.
[16] Schmitt M, Feiweier T, Horger W, et al. Improved uniformity of RF-distribution in clinical whole body-imaging at 3T by means of dielectric pads. Proc Int Soc Magn Reson Med 2004;12:197.
[17] Mugler JP 3rd, Epstein FH, Brookeman JR. Shaping the signal response during the approach to steady state in three-dimensional magnetization-prepared rapid gradient-echo imaging using variable flip angles. Magn Reson Med. 1992;28:165–185.
[18] Hennig J, Scheffler K. Hyperechoes. Magn Reson Med. 2001;46:6–12.
[19] Hennig J, Weigel M, Scheffler K. Multiecho sequences with variable refocusing flip angles: optimization of signal behavior using smooth transitions between pseudo steady states (TRAPS).Magn Reson Med. 2003;49:527–35.
[20] Pruessmann KP. Parallel imaging at high field strength: synergies and joint potential. Top Magn Reson Imaging. 2004;15:237–244.
[21] de Bazelaire CM, Duhamel GD, Rofsky NM, Alsop DC. MR imaging relaxation times of abdominal and pelvic tissues measured in vivo at 3.0 T: preliminary results. Radiology. 2004;230:652–659.
[22] Norris DG. High field human imaging. J Magn Reson Imaging. 2003;18:519-29. (Erratum in: J Magn Reson Imaging. 2004;19:513.)
[23] Wang Y, Li D, Haacke EM, Brown JJ. A three-point Dixon method for water and fat separation using 2D and 3D gradient-echo techniques. J Magn Reson Imaging. 1998;8:703–710.
[24] von Falkenhausen M, Gieseke J, Morakkabati N, et al. 3T MRI of the Liver. Establishing a Comprehensive Highfield Clinical Imaging Protocol and Comparison to 1.5T. Proc Int Soc Magn Reson Med 2004;12:902.
[25] Leiner T, de Vries M, Hoogeveen R, Vasbinder GB, Lemaire E, van Engelshoven JM. Contrast-enhanced peripheral MR angiography at 3.0 Tesla: initial experience with a whole-body scanner in healthy volunteers. J Magn Reson Imaging. 2003;17:609–614.
[26] Israel GM, Hindman N, Bosniak MA. Evaluation of cystic renal masses: comparison of CT and MR imaging by using the Bosniak classification system. Radiology 2004;231:365–371.
[27] Granata A, Sessa A, Righetti M, et al. Juvenile renal cell carcinoma as first manifestation of von Hippel-Lindau disease. J Nephrol. 2004;17:306–310.
[28] Mosetti MA, Leonardou P, Motohara T, Kanematsu M, Armao D, Semelka RC. Autosomal dominant polycystic kidney disease: MR imaging evaluation using current techniques. J Magn Reson Imaging. 2003;18:210–215.
[29] Burrel M, Llovet JM, Ayuso C, et al. Barcelona Clinic Liver Cancer Group. MRI angiography is superior to helical CT for detection of HCC prior to liver transplantation: an explant correlation. Hepatology. 2003;38:1034–1042.
[30] Heim P, Steiner P, Schoder V, Dieckmann C, Kuhlencordt R, Adam G. Detection of liver lesions with gadolinium-enhanced VIBE sequence in comparison with SPIO-enhanced MRI. Rofo. 2003;175:1376–1383.
[31] McKenzie CA, Lim D, Ransil BJ, et al. Shortening MR image acquisition time for volumetric interpolated breath-hold examination with a recently developed parallel imaging reconstruction technique: clinical feasibility. Radiology. 2004;230:589–594.
[32] Zech CJ, Schoenberg SO, Herrmann KA, Dietrich O, Menzel MI, Lanz T, Wallnofer A, Helmberger T, Reiser MF. Modern visualization of the liver with MRI. Current trends and future perspectives. Radiologe. 2004;44:1160–1169.
[33] Morakkabati-Spitz N, Gieseke J, Kuhl C, et al. 3.0-T high-field magnetic resonance imaging of the female pelvis: preliminary experiences. Eur Radiol. 2004; [Epub ahead of print].
[34] Sheu MH, Chang CY, Wang JH, Yen MS. Preoperative staging of cervical carcinoma with MR imaging: a reappraisal of diagnostic accuracy and pitfalls. Eur Radiol. 2001;11:1828–1833.
[35] Branagan G, Chave H, Fuller C, McGee S, Finnis D. Can magnetic resonance imaging predict circumferential margins and TNM stage in rectal cancer? Dis Colon Rectum. 2004;4:1317–22.
[36] Beets-Tan RG, Beets GL, Vliegen RF, et al. Accuracy of magnetic resonance imaging in prediction of tumour-free resection margin in rectal cancer surgery. Lancet. 2001;357:497–504.
[37] Kim JH, Beets GL, Kim MJ, Kessels AG, Beets-Tan RG. High-resolution MR imaging for nodal staging in rectal cancer: are there any criteria in addition to the size? Eur J Radiol. 2004;52:78–83.
[38] Schmitz S, Allsop J, Zeka J, et al. MRCP, Initial Experience at 3Tesla. Proc Int Soc Magn Reson Med. 2004;12:899.
[39] Fulcher AS, Turner MA, Franklin KJ, et al. Primary sclerosing cholangitis: evaluation with MR cholangiography-a case-control study. Radiology. 2000; 215:71–80.
[40] Talwalkar JA, Angulo P, Johnson CD, Petersen BT, Lindor KD. Cost-minimization analysis of MRC versus ERCP for the diagnosis of primary sclerosing cholangitis. Hepatology. 2004;40:39–45.
[41] Porayko MK, Wiesner RH, LaRusso NF, et al. Patients with asymptomatic primary sclerosing cholangitis frequently have progressive disease. Gastroenterology. 1990;98:1594–1602.
[42] Beuers U, Spengler U, Sackmann M, Paumgartner G, Sauerbruch T. Deterioration of cholestasis after endoscopic retrograde cholangiography in advanced primary sclerosing cholangitis. J Hepatol. 1992;15:140–143.
[43] Vasbinder GB, Nelemans PJ, Kessels AG, et al. Renal Artery Diagnostic Imaging Study in Hypertension (RADISH) Study Group. Accuracy of computed tomographic angiography and magnetic resonance angiography for diagnosing renal artery stenosis. Ann Intern Med. 2004;141:674–682.

Accurate Prostate Cancer Staging with MR

Tom Scheenen, Ph.D.; Stijn Heijmink, M.D.; Jelle Barentsz, M.D., Ph.D.

Radboud University Nijmegen Medical Centre, Dept. of Radiology

Patient History

A 65-year-old patient with prostate cancer was referred to MR for clinical staging of the disease. The PSA level was 25 µg/l and the biopsy of the prostate had shown a Gleason grade 5.

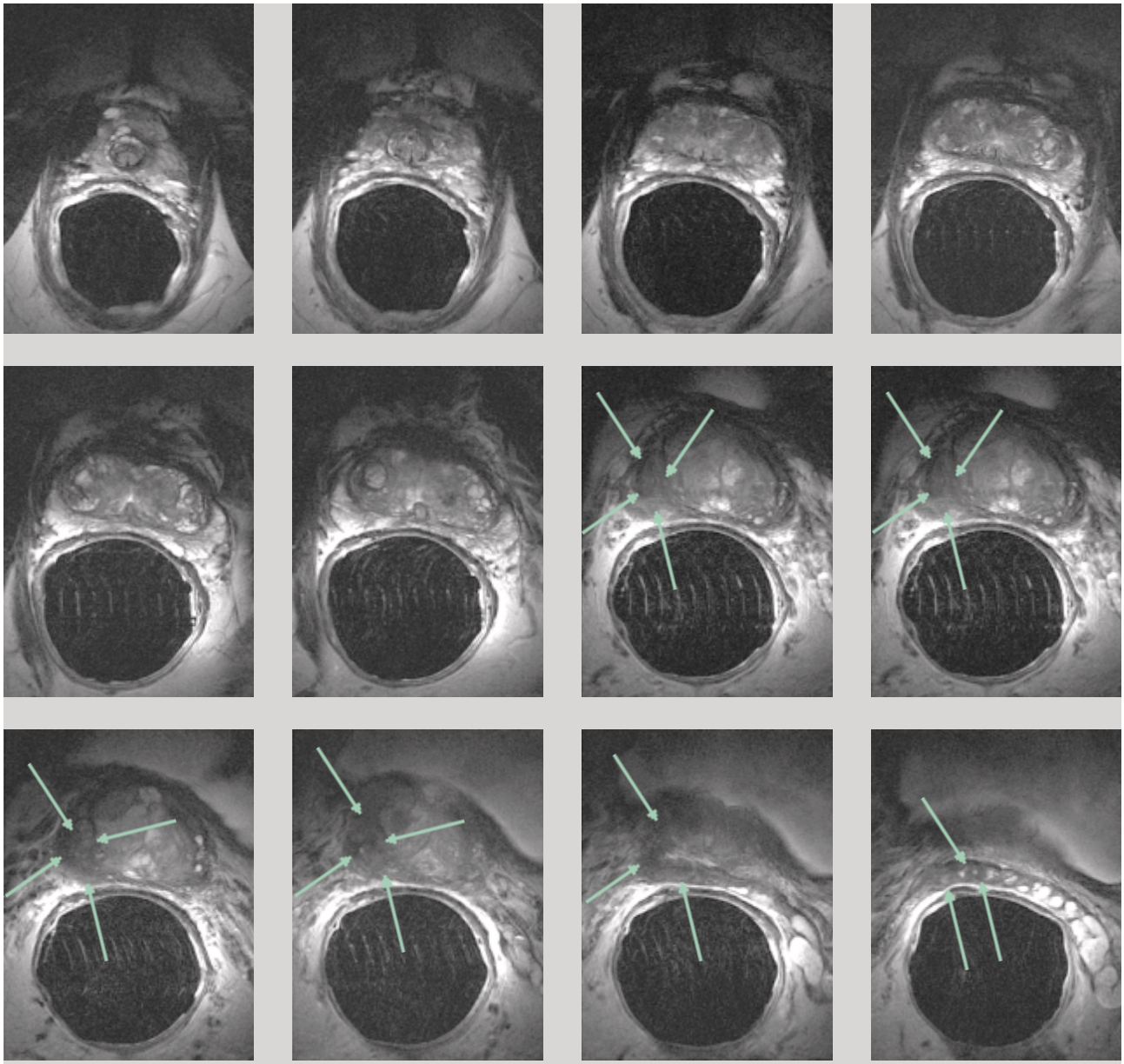

[Figure 1] *T2-weighted axial images of the prostate of a 65-year-old patient with prostate cancer. The complete prostate is visualized from apex to base. The large tumor is visible in the right base of the prostate extending into the seminal vesicles (arrows).*

Measurement Details

- A prototype of an endorectal coil and interface for 3T (Medrad, Pittsburgh, USA) was used for signal reception. The body coil was used for signal excitation.

- **Multislice axial T2-weighted TSE sequence:**
  15 axial slices, TR 4490 ms, TE 153 ms, turbo factor 17, FoV 200 x 100 mm, matrix 768 x 384, slice thickness 2.5 mm. Hyperechoes were used to decrease SAR.

- **Multislice coronal T2-weighted TSE sequence:**
  13 coronal slices, TR 4000 ms, TE 116 ms, turbo factor 17, FoV 180 x 90 mm, matrix 512 x 256, slice thickness 4 mm. Hyperechoes were used to decrease SAR.

- **T1-weighted 3D sequence:**
  Axial reconstruction of 32 partitions, TR 8.6 ms, TE 4.0 ms, flip angle 15 degrees, FoV 130 x 65 x 48 mm, matrix 256 x 128 x 32, slice thickness 2.5 mm.

- **MAGNETOM Trio, software *syngo* MR 2004A**

Results & Discussion

On axial and coronal T2-weighted imaging (Fig. 1 and 2) a large hypo-intense region is visible on the right side in the base of the prostate, extending into the seminal vesicles. After contrast agent administration this lesion, including seminal vesicle invasion, enhances on T1-weighted images (Fig. 3). Based on these findings the diagnosis is stage T3b.
The histopathological analysis of biopsy material from the seminal vesicles confirmed the presence of cancer with Gleason grade 3+4. After a negative lymph node dissection the prostate was resected. The resected prostate was cut, stained and studied (Fig. 4), confirming the clinical stage of the disease: T3b. Because of medication before the prostatectomy the Gleason score was difficult to assess.
This is an example of accurate prostate cancer staging. The combination of an endorectal coil and a magnetic field strength of 3T provides enough SNR for high resolution imaging of the complete prostate. In this case the MRI findings made the urologist decide to take biopsies from the seminal vesicles. Since these were positive for cancer, lymph nodes around the prostate were dissected. With no signs of cancer in the lymph nodes, the next step was to resect the prostate itself.

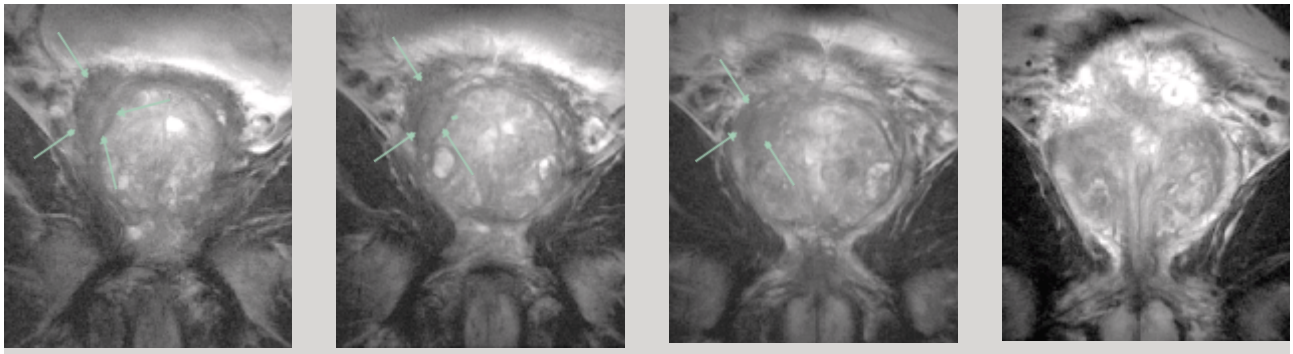

[Figure 2] *Four out of 13 T2-weighted coronal images of the prostate. As the images move towards the endorectal coil (from ventral to dorsal) the SNR of the images increases. Again the tumor with seminal vesicle invasion is indicated with the arrows.*

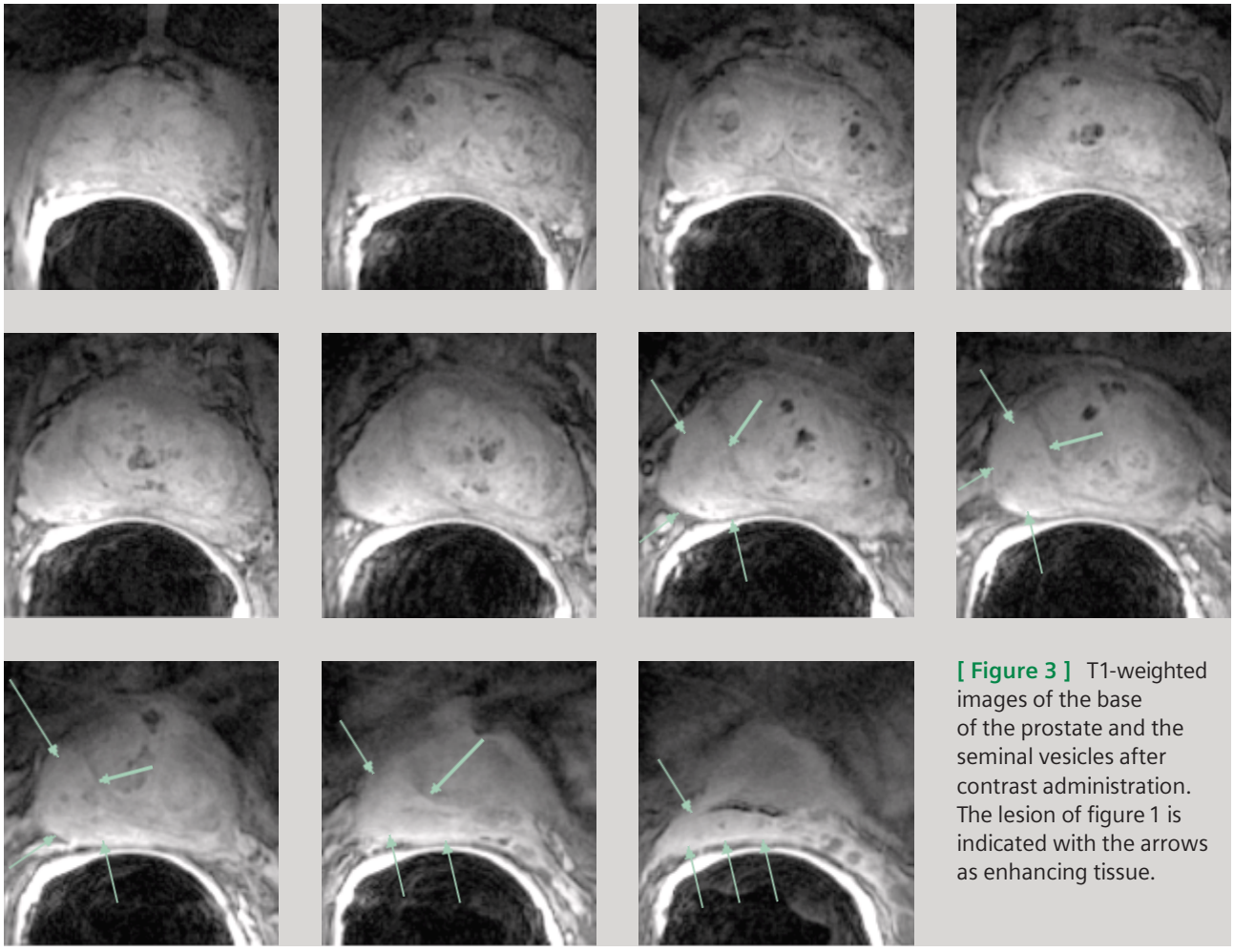

[Figure 3] T1-weighted images of the base of the prostate and the seminal vesicles after contrast administration. The lesion of figure 1 is indicated with the arrows as enhancing tissue.

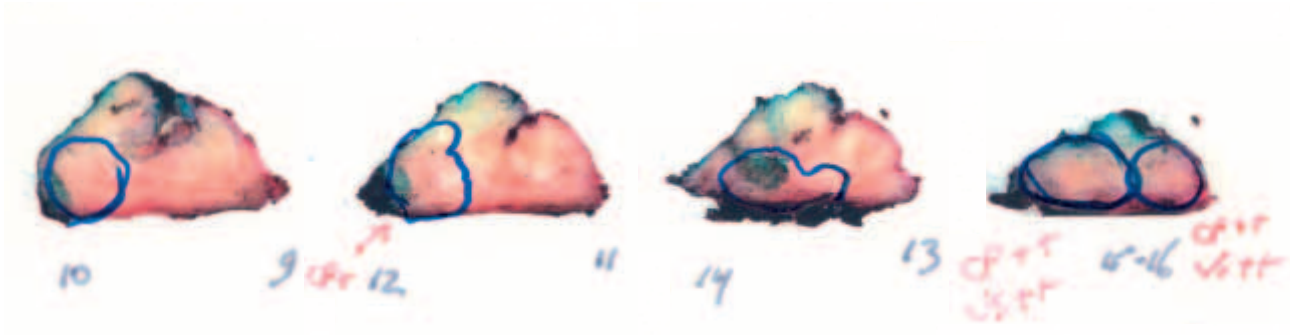

[Figure 4] Histopathology of four cuts through the base of the resected prostate. The tumor is indicated with a blue line. Extra capsular extension is indicated as CP+ and CP++, seminal vesicle invasion is indicated as VS++.

M-Z928-1-7600

Proven Outcomes with Tim (Total imaging matrix technology). Around the world, Tim® has become the new standard in MRI. With hundreds and hundreds of installations, Tim is proving every day that a new era has begun. Now, with just one mouse click you can change Tim's coils and perform a comprehensive assessment of an entire disease, not just a single body region. You can scan the smallest lesions or the entire central nervous system without a detail lost. And you can do it all at the highest speed without sacrificing resolution. Let Tim prove it to you at www.siemens.com/Tim.

Siemens **Medical Solutions** that help

SIEMENS
medical

Accurate Staging of Prostate Cancer with MR

Tom Scheenen, Ph.D.; Stijn Heijmink, M.D.; Jelle Barentsz, M.D., Ph.D.

Radboud University Nijmegen Medical Centre, Dept. of Radiology

Patient History

51 year old patient with prostate cancer. Clinical stage T2 based on digital rectal examination. For accurate staging of the disease, this patient was called for an MRI exam at 3T. With his stage, PSA and Gleason score (PSA =1.0 µg/l Biopsy: Gleason 6/10) the pretest probability of having limited disease (confined to the prostate) is between 52 and 64%, according to the Partin coefficient tables.

Measurement Details

- **A prototype of an endorectal coil** and interface for 3T (Medrad, Pittsburgh, USA) was used for signal reception. The body coil was used for signal excitation.
- **Multislice T2-weighted TSE sequence:**
  15 axial slices, TR 4490 ms, TE 153 ms, turbo factor 17, FOV 200 x 100 mm, matrix 768 x 384, slice thickness 2.5 mm. Hyperechoes were used to decrease SAR.
- **T1-weighted 3D sequence:**
  Axial reconstruction of 32 partitions, TR 8.6 ms, TE 4.0 ms, flip angle 15 degrees, FOV 130 x 65 x 48 mm, matrix 256 x 128 x 32, slice thickness 2.5 mm.
- **MAGNETOM Trio, software *syngo* MR 2004A**

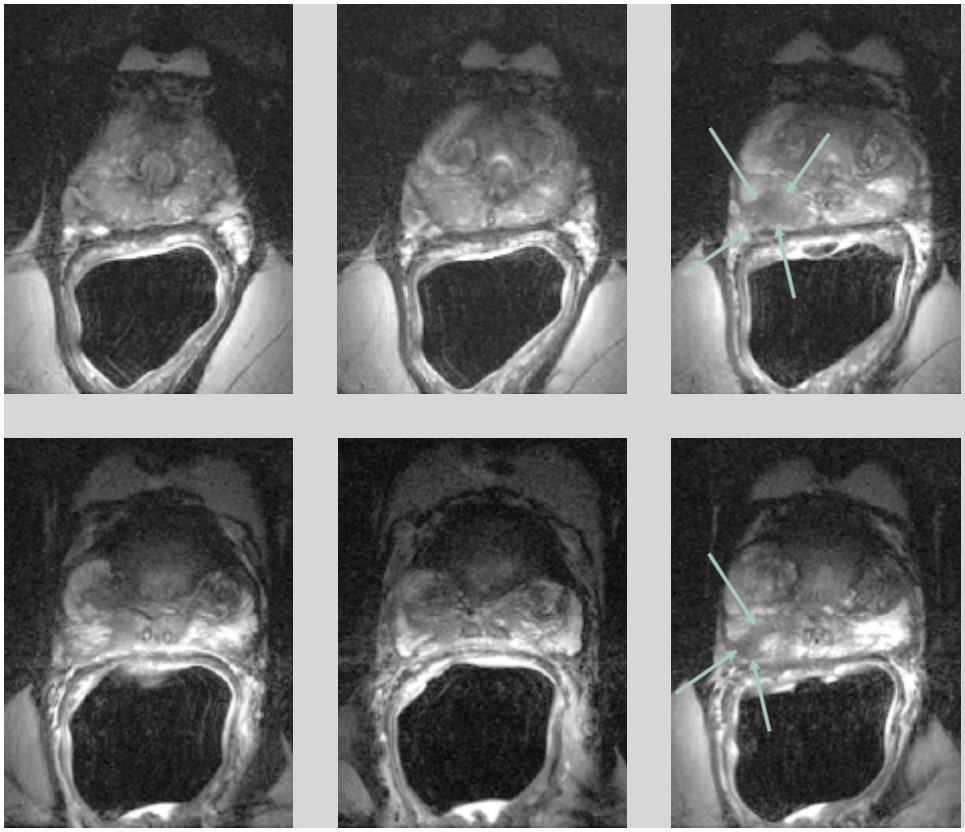

[Figure 1] *Six out of 15 T2-weighted axial images of the prostate of a 51-year-old patient with prostate cancer. The endorectal coil balloon is visible as a large void below the prostate. The arrows indicate the tumor lesion.*

Results & Discussion

On T2-weighted imaging a hypo-intense area is clearly visible in the peripheral zone of the right side of the prostate gland (arrows Fig. 1). This region enhances after administration of contrast agent (Fig. 2). There are no clear signs of extracapsular spread or seminal vesicles invasion of the disease. Based on these findings the diagnosis is stage T2a.

After staging of the disease, the patient was treated with a prostate and seminal vesicles resection. The resected prostate was cut, stained and investigated at the department of pathology (Fig. 3). The pathological stage confirmed the clinical stage of the disease but found a higher Gleason score: T2a with Gleason grade 3+5.

The attainable spatial resolution with an endorectal coil at 3T provides excellent opportunities for accurate staging of prostate cancer. In this case the MRI-examination confirms the existence of the cancerous tissue, and provides valuable information on local disease stage.

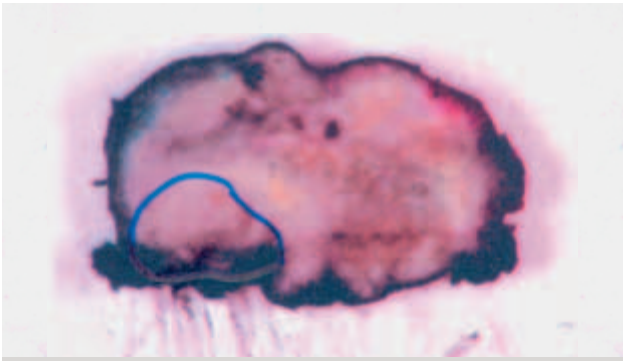

[Figure 3] *Histopathology of the corresponding cut through the resected prostate on which the tumor is indicated with a blue line.*

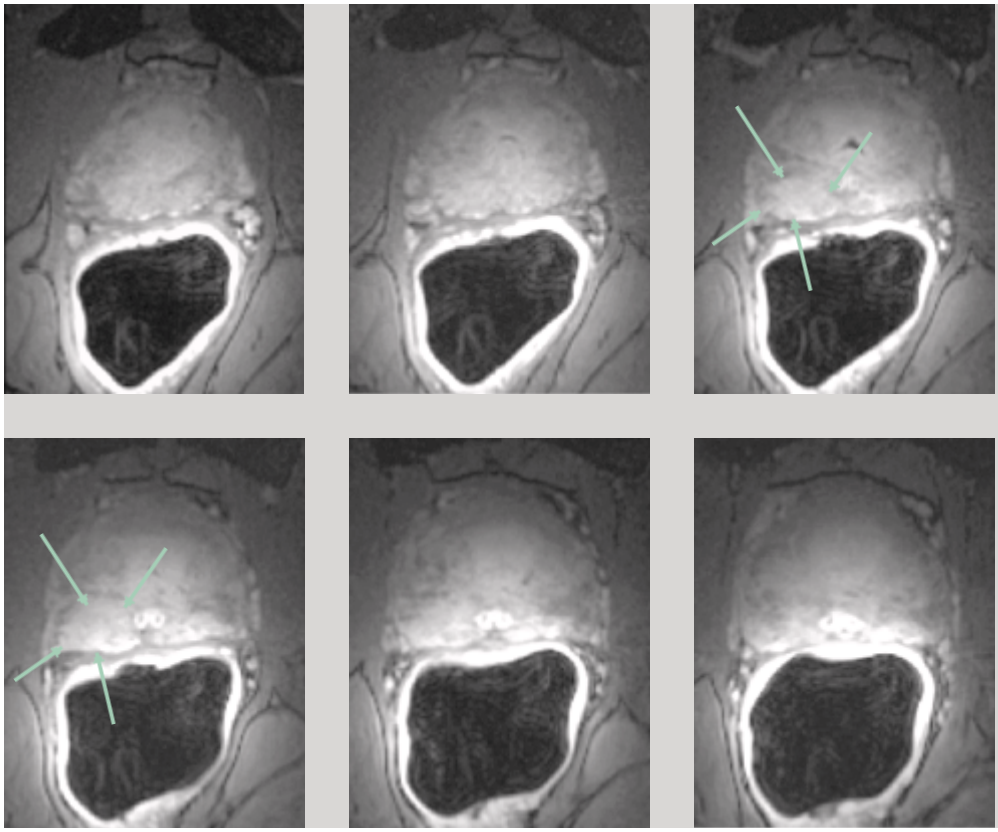

[Figure 2] *Six out of 32 T1-weighted images after contrast administration. The thickness of slices and partitions do not coincide, so the slice positions do not exactly match with T2-weighted imaging. The lesion of figure 1 is indicated with the arrows as enhancing tissue.*

We see a way to evaluate myocardial infarct and vascular disease within one exam without any patient repositioning

Tim won't let you miss a beat.

We see a way to determine regional ventricular function in real time allowing free-breathing using 12 matrix coil elements

Results may vary. Data on file.

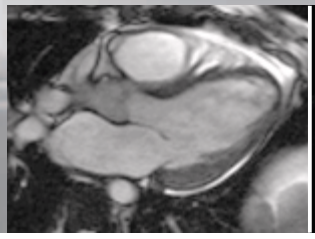

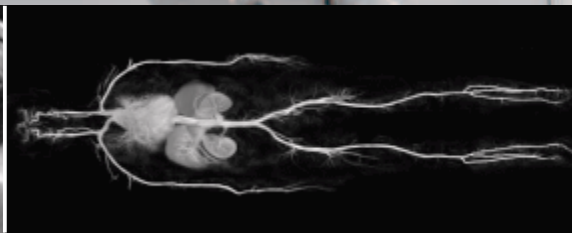

www.siemens.com/medical

M-Z906-1-7600

Proven Outcomes in Cardiology with Tim® (Total imaging matrix technology). Tim offers unmatched MRI capabilities for all cardiovascular exams without repositioning the patient. Ideal not only in diagnosing subendocardial infarct and congenital heart disease, but also systemic diseases like diabetes and atherosclerosis. With its 76 matrix coil elements and up to 32 RF channels, you enjoy revolutionary acquisition speed with virtually unlimited Parallel Imaging even in double oblique slice orientations. Tim transforms workflow from an exam limited by the dimensions of local RF-coils to one determined by the disease. Tim. Very heart smart.

SIEMENS
medical

Siemens **Medical Solutions** that help

Cardiac

CMR particularly benefits from the high SNR of MAGNETOM Trio, A Tim System. Applications like myocardial viability and cardiac perfusion improve significantly. This is also due to synergies between new advanced parallel imaging techniques like T-SENSE and the high element density of the MAGNETOM Trio Matrix coils.

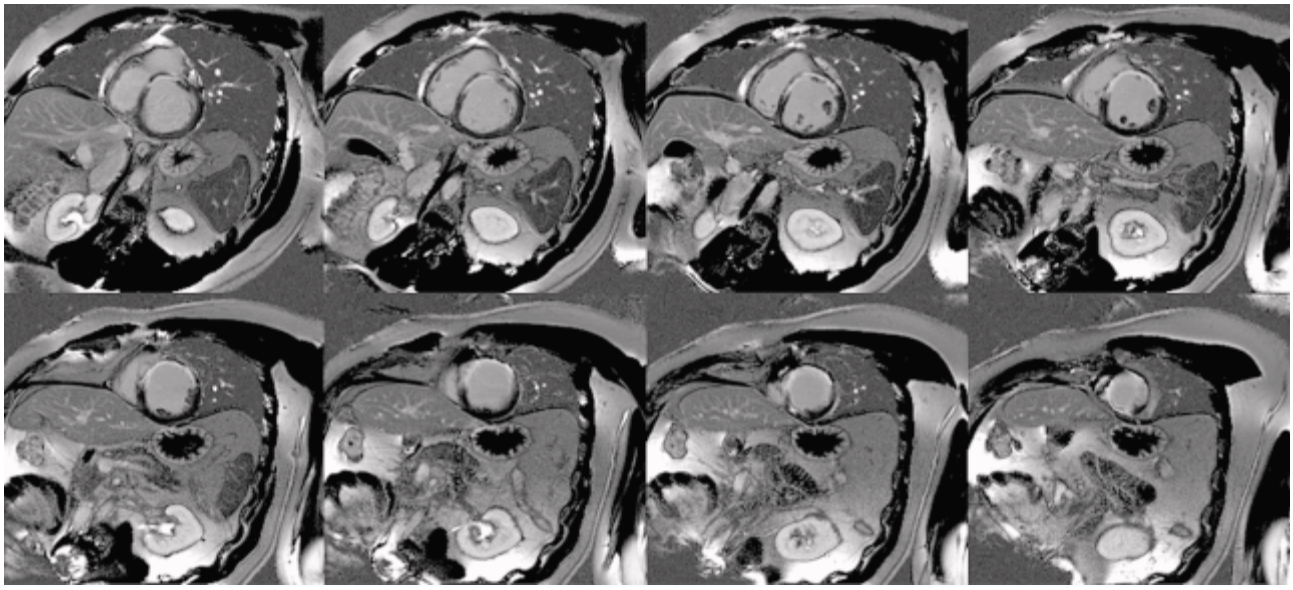

Advances in Cardiac MRI at 3T – Benefits of Multi-Channel MR Systems

Bernd J. Wintersperger, M.D.; Stefan O. Schoenberg, M.D.; Olaf Dietrich, Ph.D; Maximilian F. Reiser, M.D.

Department of Clinical Radiology, University Hospitals-Grosshadern, Ludwig-Maximilians-University, Munich, Germany

Introduction

The challenges for cardiac MR imaging are three-fold: spatial and temporal resolution, signal-to-noise ratio and the limitations induced by the need for breath-hold imaging (Figure 1). With the advance of multi-channel whole-body MRI systems at 3T, all these limitations can now be effectively overcome. Parallel acquisition techniques (PAT) allow increasing temporal or spatial resolution at virtually no costs in acquisition time. The higher field strength at 3T makes up for the loss of signal-to-noise ratio (SNR) induced by fast scanning with PAT. With the combination of PAT and 3T, real-time acquisitions have now become feasible without obviating the need for breath-hold cardiac MRI (Figure 1).

Different Aspects of MR imaging

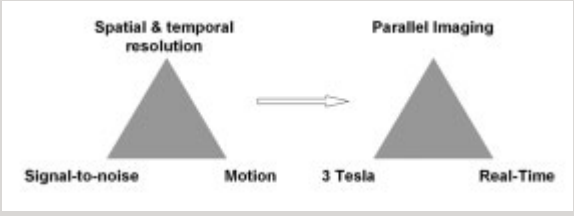

[Figure 1] *Relationship of different aspects of MR imaging specially in respect to resolution, SNR and motion (left); possible solutions to the problems as offered by 3T multi-channel MRI.*

Basic Concepts of Parallel Imaging at 3T

The concept of parallel imaging is the under-sampling of k-space by sampling only every n^{th} line in k-space compared to a full k-space acquisition. This reduces the acquisition time to 1/n of the non-accelerated acquisition and is typically referred to as imaging with an acceleration or reduction factor R. However, parallel imaging requires multi-element coils for spatially resolved signal detection. The so-called coil sensitivity profiles are then used to reconstruct an image equivalent to a full k-space acquisition without increase in acquisition time and without aliasing artifacts caused by under-sampling. Parallel imaging and 3T have a unique synergistic effect. One limitation of 3T MRI is the higher specific absorption rate (SAR) induced by the higher Larmor frequency of the RF pulses, which is effectively compensated by parallel imaging where fewer RF pulses are required to sample an equivalent data set. Nevertheless, the lower SNR induced by the use of PAT which decreases the SNR by at least a factor of one over the square root of the acceleration factor ($1/\sqrt{R}$) is nicely compensated by the higher SNR at 3T. Looking at the performance of PAT at 3T compared to 1.5T, it is easy to see that the loss of SNR introduced by an acceleration factor of R=4 with parallel imaging is approximately compensated by the SNR increase of a factor of 2 from 1.5 to 3.0T. Therefore a four-fold gain in acquisition speed is feasible at 3 Tesla with virtually no penalty in SNR compared to 1.5T.

These methodological advantages result in a number of shifts of paradigms in cardiac MRI at 3T:

- Multi-breath-hold imaging becomes single breath-hold imaging.
- 128 matrix becomes 256 matrix.
- Gated breath-hold CINE MRI becomes free breathing real-time CINE MRI.
- 2D CINE cardiac MRI becomes 3D CINE cardiac MRI.

Cardiac CINE MRI @ MAGNETOM Trio with Tim

It has already effectively been shown that single breath-hold multi-slice cardiac MRI is feasible already at 1.5T. In a study by Wintersperger et al., 11 short axis slices using TrueFISP cardiac functional analysis have been feasible within a single breath-hold of ~20 heart beats (1). As other studies have shown that temporal resolution is more critical for the accuracy of cardiac function analysis than spatial resolution (2), a temporal resolution of <50ms could have been maintained in this study with an acquisition matrix of 128 (1). For those

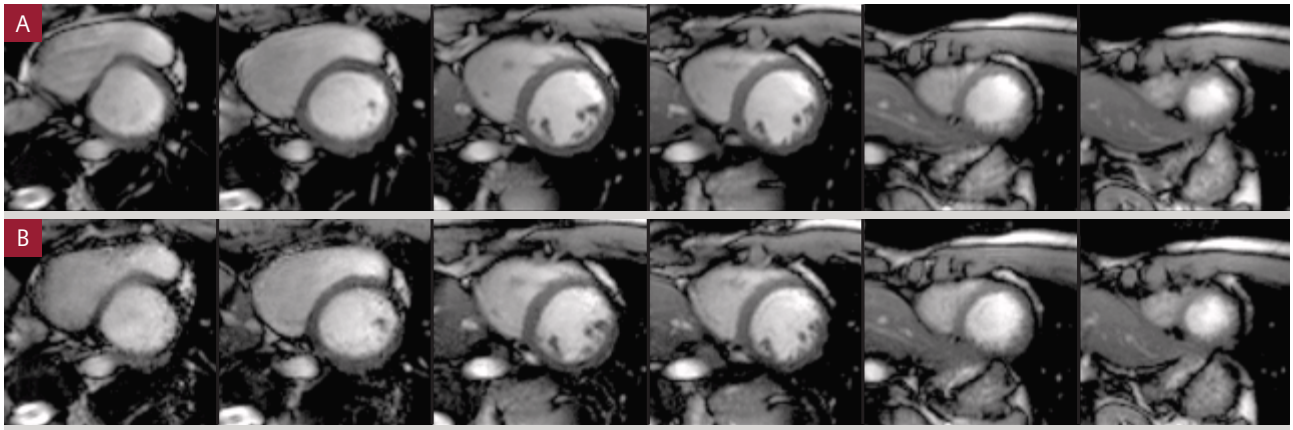

[Figure 2] *Comparison of (a) segmented CINE TrueFSIP acquiring a single slice per breath-hold and (b) fourfold (R=4) TSENSE accelerated CINE TrueFISP with whole short axis data acquired in just 2 breath-holds on a MAGNETOM Trio, A Tim System. Note that the slightly increased noise does not interfere with depictability of subtle details.*

studies typically an acceleration factor of R=2 was used with a GRAPPA (generalized auto-calibrating partially parallel acquisition) reconstruction algorithm. A limitation of the integrated auto-calibration in the GRAPPA algorithm in CINE imaging is caused by the fact that within each image frame additional central lines in k-space (reference lines) have to be acquired for auto-calibration of the coil sensitivity profiles. This results in a net loss of the effective acceleration factor R which is typically reduced by approximately 20–40%, depending on the number of reference lines. More recent reconstruction algorithms such as TSENSE or TGRAPPA effectively overcome this limitation by eliminating the need for additional reference line or ACS (auto-calibration signal) measurements by exploiting the data of an interleaved k-space line sampling covering the full k-space in subsequent dynamic CINE frames (3, 4). These techniques allow for a marked acceleration of CINE TrueFISP imaging as already shown at 1.5T by Reeder et al. with no significant loss in image quality and accuracy for cardiac functional analysis at R=3 (5). The combination of the TSENSE algorithm with higher field strengths and multi-channel MRI at 3T exceeds this performance by far.

On a MAGNETOM Trio, A Tim System, four-fold faster cardiac acquisitions at full 256 matrix size with no loss in diagnostic accuracy compared to the unaccelerated images have been successfully demonstrated in clinical applications. In a study of 10 patients with myocardial infarction, an excellent visualization of regional wall motion abnormalities and evaluation of global ventricular function was possible due to the high spatial and temporal resolution of a full 256 matrix and 50 ms temporal resolution in a multi-slice approach (Figure 2). This is a clear gain in diagnostic accuracy for single breath-hold cardiac MRI compared to 1.5T, since it has been shown earlier that with real-time CINE regional function analysis is not reliably feasible at 1.5T due to the limits in spatial resolution. Another advantage of the combination of parallel imaging with a multi-channel MAGNETOM Trio, A Tim System compared to conventional 3T MRI scanner is that the under-sampling of k-space with parallel acquisition techniques results in the possible use of higher flip angles for TrueFISP imaging. Due to the square relationship between the excitation angle and the specific absorption rate (SAR), cardiac MRI at 3T was traditionally limited to lower flip angles within the range of ~40° to 50°. Using TSENSE in combination with a MAGNETOM Trio, A Tim System, flip angles of 60° or even higher could be realized resulting in a better blood-to-myocardium contrast. The contrast of multi-slice acquisitions at 3T accelerated by T-SENSE is therefore comparable to unaccelerated images at 1.5T.

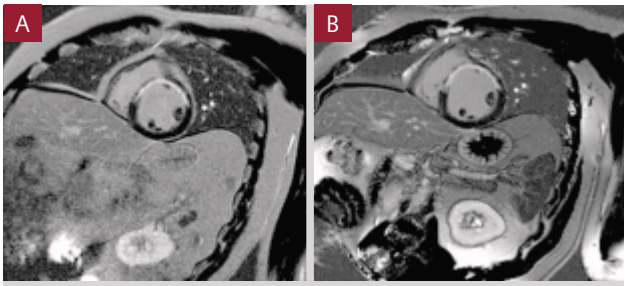

[Figure 3] *PSIR single-shot TrueFISP in a patient with extensive LAD infarction; while this technique at 1.5T (a) comes along with a considerable level of noise, at 3T (b) image quality improves also based on the substantial lower noise level.*

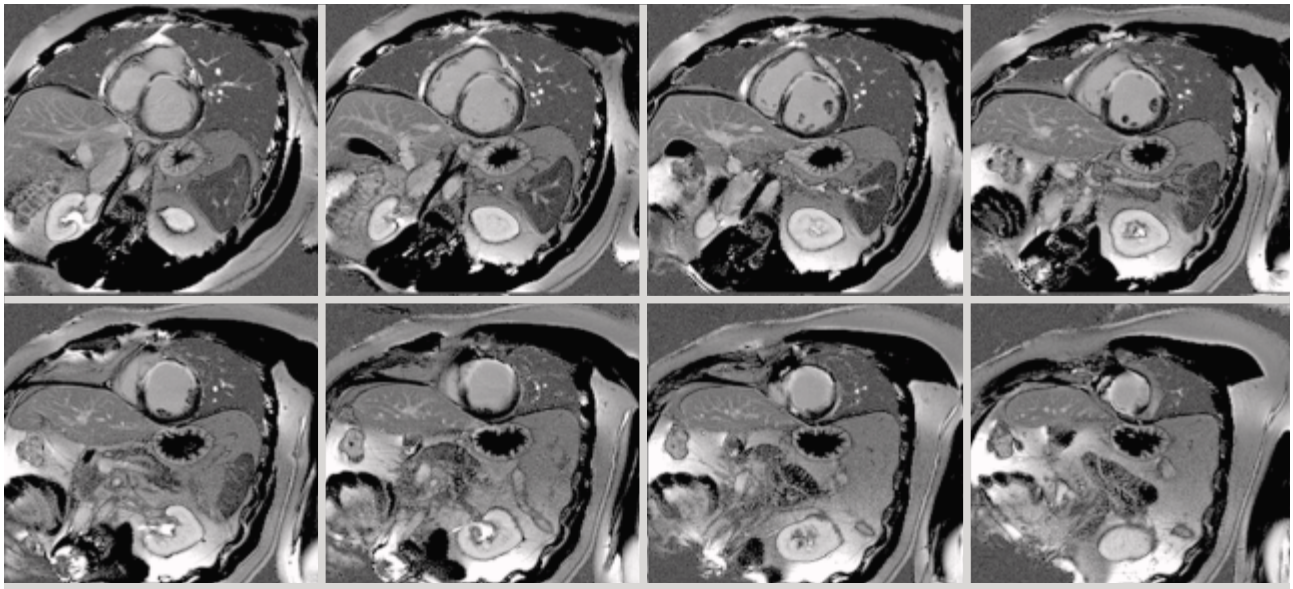

[Figure 4] *MAGNETOM Trio, A Tim System short axis data set acquired in multiple breath-holds using a segmented PSIR TrueFISP technique showing the whole extent of the LAD infarction in the same patient as shown in figure 3.*

Delayed Enhancement* @ MAGNETOM Trio, A Tim System

Additionally, for use in delayed enhancement (DE) imaging assessing myocardial infarction and viability, multi-channel 3T MRI allow for new possibilities and options. Despite all the effectiveness and value of DE imaging for assessment of myocardial infarction, this technique remains quite time-intensive in clinical routine due to the need for inversion time adjustments to allow optimized contrast between the infarcted and normal myocardium. Already at 1.5T it had been shown that a new technique termed phase sensitive IR (PSIR) reconstruction obviates the need for exact optimization of the inversion time (6).

Huber et al. demonstrated that PSIR allows an accurate assessment of the area of infarcted myocardium at virtually any arbitrary chosen inversion time (7). The combination with TrueFISP based acquisition speeds up data sampling allowing single breath-hold multi-slice coverage of the entire left ventricle for the exact assessment of the extent of myocardial infarction (8). However at 1.5T these images are somewhat noisy and sometimes influenced by artifacts due to the ambiguousness of the phase information at low signal-to-noise ratios (Figure 3). At 3T the higher SNR allows for excellent multi-slice single breath-holds TrueFISP PSIR imaging of the entire left ventricle with high image quality (Figure 4). The combination with PAT techniques like GRAPPA again allows preventing possible SAR limitations using TrueFISP at 3T.

If TSENSE TrueFISP acquisitions of cardiac function and PSIR TrueFISP acquisition of delayed contrast enhancements are combined at multi-channel 3T MRI, a complete assessment of function and viability with high temporal and spatial resolution is feasible with only a few breath-holds.

At 3T the contrast-to-noise ratio of the TrueFISP based PSIR technique even exceeds the SNR of the best technique at hand used 1.5T, e.g. segmented TurboFLASH magnitude reconstruction. Comparing the accuracy of single breath-hold multi-slice acquisitions to time intensive multi-breath-hold single slice acquisitions, it has been shown that the limits of agreement between both are smaller at 3T compared to 1.5T.

Myocardial Perfusion* @ MAGNETOM Trio with Tim

While CINE MRI and viability imaging have already been daily clinical routine techniques on 1.5T with sufficient high SNR levels, myocardial perfusion imaging has been a promising tool for the evaluation of coronary artery disease for years but never really took off for widespread use. This has been mainly based on limited SNR performance, artifacts and variable coexisting sequence techniques. At 3T one can envision that due the higher SNR the quality of TurboFLASH techniques, the best evaluated standard in myocardial perfusion imaging, will dramatically improve therefore enabling a reliable time-signal analysis and accurate assessment of myocardial perfusion (Figure 5). The gain in SNR could par-

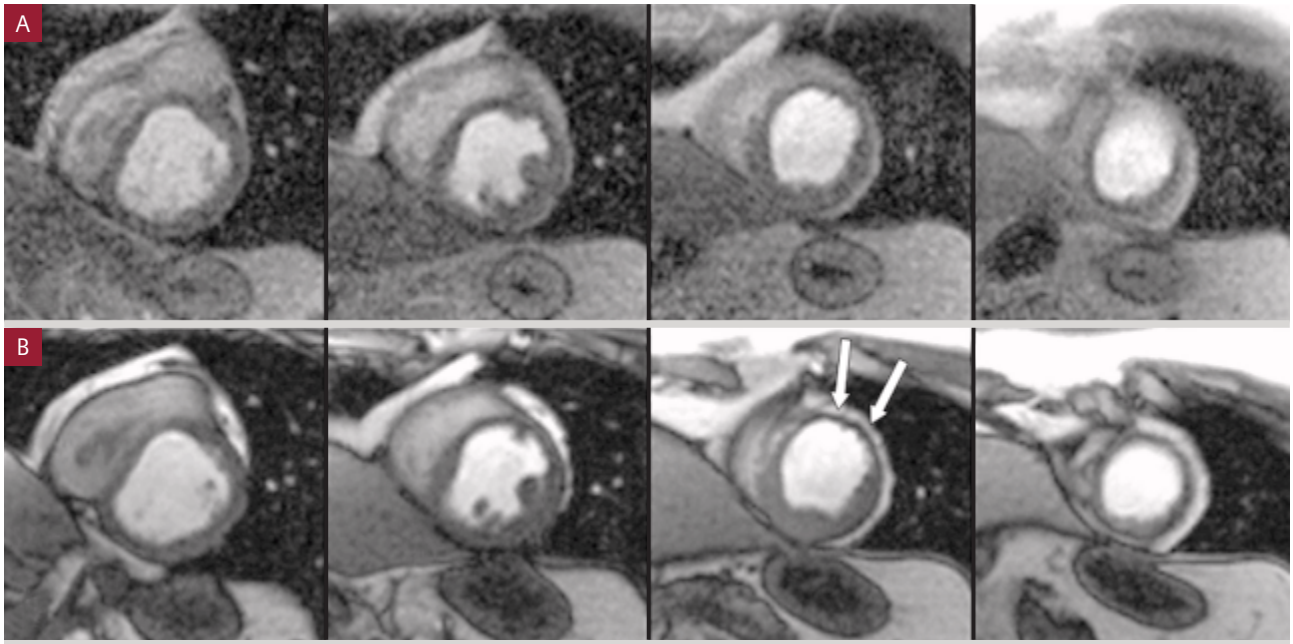

[Figure 5] *IR TurboFLASH myocardial perfusion imaging: (a) four slice data set acquired at 1.5T shows a considerable high noise level possibly interfering with quantitative analysis. (b) Data set of same patient acquired with MAGNETOM Trio, A Tim System using the same technique shows markedly reduced noise and allows better delineation of the hypoperfusion in the infarcted anterior wall (arrows).*

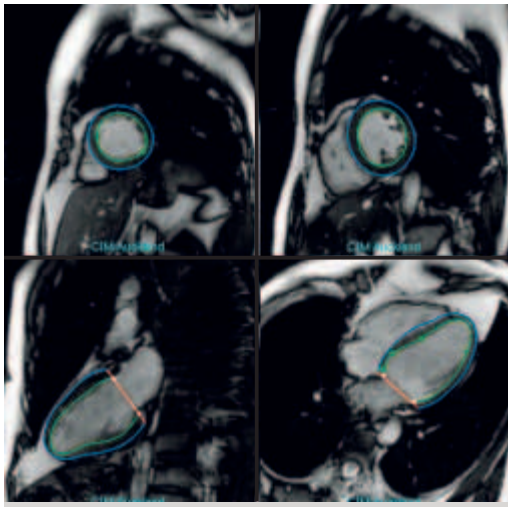

[Figure 6] *T-SENSE CINE data set showing the automated contouring of the endo- and epicardial border in multiple planes. This technique allows for better detection of valve planes and therefore increased accuracy. Functional Information of the circumferential contraction though is maintained by incorporated short axis images.*

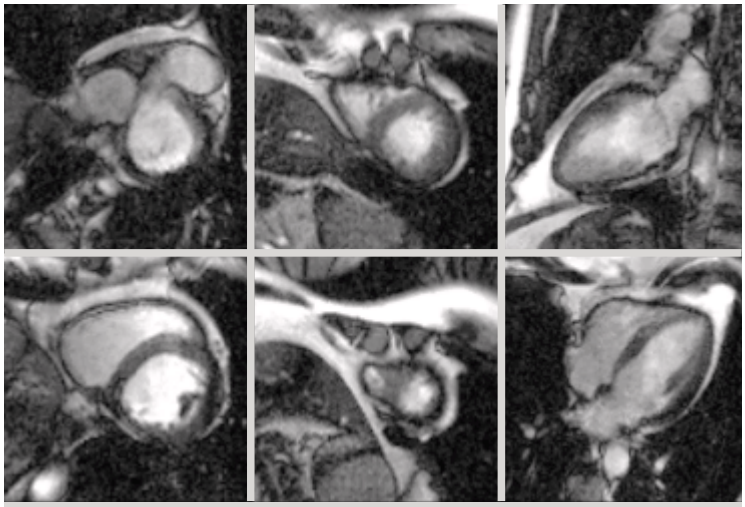

[Figure 7] *The data sampling acceleration in CINE imaging of the heart by PAT (T-SENSE) allows not only for fast acquisition of short axis data but also multiplanar data sets without the need of data registration to avoid mismatch of the data.*

*The information about this product is preliminary. The product is under developement and is not commercially available in the US. and its future availability cannot be assured.

tially be invested in even higher spatial/temporal resolution using higher acceleration factors with PAT (e.g. TENSE) or enabling coverage of the entire short axis during first pass perfusion.

Future Developments

The introduction of 4D function analysis tools allows changing the approach for cardiac functional assessment (9). Although the use of the Simpsons' rule with a contiguous coverage along the entire short axis from the apex to the AV-valve plane has major benefits in terms of accuracy based on its 3D modeling, the valve plane itself could much better be identified in 2- and 4-chamber views. The 4D analysis software allows combining the information of long and short axis cardiac MRI including a computerized LV model thereby reducing the number of required short axis views (Figure 6). This ideally combines with single breath-hold cardiac MRI at 3T accelerated with T-SENSE, since one breath-hold is sufficient to require 5–6 slices with sufficiently high temporal and spatial resolution for this analysis (Figure 7). Therefore one can envision a single breath-hold, highly accurate assessment of the LV function by the combination of MAGNETOM Trio, A Tim System and 4D Argus Software.

With the advent of multi-channel scanner systems, new dedicated coil arrays might be developed that meet the high number of the receiver channels of the MAGNETOM Trio, A Tim System ("32 elements meet 32 channels"). In a preliminary research study in collaboration with RAPID Biomedical, a dedicated flexible cardiac coil was used in close cooperation with the team of Dr. Mark Griswold. Results exceeded those already obtained at 1.5T with a previous prototype of the coil (5). Acceleration factors of 6 for TSENSE cine TrueFISP cardiac function analysis were feasible at virtually no loss in diagnostic image quality. In combination with real-time acquisitions instead of segmented CINE techniques, this would allow new three-dimensional insights in the true physiologic cardiac function without hemodynamic changes based on breath-hold induced intrathoracic pressure variations. As already shown in preliminary studies, this has promising clinical applications for the assessment of diseases such as constrictive pericarditis and the differentiation from restrictive cardiomyopathy (10).

Summary

Cardiac MRI was initially not considered the primary application for 3T due to problems with the high SAR and a number of artifacts particularly for the use of steady-state free precession techniques (TrueFISP). The advent of multi-channel cardiac MRI systems in combination with new acquisition strategies such as TSENSE and TGRAPPA now has vastly overcome these limitations and even shown new possibilities for improved diagnosis of cardiac diseases at higher field strengths.

Acknowledgement

The authors also acknowledge the work of the entire cardiac team of the Department of Clinical Radiology: Kerstin Bauner, M.D., Denise Friedrich RT, Armin Huber, M.D., Michele Picciolo, RT, Frank Stadie, RT, and of Siemens Medical Solutions: Andreas Greiser Ph.D., Edgar Müller, Ph.D., Michaela Schmidt, RT, Katrin Sprung, RT.

This work was in part supported by the "Verein zur Förderung der Forschung und Entwicklung der Magnetresonanztomographie e.V."

Authors (left to right): Bernd J. Wintersperger, M.D.; Stefan O. Schoenberg, M.D.; Olaf Dietrich, Ph.D; Maximilian F. Reiser, M.D.

References

[1] Wintersperger BJ, Nikolaou K, Dietrich O, et al. Single breath-hold real-time cine MR imaging: improved temporal resolution using generalized auto-calibrating partially parallel acquisition (GRAPPA) algorithm. Eur Radiol 2003; 13:1931–1936.

[2] Miller S, Simonetti OP, Carr J, Kramer U, Finn JP. MR Imaging of the heart with cine true fast imaging with steady-state precession: influence of spatial and temporal resolutions on left ventricular functional parameters. Radiology 2002; 223:263–269.

[3] Kellman P, Epstein FH, McVeigh ER. Adaptive sensitivity encoding incorporating temporal filtering (TSENSE). Magn Reson Med 2001; 45:846-852.

[4] Breuer FA, Kellman P, Griswold MA, Jakob PM. Dynamic auto-calibrated parallel imaging using temporal GRAPPA (TGRAPPA). Magn Reson Med 2005; 53:981–985.

[5] Reeder SB, Wintersperger BJ, Dietrich O, et al. Cardiac CINE SSFP imaging with parallel acquisition techniques and a 32-channel cardiac coil: evaluation of SNR performance. Mag Reson Med 2005; in press.

[6] Kellman P, Arai AE, McVeigh ER, Aletras AH. Phase-sensitive inversion recovery for detecting myocardial infarction using gadolinium-delayed hyperenhancement. Magn Reson Med 2002; 47:372–383.

[7] Huber AM, Schoenberg SO, Hayes C, et al. Value of phase-sensitive Inversion Recovery (PSIR) for Detection of Myocardial Infarction. Radiology 2005; in press.

[8] Huber AM, Schoenberg SO, Spannagl B, et al. Single shot inversion recovery TrueFISP for assessment of myocardial infarction. Am J Roentgenol 2005; accepted.

[9] Young AA, Cowan BR, Thrupp SF, Hedley WJ, Dell'Italia LJ. Left ventricular mass and volume: fast calculation with guide-point modeling on MR images. Radiology 2000; 216:597–602.

[10] Francone M, Dymarkowski S, Kalantzi M, Bogaert J. Real-time cine MRI of ventricular septal motion: a novel approach to assess ventricular coupling. J Magn Reson Imaging 2005; 21:305–309.

MR Angiography

1024 image acquisition matrix for Time of Flight (TOF) angiography in the head in a few minutes acquisition time as well as submillimeter isotropic resolution for contrast enhanced angiography in all body parts in less than 20 s is now everyday reality with MAGNETOM Trio, A Tim System.

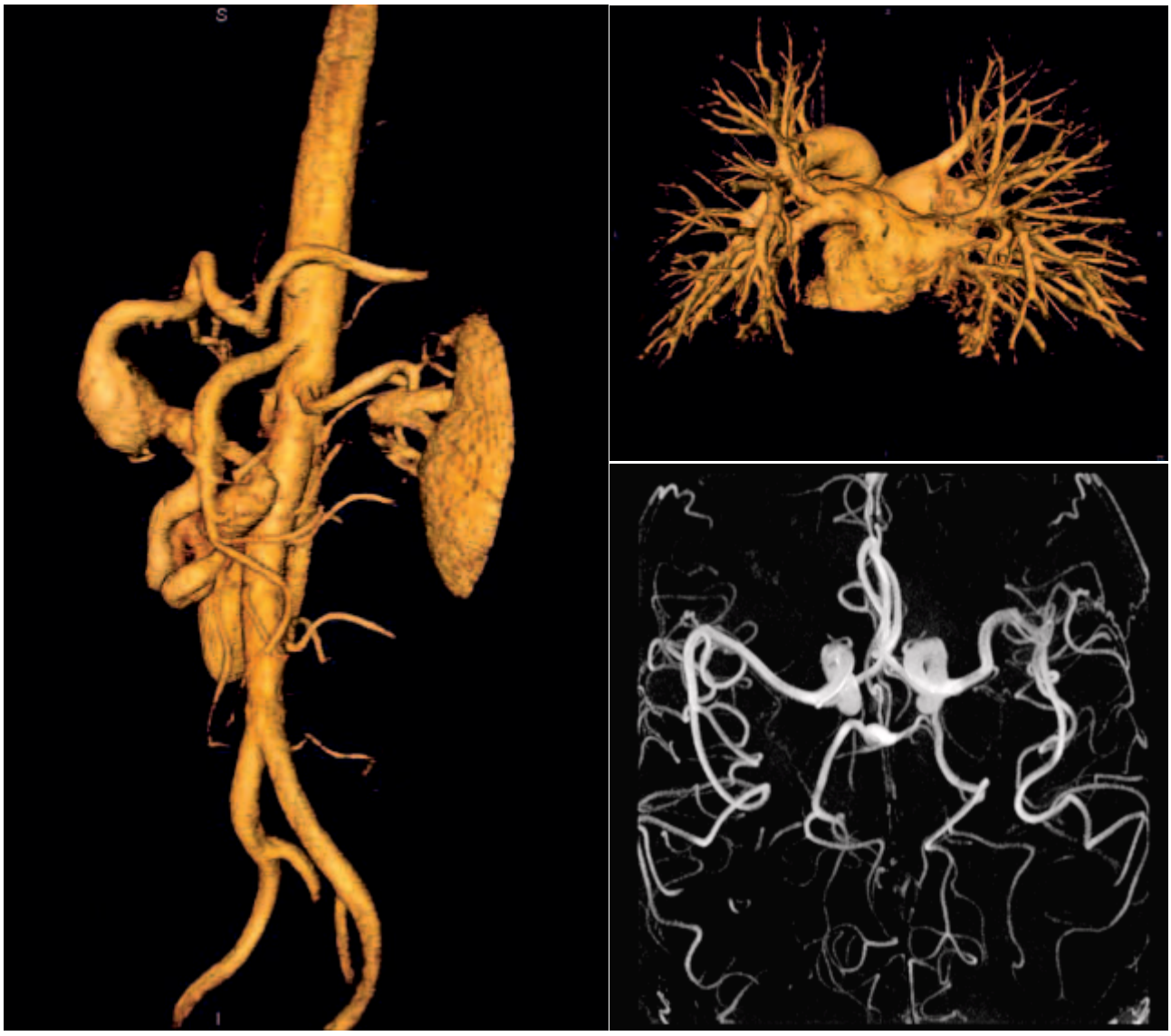

Comparison of Intracranial 3D-ToF-MRA with and without Parallel Acquisition Techniques at 1.5T and 3.0T: Preliminary Results

Jochen Gaa[1], Stefan Weidauer[2], Martin Requardt[3], Berthold Kiefer[3], Heinrich Lanfermann[2], Friedhelm E. Zanella[2]

[1]*Department of Radiology, Technische Universität München, Germany*
[2]*Department of Neuroradiology, University of Frankfurt, Germany*
[3]*Siemens Medical Systems, Erlangen, Germany*

Introduction

Magnetic resonance angiography (MRA) has undergone significant developments over the past decade. For imaging intracranial vessels, time-of-flight (ToF) MRA sequences have been widely used (5, 6, 11). With this technique the vessels give high signal intensity related to the inflow effect of blood during its passage through the acquisition volume, whereas the background tissue appears dark because a short repetition time prevents relaxation of stationary tissue.

Present available pulse sequences are well optimized for ToF-MRA at 1.5T. However, one of the principal limitations inherent to ToF-MRA is that they remain signal limited when pushed to the limits of higher resolution and shorter acquisition times. The main advantage of high B-field imaging is a significant improvement in the signal-to-noise-ratio (SNR), which increases in an approximately linear fashion with field strength in the range of 1.5T to 3.0T. Thus, the gain in SNR at 3.0T can be used for either a reduction in imaging time or an increase in resolution. ToF-MRA is a technique that can benefit from the increased SNR available at 3.0T by decreasing voxel size, resulting in improved spatial resolution compared to 1.5T. In addition, advances in coil technology have resulted in further signal gains and multichannel technology has allowed for novel acquisition strategies such as integrated parallel acquisition techniques (iPAT); (3, 4, 7, 8).

Material and Methods

Seven volunteers and 5 patients (4 aneurysms, 1 AVM) underwent 3D-ToF-MRA at 1.5T (MAGNETOM Sonata) and 3.0T (MAGNETOM Trio) with and without parallel acquisition techniques (iPAT) using similarly designed 8-channel phased-array head coils. Imaging time of the pulse sequences was set to 7.15 and 7.35 min, respectively. The pulse sequence parameters for both 1.5T and 3.0T are listed in Table 1. Images were analyzed quantitatively by calculating signal-to-noise (SNR) and contrast-to-noise (CNR) ratios of proximal M2 segments and qualitatively by using a 5-point scale.

Results

All patients tolerated the MR examination well. No sensory-motor stimulations or signs related to the increased RF deposition (such as increased sweating) particularly at 3.0T were reported. Analysis of the vessel SNR and CNR is summarized in Table 1. The results indicate a significant increase in both vessel SNR and CNR at 3.0T. ToF-MRA without iPAT at 3.0T showed a higher, statistically insignificant SNR and CNR compared with MRA at 3.0T with iPAT. Both SNR and CNR were significantly higher at 3.0T compared with 1.5T.

Overall vessel visualization was rated more highly at both MRA sequences with 3T (Table 2). A slightly higher, statistically not significant overall score was obtained for the MRA with iPAT at 3.0T compared with the 3.0T MRA without iPAT. In particular, visualization of smaller vessel segments, such

Table 1

Field Strength	SNR	CNR
3.0T no iPAT	122,6 ± 31,4**	88,9 ± 27,4**
3.0T with iPAT	107,8 ± 26,6*	75,9 ± 24,4**
1.5T no iPAT	67,3 ± 14,2	39,7 ± 13,5
1.5T with iPAT	50,3 ± 10,7	31,6 ± 11,1

**P<0.005, **P<0.001*

SNR and CNR values obtained at 1.5T and 3.0T with and without iPAT. Blood measurements were made on the proximal M2 segments of the MCA.

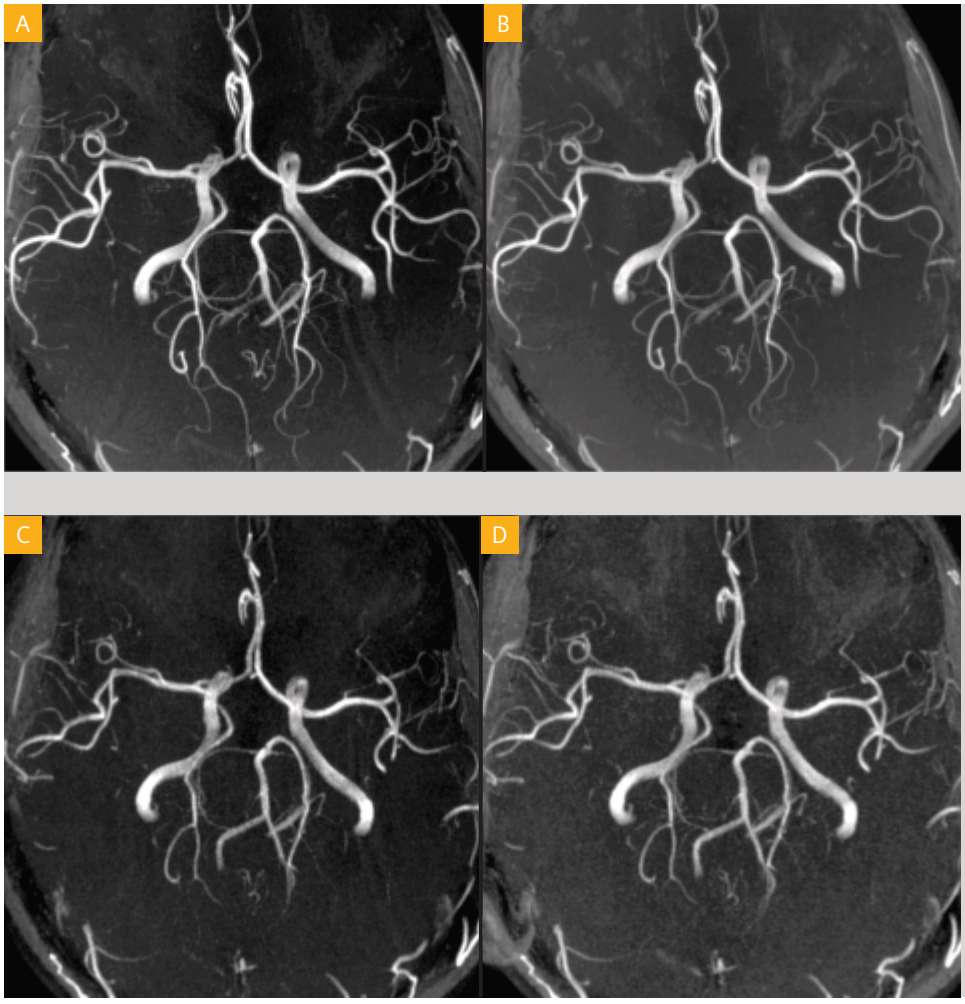

[Figure 1] *Axial collapse 3D-ToF MIP images at 3.0T with (A) and without (B) iPAT and at 1.5T with iPAT (C) and without iPAT (D). Note the better visualization of distal MCA and PCA branches as well as the right AICA at 3.0T (A, B). Minor aliasing artifacts are noticed due to the use of the iPAT reconstruction algorithm (A, C).T.*

as M3 and P3 segments as well as delineation of PICA and AICA, was rated significantly superior compared to both MRA sequences at 1.5T (Fig. 1).

Wrap around artifacts in the MRAs with iPAT were minor at both 1.5T and 3.0T and had no noticeable influence on image analysis. The increased susceptibility effects at 3.0T, especially at air-bone interfaces along the floor of the anterior cranial fossa and adjacent to the petrous portions of the temporal bones had no noticeable effects on the image quality of ToF MRA at 3.0T. Delineation of a left temporal AVM in one patient was slightly better at both MRAs at 3.0T (Fig. 2). One aneurysm of the right MCA (Fig. 3) with a size of 2.8 mm was

Table 2

Field Strength	A2	M2	M3	P2	P3	PICA	AICA	SCA	Overall
3.0T no iPAT	4,8	4,4	3,3*	4,2	3,7**	4,0**	3,8**	4,2**	4,1 ± 0,5**
3.0T with iPAT	4,8	4,8	3,7**	4,6	4,0**	4,0**	4,0**	4,6**	4,3 ± 0,4**
1.5T no iPAT	4,0	3,0	1,3	2,9	1,0	2,3	1,7	2,3	2,3 ± 0,1
1.5T with iPAT	4,0	3,4	1,3	2,9	1,0	1,7	1,3	2,3	2,1 ± 0,1

**P<0.005, **P<0.001*

Confidence of vessel visualization at 1.5T and 3.0T with and without iPAT. Five-point scale with scores of 1 = unsatisfactory, 2 = fair, 3 = average, 4 = good, and 5 = exellent.

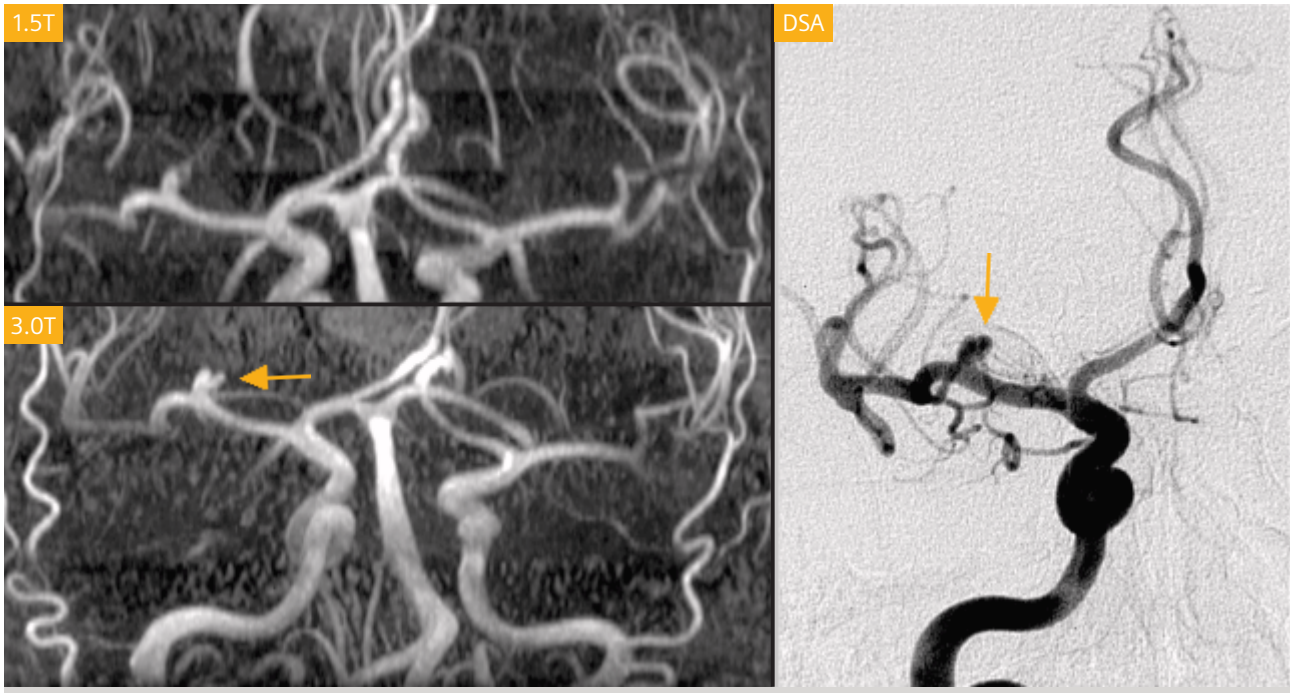

[Figure 2] *One aneurysm of the right MCA with a size of 2.8 mm was reliably detected only at 3.0T.*

reliably detected only at 3.0T, while the other aneurysms – sized between 6 and 10 mm – were detected at both field strengths.

Discussion

ToF-MRA is commonly used in the evaluation of intracranial vascular pathology. Present available pulse sequences are well optimized for ToF-MRA at 1.5T. However, one of the principal limitations inherent to ToF-MRA is that they remain signal limited when pushed to the limits of higher resolution and shorter acquisition times.

There are various factors which enhance the overall image quality in ToF-MRA at 3.0T compared with MRA at lower field strengths. The increased SNR available at 3.0T was used in our study to increase spatial resolution, which reduces the amount of partial volume artifact. Smaller voxels are less subject to intravoxel dephasing because they contain a smaller heterogeneity of spins, providing further improvements in MRA. In addition, the effects of magnetic-field strength-related T1-lengthening of brain parenchyma and background tissue are beneficial for ToF-MRA at 3.0T, providing better suppression of background signal. Furthermore, there is little change in the T1 relaxation of blood, making in-plane saturation effects similar at 1.5T and 3.0T for ToF techniques (2). The lengthened T1 of background tissue allows ToFMRAat 3.0T with smaller flip angles, decreasing saturation effects within in-plane blood. Since high resolution scanning increases the total number of phase encoding- and 3D-encoding steps, a prolongation of measurement time will result. Owing to the prolonged T1-relaxation constants it was useful to remove the MT pulse in our measurement protocol. MT pulses increase the TR of a measurement protocol by typically 8-12 ms, depending on field strength. Therefore, by removing the MT pulse, a 30% higher resolution within the same total measurement time can be achieved. In addition, the field strength of 3.0T allows an echo time of 3.8 ms to be used as the opposed phase condition. This echo time is shorter than the corresponding 7 ms at 1.5T, which will result in decreased intravoxel dephasing.

In our study, a significantly higher confidence of small vessel visualization was obtained with both ToF-MRA sequences at 3.0T. Despite a lower SNR and CNR, small vessel conspicuity was rated best at 3.0T with iPAT, which was the result of a higher resolution matrix (512 x 640 vs. 296 x 512) and smaller voxel sizes (0.08 vs. 013 mm^3) compared with the MRA at 3.0T without iPAT.

Main applications of iPAT are the reduction of examination time by faster imaging or the increase of spatial resolution in a given acquisition time. However, the trade-off for reducing the number of acquired k-space lines using iPAT is a decreased

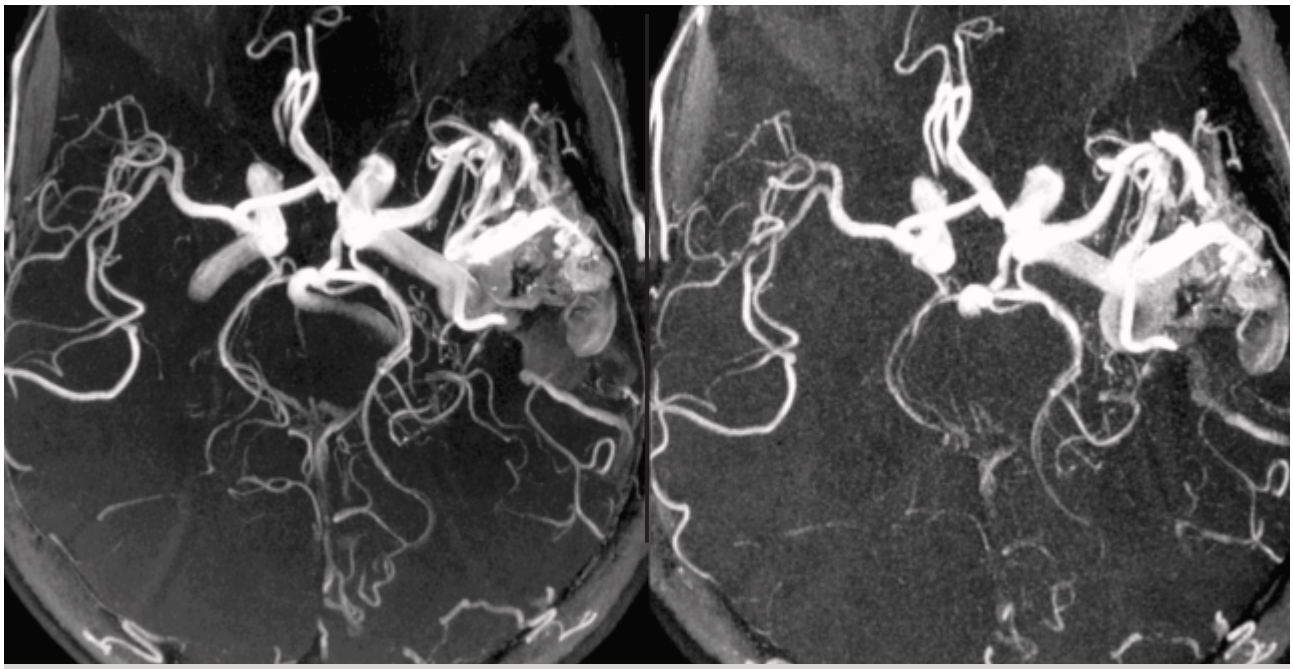

[Figure 3] *Patient with left temporal AVM. Note the superior image quality as well as the superior small vessel delineation at 3.0T (left) compared to 1.5T (right).*

SNR. Owing to this loss of SNR, parallel acquisition techniques are particularly useful when the corresponding image has a high intrinsic SNR like in 3D-ToF-MRA at 3.0T.

Several techniques have been suggested for the iPAT image reconstruction from the reduced data sets (3, 4, 7, 8). They can be divided into two different groups, such as techniques working on the data in frequency domain (e.g. SMASH, GRAPPA) and techniques working on the Fourier transformed data in the image domain (e.g. SENSE). However, one general limitation of the iPAT approach is the propagation of wrap-around artifacts into the center of the image. We therefore decided to use an AUTO-SMASH-like algorithm such as GRAPPA, since these artifacts are less prominent compared to the SENSE technique (4). In our study, aliasing artifacts were only mild and therefore did not limit the accurate assessment of fine vessel detail.

In conclusion, we have demonstrated that 3D-ToF-MRA at 3.0T is superior to that at 1.5T. The combined use of a multichannel phased-array head coil in conjunction with iPAT allows for high resolution intracranial vessel imaging with adequate SNR in reasonable imaging times. With continued optimization and refinements, ToF-MRA at 3.0T will further reduce the need for conventional digital subtraction angiography, which is still an invasive method with possible serious complications.

References

[1] Bernstein MA, Huston J, Lin C, et al. High-resolution intracranial and cervical MRA at 3.0T: technical considerations and initial experience. Magn Reson Med 2001;46:955–62.

[2] Campeau NG, Huston J, Bernstein MA, et al. Magnetic resonance angiography at 3.0 Tesla: initial clinical experience. Topics Magn Reson Imaging 2001;12: 183–204.

[3] Dietrich O, Nikolaou K, Wintersperger BJ, et al. iPAT: applications for fast and cardiovascular MR imaging. Electromedica 2002;70:133–46.

[4] Griswold MA, Jakob PM, Heidemann RM, et al. Generalized autocalibrating partially parallel acquisitions (GRAPPA). Magn Reson Med 2002; 47:1202–10.

[5] Heiserman JE, Drayer BP, Keller PJ, et al. Intracranial vascular stenosis and occlusion: evaluation with threedimensional time-of-flight MR angiography. Radiology 1992;185:667–73.

[6] Marchal G, Bosmans H, van Fraeyenhoven L, et al. Intracranial vascular lesions: optimization and clinical evaluation of three-dimensional time-of-flight MR angiography. Radiology 1990;175:443–8.

[7] Pruessmann KP, Weiger M, Scheidegger MB, et al. SENSE: sensitivity encoding encoding for fast MRI. Magn Reson Med 1999;42:952–62.

[8] Sodickson DK, Manning WJ. Simultaneous acquisition of spatial harmonics (SMASH): fast imaging with radiofrequency coil arrays. Magn Reson Med 1997;38: 591–603.

[9] Thomas SD, Al-Kwifi O, Emery DJ, et al. Application of magnetization transfer at 3.0T in three-dimensional time-of-flight magnetic resonance angiography of the intracranial arteries. J Magn Res Imag 2002;15:479–83.

[10] U.S. Department of Health and Human Services, Food and Drug Administration, Center for Devices and Radiological Health. Guidance for the submission of premarket notifications for magnetic resonance diagnostic devices. Washington, DC: 14 Nov., 1998.

[11] Wentz KU, Roether J, Schwartz A, et al. Intracranial vertebrobasilar system: MR angiography. Radiology 1994;190:105–10.

An Overview of Three Dimensional Contrast-Enhanced MRA at 3.0 Tesla

Kambiz Nael, M.D.[1]; Gerhard Laub, Ph.D.[2]; J. Paul Finn, M.D.[1]

[1]*University of California at Los Angeles, David geffer School of Medicine, L.A., USA*
[2]*Siemens Medical Solutions, USA*

Over the past decade, thanks to steady advances in pulse sequences and scanner design, contrast-enhanced MR angiography (CE-MRA) has made significant advances in image quality and reliability. For a variety of applications, 3D CE-MRA has advantages over other modalities such as CTA, or digital subtraction angiography (DSA), and in many institutions it is often the imaging test of first choice.
Recently, whole body, 3.0T MR systems have become available, with the promise of greatly improved signal-to-noise ratio (SNR) in comparison to 1.5T. Also, since the longitudinal relaxation time (T1) of background increases with field strength, sensitivity to injected gadolinium agents for CE-MRA is heightened, so that smaller contrast doses may be used. Whilst there are also challenges and disadvantages to 3.0T imaging, such as SAR limitations, dielectric resonances and radiofrequency (RF) eddy currents, nevertheless, CE-MRA at 3.0T can often generate spectacular studies, providing very high spatial resolution 3D data over a large field of view (FoV). This article describes existing 3D CE-MRA techniques at 3.0T, as implemented on the Siemens MAGNETOM Trio scanner. We also summarize clinical experience with CE-MRA to date over a variety of vascular territories.

Background

1. Conventional CE-MRA:
CE-MRA relies on the T1 shortening effect of paramagnetic contrast agents and is performed with a T1-weighted fast spoiled 3D gradient echo (GRE) pulse sequence. The sequence parameters and the contrast administration scheme should be carefully planned, to achieve the best compromise between the expendable signal-to-noise (SNR) and the required spatial and temporal resolution. With gradient slew rates of up to 200 mT/m/s and up to 45 mT/m gradient amplitudes, TRs of the order of 2.5–3 ms and TE of the order of 1.2 ms are achievable, for 512 matrix acquisitions. Pulse sequence features such as asymmetric echo and different k-space sampling schemes have also improved the performance of CE-MRA. Parallel acquisition has greatly increased the performance of CE-MRA at 3.0T, where the higher baseline SNR provides a firmer base to support aggressive acceleration factors. Precise contrast administration is an essential prerequisite for CE-MRA, where the center of k-space should be aligned with the peak vascular enhancement. Timing can be easily optimized by use of a test bolus, but real-time triggering algorithms provide an alternative, if less flexible, method. Contrast doses between 0.1 and 0.2 mmol/kg body weight Gd-based contrast agent have been reported to be sufficient for most single-station MRA examinations.

2. Time-resolved CE-MRA:
Advances in ultrafast MR techniques can now generate temporally resolved 3D MRA, which depict the transit of the paramagnetic contrast agent through the vascular system. Time resolved MRA has the ability to provide supplemental functional information about cardiovascular hemodynamics. Other strengths of time resolved MRA include relative insensitivity to motion and the requirement for only very small doses of contrast.
A general limitation of all time-resolved MRA techniques is that the spatial resolution of the individual 3D data set is limited when compared to single-phase MRA acquisitions. Nonetheless, for many applications, in-plane resolution can be preserved while through-plane resolution is traded for rapid temporal sampling. Unless off-axis reconstruction of the time-resolved data is required (in our experience an uncommon requirement), there is little to be gained from spending a lot of time on through-plane phase-encoding. The MIP images are then viewed in a cine format in the plane of acquisition. Temporal resolution of one second or better is readily achieved with this approach.

Recent advances:

The introduction of parallel imaging is one of the most promising recent advances in MR imaging, and it has significantly improved the performance of MRA applications by changing the way that data are acquired and processed. In these tech-

niques, component coil signals in a radiofrequency coil array are used to partially encode spatial information by substituting for phase-encoding gradient steps that have been omitted. Therefore only a subset of the k-space data, defined by the 'acceleration factor' is sampled and then the whole dataset is reconstructed afterward. The major drawback to parallel acquisition is that SNR is diminished, and this represents a fundamental challenge as acceleration factors are increased. Among the strategies to counteract the SNR loss of parallel imaging are the use of higher magnetic field, improvement and adjustment in array coil geometry and sensitivity, and the optimal infusion of contrast agent.

The availability of whole body 3.0T MR systems with higher baseline SNR, promises more efficient use of parallel acquisition. Recently integrated multicoil technology has also become available at 3.0T (Tim, Siemens). Appropriately designed array coils with more optimal sensitivity profiles and more channels, will improve overall SNR and CE-MRA performance. 32-channel MR systems are now available at 3.0T, with 102 coil elements which can be sited simultaneously, if required. These multiple RF receiver coils, with associated multi-RF receiver channel electronics, combine for more effective parallel acquisition strategies. The improved CE-MRA performance can be used in any combination to increase coverage, speed or spatial resolution.

The clinical application of CE-MRA in different vascular territories:

Head & Neck

3D CE-MRA in craniocervical vasculature is useful for atherosclerotic arterial disease (Fig.1), aneurysms (Fig.2), AVMs, and pre-operational assessment of tumors.

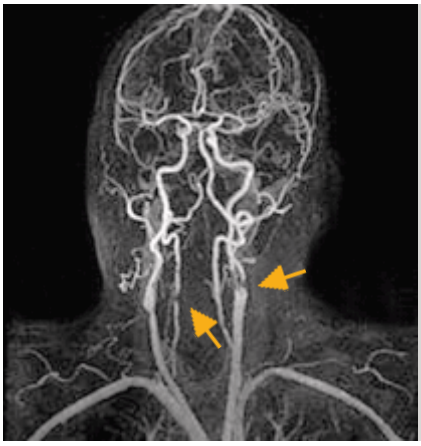

[Figure 1] *Coronal MIP from CE-MRA shows severe stenosis of the left carotid bifurcation and right vertebral artery (arrows) (voxel: 0.8 x 0.7 x 0.7 mm in a 21 second breath hold).*

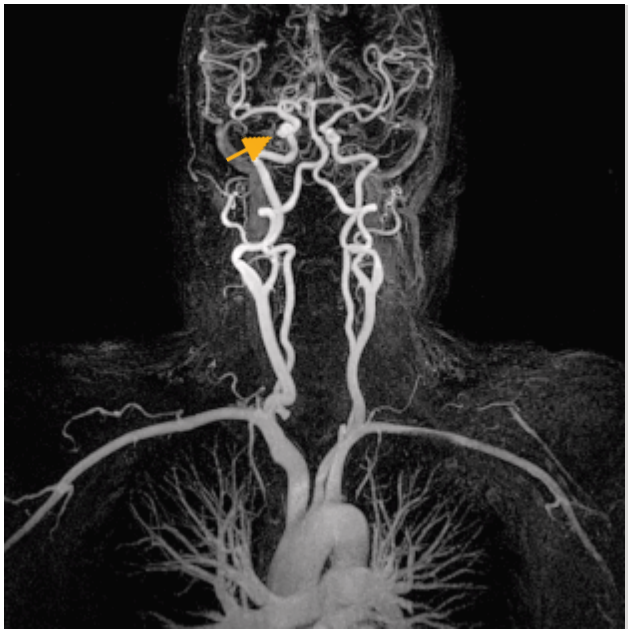

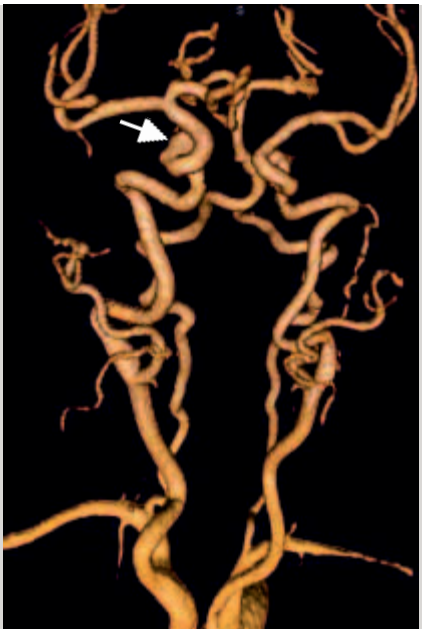

[Figure 2] *Coronal MIP and VR from CE-MRA show an arterial aneurysm at the level of the right cavernous ICA (voxel: 0.8 x 0.7 x 0.7 mm in a 21 seconds breath hold).*

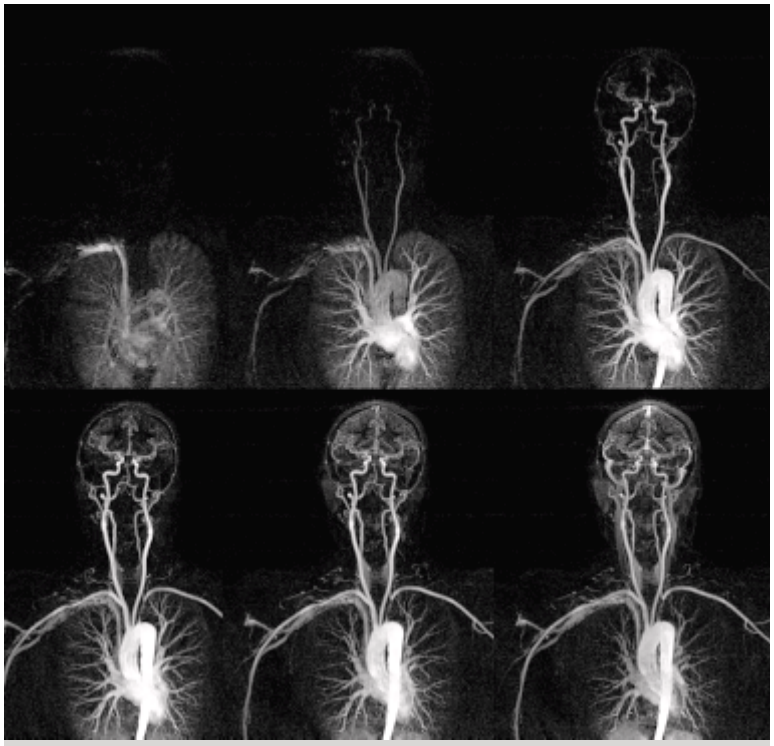

[Figure 3] *MIP images from time resolved CE-MRA show subclavian steal syndrome (left side) (voxel: 1 x 1.2 x 3 mm over a 500 mm FOV, 3D volume was updated every 2 seconds, after injection of 6 ml of contrast).*

Pulmonary

Clinical applications for pulmonary CE-MRA include the evaluation of pulmonary embolism, pulmonary perfusion (Fig. 5), pulmonary hypertension (Fig. 6), pulmonary AVM, congenital heart disease, lung tumors, and pulmonary venous mapping (Fig. 7).

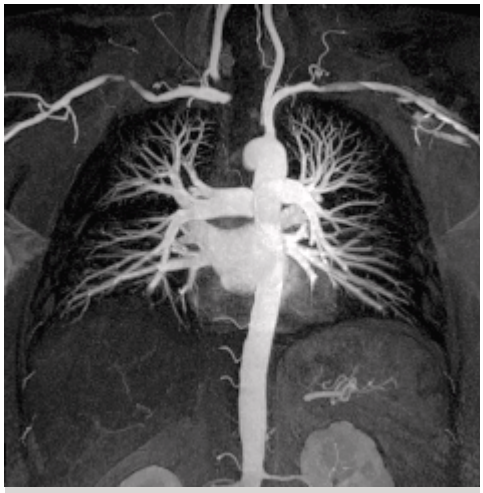

[Figure 4] *Coronal partial thickness MIP from high spatial resolution pulmonary CE-MRA at 3.0T, acquired during a 20 seconds breath hold, showing up to 5th order pulmonary arterial branches (voxels 0.8 x 0.9 x 1 mm over a 450 mm FOV).*

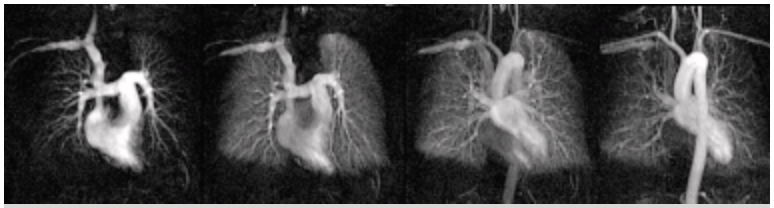

[Figure 5] *Coronal MIP images from time resolved MRA at 3.0T demonstrate the sequential filling of the pulmonary and systemic arteries and pulmonary perfusion (voxel size: 1.6 x 1.2 x 5 mm, each 3D volume was updated in 1.5 s).*

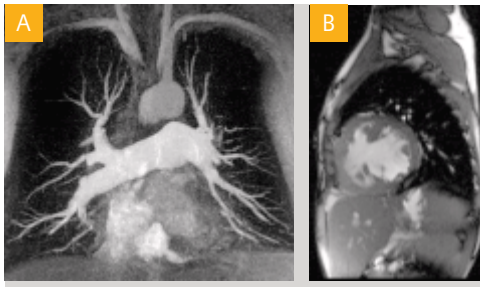

[Figure 6] *Coronal MIP image (A) from CE-MRA at 3.0T shows dilatation of central pulmonary vessels and abnormal proximal-to-distal tapering of the pulmonary arteries. These findings are consistent with pulmonary hypertension which is secondary to a large ventricular septal defect (VSD) (B).*

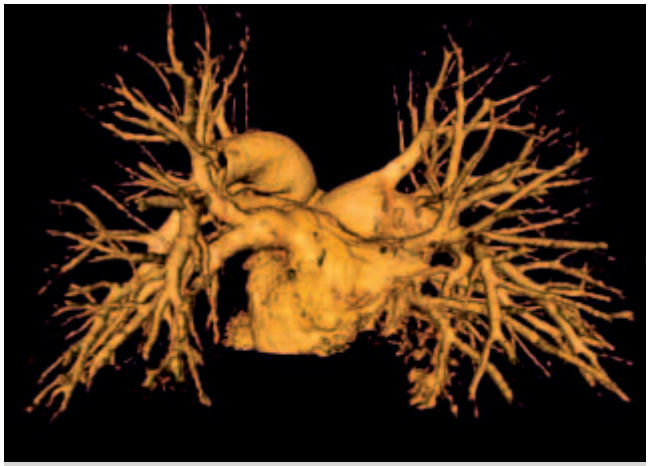

[Figure 7] *3D VR image from CE-MRA defines pulmonary venous anatomy, which can improve pre-procedural planning and fluoroscopic procedural time during the ablation treatment for patients with atrial arrhythmias.*

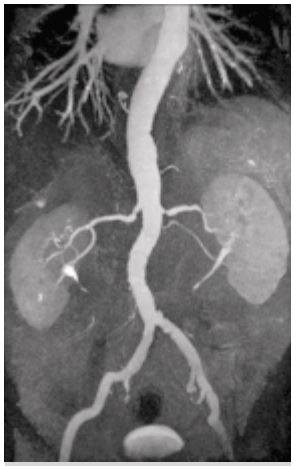

[Figure 8] *Coronal MIP from CE-MRA at 3.0T showing the irregularity and tortuosity of the abdominal aorta and bilateral renal artery stenosis due to atherosclerosis.*

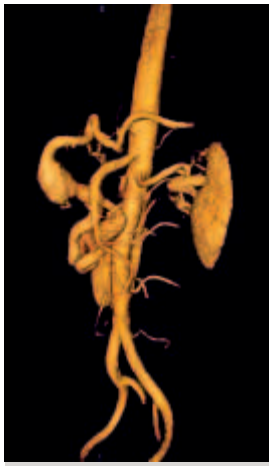

[Figure 9] *Sagittal oblique 3D VR from CE-MRA at 3.0T shows aneurysmal dilatation of the superior mesenteric artery (voxel size: 0.8 x 0.8 x 1mm; 21 second breath hold). The origin of the celiac artery is occluded.*

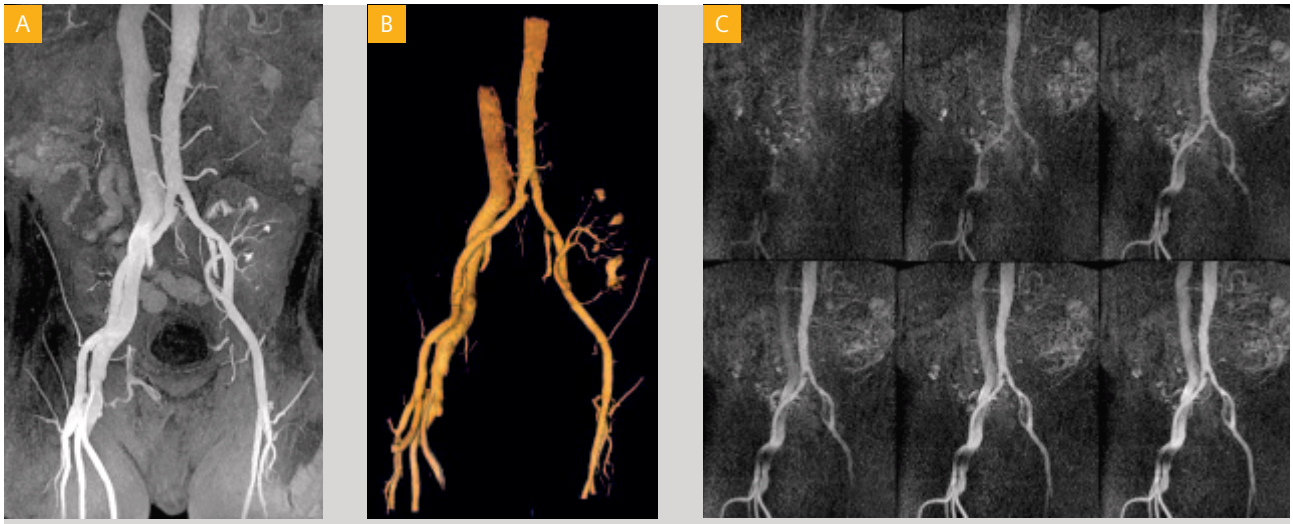

[Figure 10] *Coronal MIP (A) and 3D VR (B) from CE-MRA at 3.0T demonstrate widely patent transplant renal artery (voxel size: 0.8 x 0.8 x 0.9, FOV: 440, time: 21 s). Time resolved MRA (C) shows an AV-fistula between the right common iliac artery and vein results in early filling of the inferior vena cava. Metal in the right inguinal region from prior surgery causes focal signal loss.*

M-Z899-1-7600

Proven Outcomes with Clinical 3T MRI.
Now MRI's most innovative new technology, Tim (Total imaging matrix) has been combined with the amazing power of 3T. Together, they go places no 3T has gone before. Now, what was only possible in research can be done daily in clinical practice. You'll see what couldn't be seen. And do things faster than they've ever been done before.

Imagine visualizing 0.4 mm cervical spine nerve roots in less than two minutes. Performing 3-D abdominal imaging with submillimeter resolution in 15 seconds. Or a full head protocol in less than three minutes. With 3T and Tim, the extraordinary will become routine. Everyday.

Siemens **Medical Solutions** that help

SIEMENS
medical

Neurology

Unprecedented image resolutions can be achieved within clinically reasonable acquisition times thanks to the unique capabilities of the 12-channel 3T Head Matrix coil as well as the 24-channel 3T Spine Matrix coil. These coils are capable of massive parallel imaging in all 3 directions providing unique flexibility at 3T.

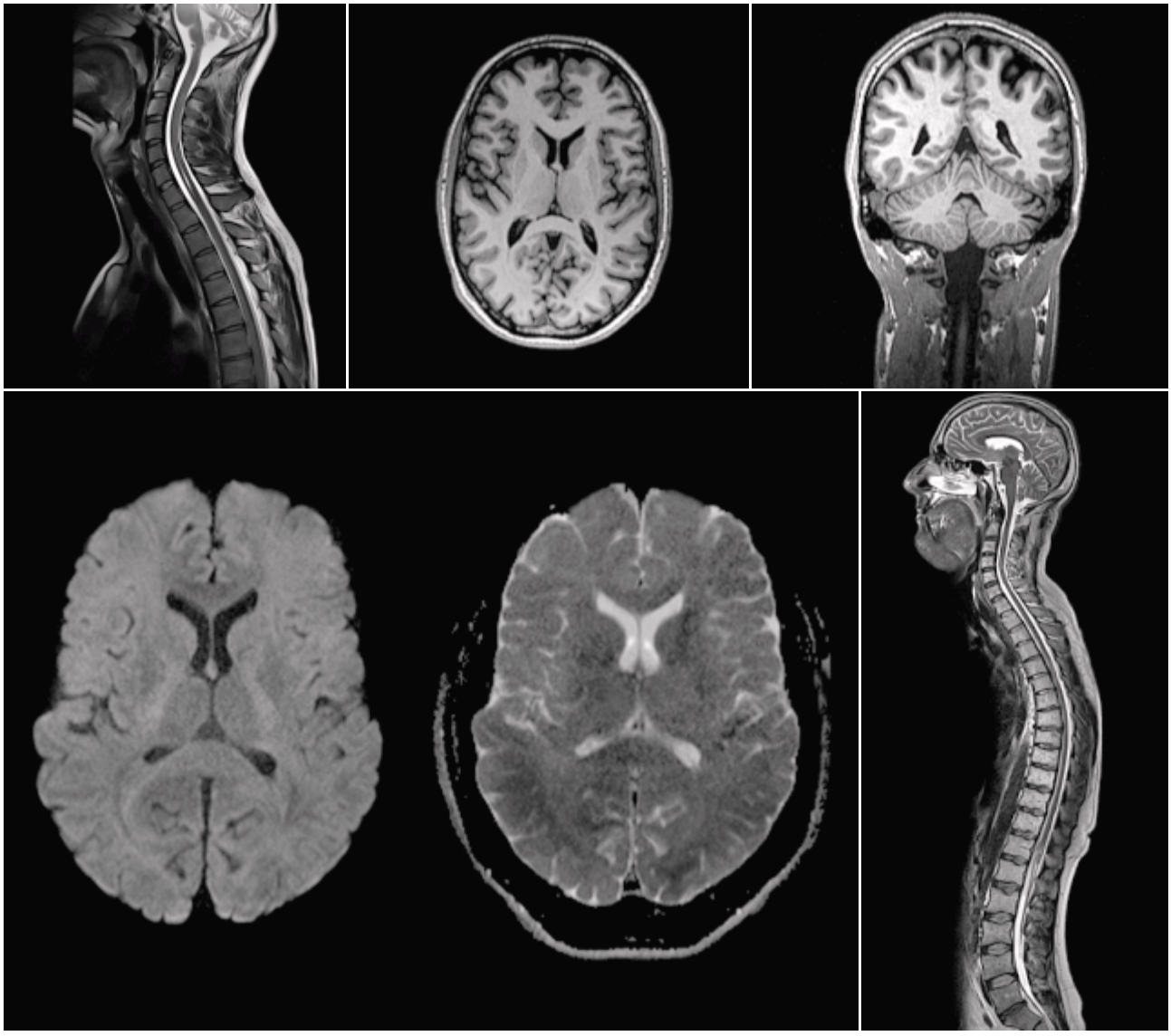

CSI-Measurements of the Human Brain at 3T

U. Klose[1,2], E. Bültmann[2], F. Jiru[1,2], T. Nägele [2]

[1]Section on experimental MR of the CNS, [2]Department for Neuroradiology, University Hospital Tübingen

Introduction

One of the advantages of using MR scanners working at higher field strengths is the improvement in MR spectroscopy. In proton spectroscopy, the relevant frequency range for analysis of spectra is increased. In addition, an increased signal-to-noise ratio can be expected if appropriate coils are used. Since both effects contribute to a more reliable data analysis, high field systems are of great interest for the clinical MR spectroscopy. In the systems equipped with a multi-channel receiver, the sensitivity of the measurement can be additionally improved by the use of multi-array coils [1] and by the subsequent combination of the signals from particular channels [2]. A disadvantage of a higher field is, however, the decreased value of T2*-relaxation time compared to the lower field strengths [3, 4]. This fact compromises the signal-to-noise ratio, especially when long echo times are used. Also, more pronounced susceptibility effects in higher field strengths lead to a worse field homogeneity in the examined volume. To evaluate benefits of a 3T MR scanner for the diagnosis of brain diseases, a short echo time proton spectroscopic imaging at a whole body 3T scanner of the newest generation was performed. Spectroscopic imaging (CSI) enables the measurement of both spectral information and a spatial distribution of the spectra. To prevent a contamination of the spectra by unwanted signals originating mainly in the subcutaneous fat tissue, a combination of volume pre-selection (PRESS) and an outer volume saturation [5, 6] was used. Since spatial selective saturation pulses used in outer volume saturation technique may interfere with the measured signal , the advantages and disadvantages of using outer volume saturation was evaluated in a volunteer examination. The quality and the significance of the short echo CSI spectra for clinical diagnostics at 3T are shown in an exemplary patient examination.

Methods and Subjects

All CSI measurements were performed at a whole body 3T scanner (MAGNETOM Trio, A Tim System, Siemens AG) using a twelve-channel Head Matrix coil. A volume pre-selected PRESS CSI sequence with a repetition time of 1.6 s and an echo time of 30 ms was used in all examinations. For the data acquisition, a 16 x 16 matrix size was used covering a field of view of 15 cm x 15 cm. The exited cubical volume had a slice thickness of 1.5 cm and in-plane dimensions as adjusted to the brain anatomy, varying between 8 cm x 9 cm and 6 cm x 10.5 cm. Four averages were acquired combined with an elliptic weighted data acquisition [7] (omitting the k-space corners and averaging only data in the center of the k-space). Measurement time was 7.5 minutes for each measurement. The delta frequency (the excitation frequency expressed as a difference from the water frequency) for the spatial selective rf pulses was 2.7 ppm, corresponding to the chemical shift of NAA.

A first evaluation of the acquired data was performed with the spectroscopy software at the host computer of the MR scanner. In a second step, the measured time signals from all calculated voxels were transferred to a separate workstation and evaluated with an own software CULICH [8]. Within this evaluation, the spectral fitting by means of LC Model program [9] was performed. The LC Model decomposed the analysed spectra using 15 base spectra of water solutions of particular metabolites measured in vitro. The base spectra were obtained from the single voxel measurements at 3 T, using a PRESS sequence with an echo time of 30 ms. In addition, calculated base spectra from lipids were included in the evaluation as proposed by Seeger et al. [10].

Measurements were performed in a healthy volunteer (female, 29-years-old) to examine the benefit of the outer volume saturation by spatial selective pulses and in a 45-year-old patient, who was examined routinely at 1.5T and was transferred to a spectroscopic examination at 3T for a further characterization of an unclear diagnostic finding.

Results

In the examination of a healthy volunteer, two CSI measurements from an axial slice of the brain were performed with identical parameters except for the application of six addi-

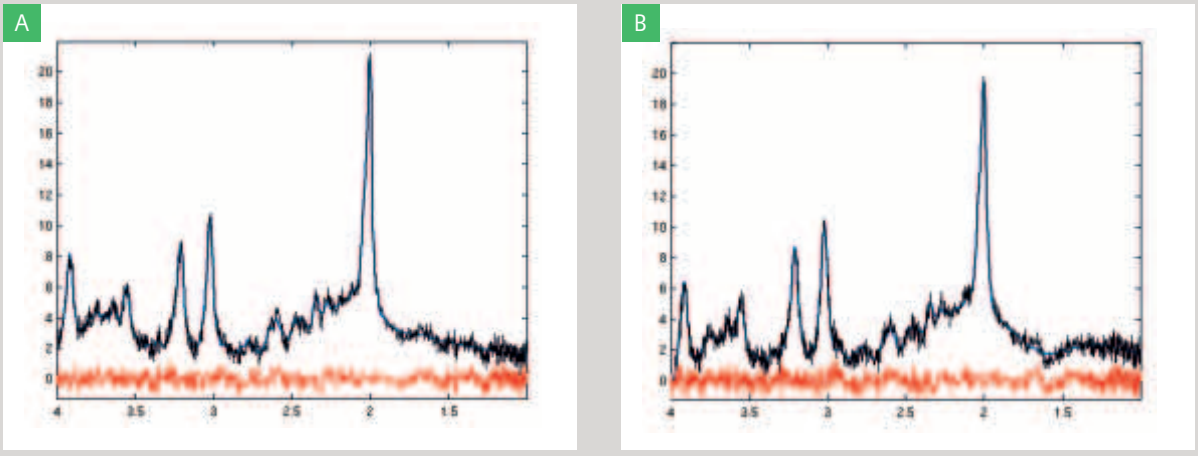

[Figure 1] *Spectra of corresponding voxels in two hemispheres of a healthy subject from a measurement without saturation pulses. The measured spectrum (black), the fitted signal (blue) and the residuum (red) is shown.*

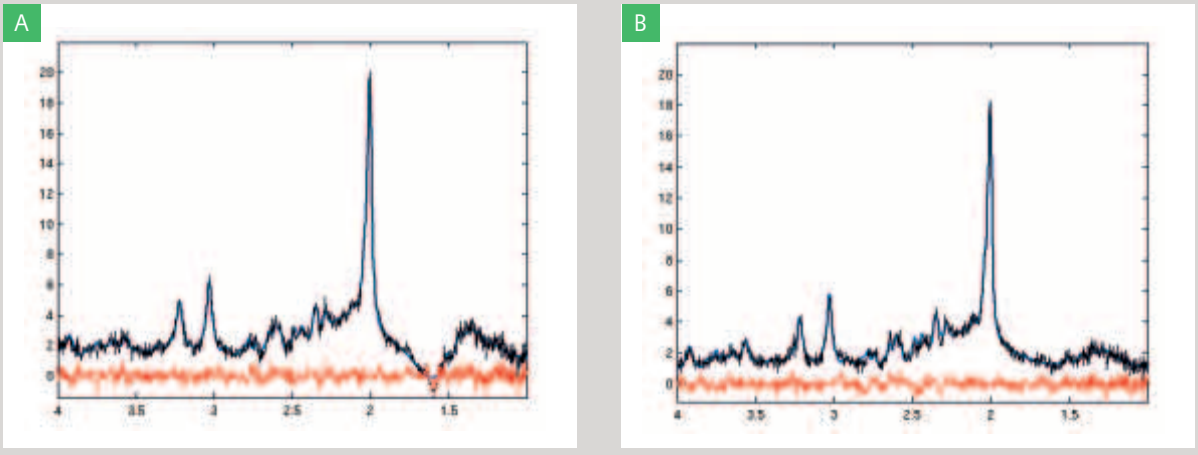

[Figure 2] *Spectra from measurements from the same voxel of a healthy subject without (A) and with (B) additional outer volume saturation pulses. Without saturation pulses, artifacts from lipids occur in the frequency range of 1 to 2 ppm. The measured spectrum (black), the fitted signal (blue) and the residuum (red) is shown.*

tional spatial saturation pulses (outer volume suppression, OVS, [5]). Even in the measurement without OVS, spectra without any signal contamination in the spectral range of lipids were obtained in most voxels of the CSI data set. As an example, two spectra from the left and right basal ganglia are shown in Fig. 1. In both cases, a very good fit was achieved and both spectra showed a very good congruence. In the frequency range of lipids, only minor signal variations were observed in these spectra. Lipid signals with a higher intensity were found near the edges of the excited volume (Fig. 2A) in the measurement without OVS. The negative amplitude of the signal was used as a hint indicating the contamination. In the measurement with OVS (Fig. 2B) the erroneous lipid signals are diminished, but the NAA signal is also reduced compared to the measurement without OVS. An additional negative side effect of the measurement with OVS was significantly inferior water saturation in some areas of the excited volume. This effect caused problems with the automatic spectrum evaluation using the LC Model. For these reasons, the measurement without OVS was performed in the patient. The patient was examined due to vertigo and unspecific headache within the last three months.

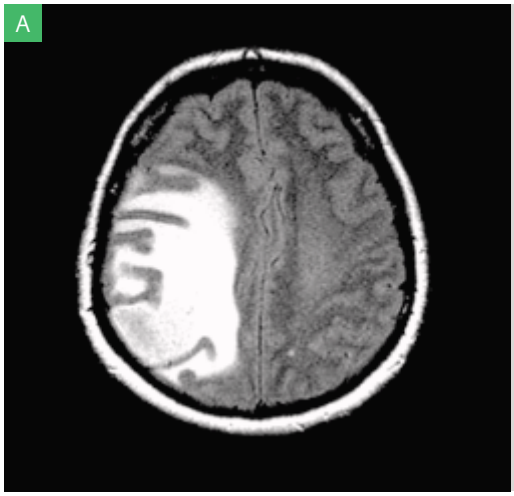

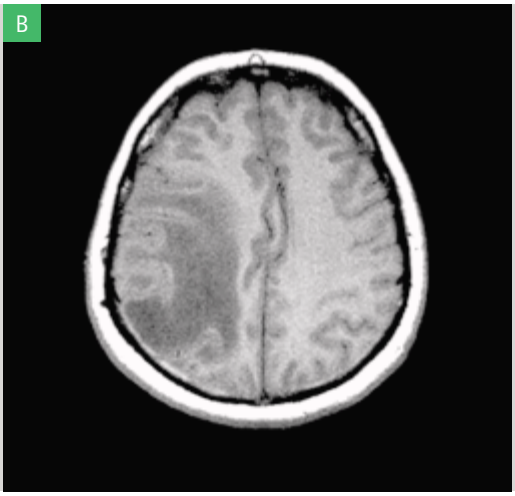

[Figure 3] *Images acquired with a FLAIR (A) and a T1-weighted spin-echo sequence (B) from a slice through the lesion of the examined patient.*

In the MR image examination at 1.5T, a tumorous lesion was found right parietal with a large edema. In the T1-weighted image no differentiation was possible within the lesion, whereas in the FLAIR-image (TR 8,8 s TI 2,5 s, TE 118 ms) the lesion was slightly hyperintense in the posterior part. (Fig. 3). For further specification of the lesion, two CSI measurements at 3T were performed, which differed in the extent of the excited volume. To avoid an excitation of the extra cranial lipids in both measurements, the shape of the exited volume was nearly quadratic in first case and had the shape of a narrower rectangle in the second. The extension of both volumes and the position of the excited slice are shown in Fig. 4A and 4B. Results of both measurements were consistent in the spectral range of the main metabolites, but differences were observed in the frequency range of lipids (0.5–1.8 ppm). Examples of the similarity of spectra from the non affected brain hemisphere and from the lesion are shown in Fig. 4B–E. The signal variations within the frequency of lipids in Fig. 4C and 4D with partly negative peak amplitudes indicate, that these signals most probably represent erroneous contaminations from areas outside the field of view, which are excited in a different way in both measurements. The variable lipid signal also influenced the automatic phase correction and therefore the signal variation at the edge of the NAA peak can be seen. On the opposite side of the slice the lipid signals within the lesion (Fig. 4E,F) are much more intensive and largely consistent in both measurements. This suggests that the major part of the lipid signals within the lesion originated from the examined voxel.

As a consequence of these findings, the quantitative evaluation was limited to the spectral range of the main metabolites. All spectra within the excited volumes could be successfully evaluated with the automatic evaluation procedure and for all voxels, the fitting of a sum of adjusted base spectra to the measured spectra was possible. Evaluated spectra from the unaffected hemisphere and from the lesion measured with and without outer volume suppression are shown together with the fitted spectrum and the residuum in Fig. 5. The quantitative evaluation of single metabolites in all voxels of the excited slice could be used for the calculation of parameter maps showing the relative concentration of selected metabolites as well as of the chosen metabolite ratios.

The metabolite maps of creatine and NAA as well as the ratios Creatine to NAA and Choline to Creatine are shown in Fig. 6. Within the lesion, they reveal a decreased NAA, a slightly decreased creatine and interestingly also a strong decrease of Choline. This pattern of metabolite changes leads the Choline to Creatine ratio to be seen as the most relevant parameter for the characterization of the lesion. Accordingly, a biopsy was planned under special consideration of the map of this ratio (Fig. 6D) . A prominent peak of the Creatine to Choline ratio was found in the posterior part of the lesion, which seems to mark the central part of the lesion. This location was used as a guidance for the biopsy. The histological result of the biopsy was a low-grade glioma. This finding correlates with the large lipid signals within the lesion, but the decreased intensity of the Choline signal compared with the Creatine signal is an atypical pattern for this tumor type.

Discussion

The acquisition of proton spectra at a field strength of 3T offers the advantage of larger frequency range in the spectra enabling separation of metabolites such as glutamate and glutamine [11] and brings an increased sensitivity allowing an increase of the spatial resolution of CSI measurement.

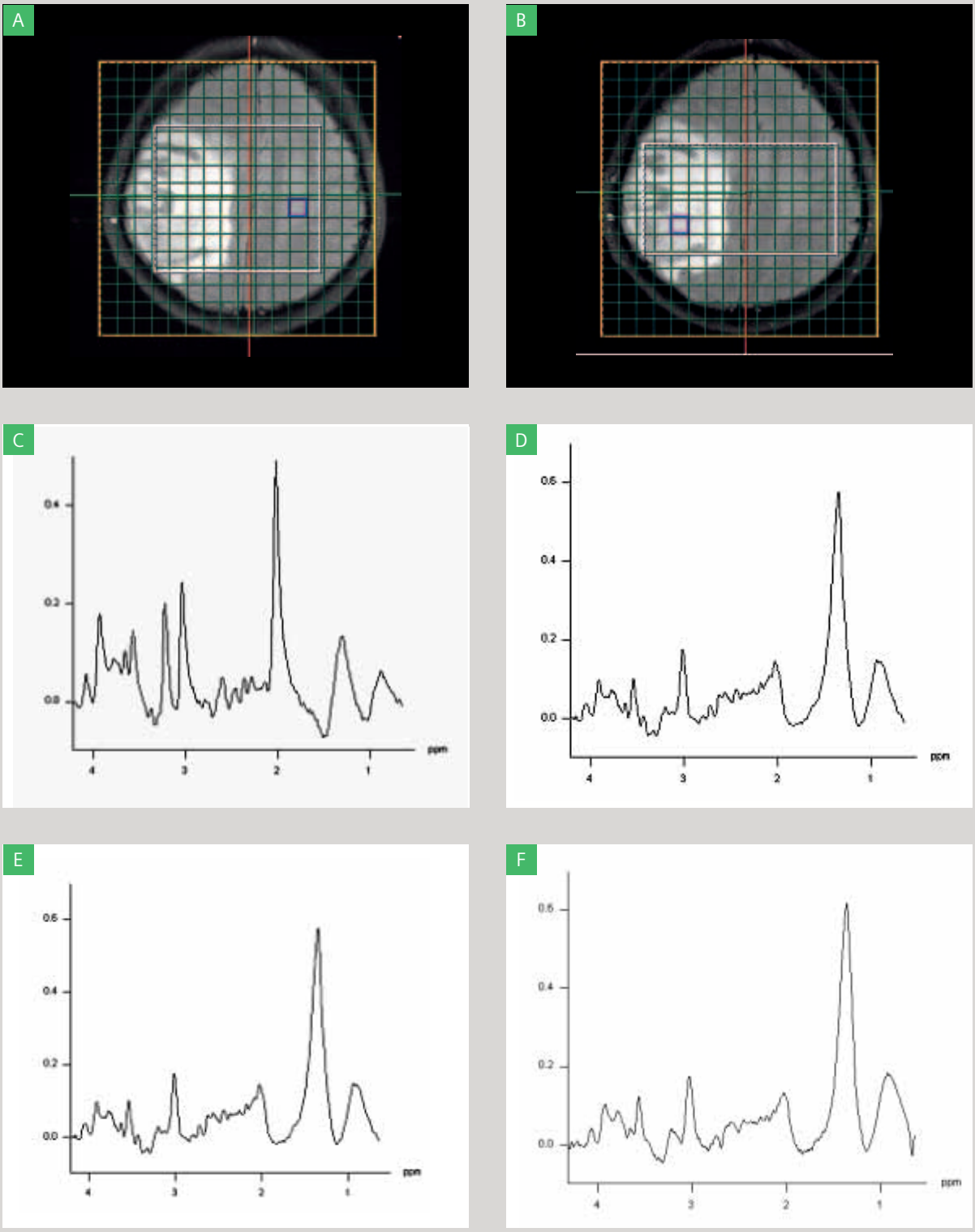

[Figure 4] *Spectra and locations (blue quadrates) from voxels of the not affected hemisphere (A,C,E) and from the lesion (B,D,F), acquired with a more rectangular (C,E) and with a more quadratic (D,F) excitation volume (white rectangle). In A) the more rectangular, in B) the more quadratic volume is depicted.*

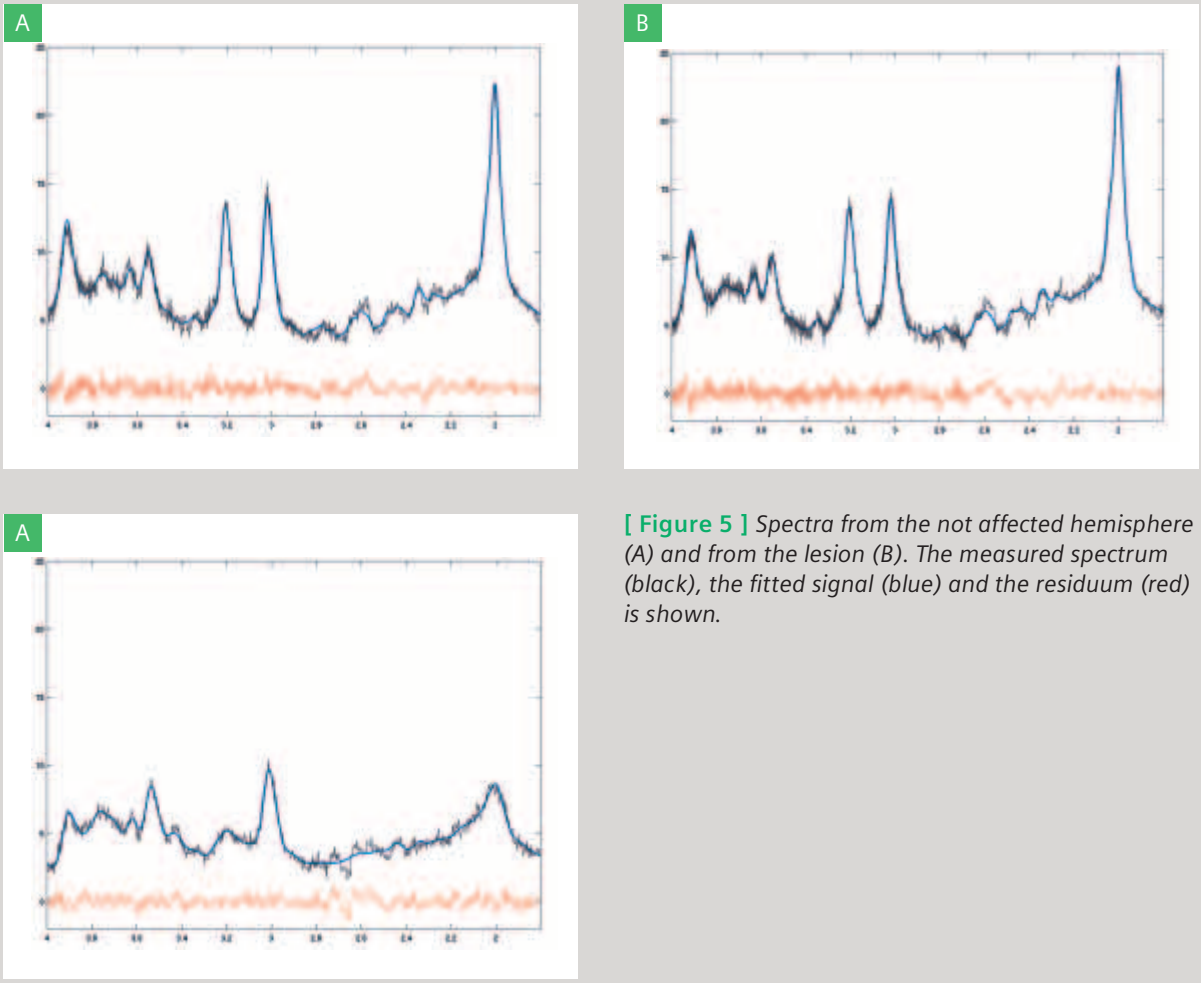

[Figure 5] *Spectra from the not affected hemisphere (A) and from the lesion (B). The measured spectrum (black), the fitted signal (blue) and the residuum (red) is shown.*

The signal-to-noise ratio can be further improved by the use of multi-channel coils. In this work it was shown that the combination of both technical improvements allows to perform CSI measurements with the high spatial resolution and good signal-to-noise ratio and to evaluate the results with a high level of reliability.

The quantitative evaluation of the CSI spectra was performed using the LC Model program. This technique is used for the calculation of absolute metabolite concentrations in single voxel spectroscopy. The absolute concentrations are calculated based on the known concentrations of the model solutions in the basis set. A prerequisite of this calculation is the identical measurement technique used both for the acquisition of spectra in the subject and in the model solutions.

For a correct fitting procedure of CSI spectra, CSI measurements of metabolite solutions with exactly the same spatial excitation as in the patient examination would be required. The acquisition of such reference data would take extremely long measurement times, since generally the different size of the PRESS voxel is used in each examination. Therefore, reference spectra from single volume measurements were used in this study. Sequence type (PRESS), a repetition time and an echo time were the same as in the CSI measurement. Nevertheless, the differences between single voxel and CSI measurements can lead to errors of the fitting procedure. In single voxel measurements the whole excited volume including the edges of the voxel, where flip angle is lower than the nominal flip angle value, contribute to the measured signal, whereas in 2D-CSI measurements, the non-ideal excitation profiles of the rf pulses lead to variable flip angles among particular voxels. Due to this effect the spectra from the voxels in the CSI grid are not identical to the base spectra. This behavior is pronounced mainly in metabolites with coupled resonances. As a consequence, the evaluation tech-

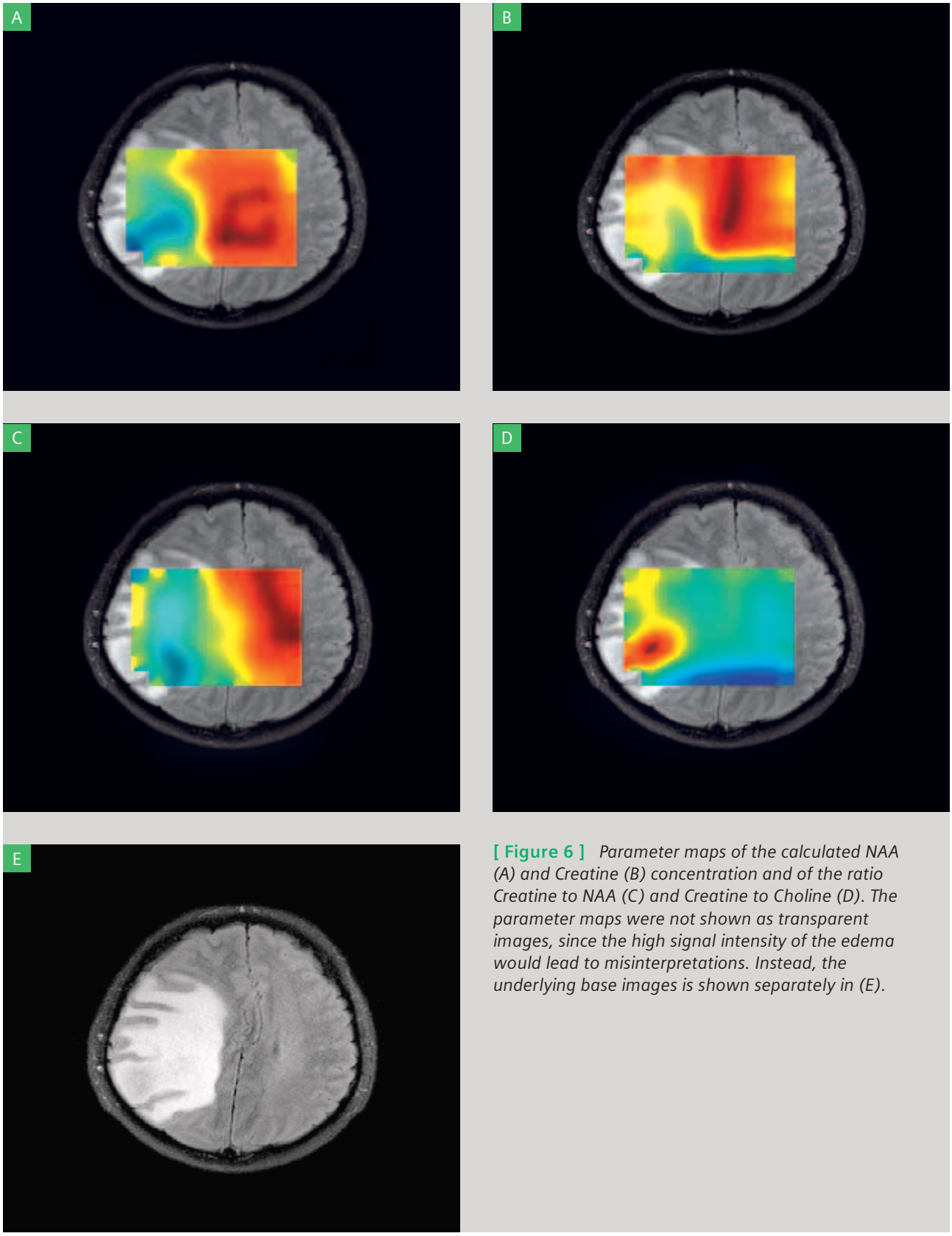

[Figure 6] *Parameter maps of the calculated NAA (A) and Creatine (B) concentration and of the ratio Creatine to NAA (C) and Creatine to Choline (D). The parameter maps were not shown as transparent images, since the high signal intensity of the edema would lead to misinterpretations. Instead, the underlying base images is shown separately in (E).*

nique cannot be used for the absolute quantification of metabolites. However, it allows the calculation of reliable relative concentrations of metabolites, which can be used to calculated metabolite and ratio maps. Despite these systematic obstacles, the fitting procedure lead to very good results within the selected frequency range, except for the region near the frequency corresponding to 2.7 ppm where minor systematic deviations were visible in the residuum. This can be ascribed to the mentioned deviations between acquired CSI data and the used single voxel reference data.

The quality of the short echo time CSI spectra can be hampered by the signal contamination from the extracranial fat tissue. A reduction of this artifact can be obtained by the use of the OVS technique [5]. However, the application of six saturation pulses in combination with a short echo time can lead to the interferences with the signal from the measured volume and in turn to inferior spectra quality, as was found in volunteer measurements. Therefore the patient examination was performed without OVS technique. To reduce the impact of the possible artifacts occurring in the lipid region on the remaining metabolites in the spectrum, the fitting was restricted to the frequency range 1.8 to 4.0 ppm. This procedure does not allow a quantification of lipid and lactate signals, but within the frequency range of the main metabolites, a very good fit with random residuals was obtained. The described measurement technique is not free from artifacts within the frequency range of lipid signal. These artifacts, however, have a limited amplitude and therefore the occurrence of increased lipid signals can be observed within the original spectra, if the amplitude of lipid signals e.g. in lesions is much higher than the amplitude of the contaminating signals as in Fig. 4C and D. The performed experiments show that high quality spectroscopic imaging measurements at the 3T scanner equipped with the multi channel head coil can be performed. This enables a reliable quantification of short echo time spectra, which is of high importance for clinical MR spectroscopy.

We used the CSI technique for the examination of a patient with low grade glioma. In general, Choline as a phospholipid and membrane marker is increased in all cerebral lesions with disintegration of cell membranes such as brain tumors [12, 13], inflammations [14] and also metastases [15]. In our case of a histologically-confirmed low grade glioma an atypical pattern was found. Whereas a strong decrease of NAA and slight decrease of Creatine is well known in case of glioma [12], a strong decrease of Choline has up to now only be described for radiation necrosis [16] and in Lhermitte-Duclos disease [17].

References

[1] Roemer, P. B., Edelstein, W. A., Hayes, C. E., Souza, S. P., Mueller, O. M.: The NMR phased array. Magn Reson Med 16 (1990) 192–225.
[2] Schaffter, T., Bornert, P., Leussler, C., Carlsen, I. C., Leibfritz, D.: Fast 1H spectroscopic imaging using a multi-element head-coil array. Magn Reson Med 40 (1998) 185–193.
[3] Mlynarik, V., Gruber, S., Moser, E.: Proton T (1) and T (2) relaxation times of human brain metabolites at 3 Tesla. NMR Biomed 14 (2001) 325–331.
[4] Barker, P. B., Hearshen, D. O., Boska, M. D.: Single-voxel proton MRS of the human brain at 1.5T and 3.0T. Magn Reson Med 45 (2001) 765–769.
[5] Duyn, J. H., Gillen, J., Sobering, G., van Zijl, P. C., Moonen, C. T.: Multisection proton MR spectroscopic imaging of the brain. Radiology 188 (1993) 277–282.
[6] Salibi, N., Roell, S.: MR spectroscopy with syngo MR 204 A/V: automation with flexibility SVS, 2D-CSI and 3D-CSI, with longa and short TE. Magnetom Flash 28 (2004) 8–12.
[7] Wilman, A. H., Riederer, S. J., King, B. F., Debbins, J. P., Rossman, P. J., Ehman, R. L.: Fluoroscopically triggered contrast-enhanced three-dimensional MR angiography with elliptical centric view order: application to the renal arteries. Radiology 205 (1997) 137–146.
[8] Jiru, F., Burian, M., Skoch, A., Hajek, M.: LCModel for spectroscopic imaging. Magma 15 (2002) S368.
[9] Provencher, S. W.: Estimation of metabolite concentrations from localized in vivo proton NMR spectra. Magn Reson Med 30 (1993) 672-679.
[10] Seeger, U., Klose, U., Mader, I., Grodd, W., Nagele, T.: Parameterized evaluation of macromolecules and lipids in proton MR spectroscopy of brain diseases. Magn Reson Med 49 (2003) 19–28.
[11] Naegele, T., Seeger, U., Hass, H., Kueker, W., Heckl, S., Klose, U.: Localized proton spectroscopy in hepatic encephalopathy: advantage of 3T high field for discrimination of glutamine and glutamate. Magnetom Flash 28 (2004) 50–53.
[12] Meyerand, M. E., Pipas, J. M., Mamourian, A., Tosteson, T. D., Dunn, J. F.: Classification of biopsy-confirmed brain tumors using single-voxel MR spectroscopy. AJNR Am J Neuroradiol 20 (1999) 117–123.
[13] Negendank, W. G., Sauter, R., Brown, T. R., Evelhoch, J. L., Falini, A., Gotsis, E. D., Heerschap, A., Kamada, K., Lee, B. C., Mengeot, M. M., Moser, E., Padavic Shaller, K. A., Sanders, J. A., Spraggins, T. A., Stillman, A. E., Terwey, B., Vogl, T. J., Wicklow, K., Zimmerman, R. A.: Proton magnetic resonance spectroscopy in patients with glial tumors: a multicenter study. J Neurosurg 84 (1996) 449–458.
[14] Rudkin, T. M., Arnold, D. L.: Proton magnetic resonance spectroscopy for the diagnosis and management of cerebral disorders. Arch Neurol 56 (1999) 919–926.
[15] Harada, M., Tanouchi, M., Nishitani, H., Miyoshi, H., Bandou, K., Kannuki, S.: Non-invasive characterization of brain tumor by in-vivo proton magnetic resonance spectroscopy. Jpn J Cancer Res 86 (1995) 329–332.
[16] Preul, M. C., Leblanc, R., Caramanos, Z., Kasrai, R., Narayanan, S., Arnold, D. L.: Magnetic resonance spectroscopy guided brain tumor resection: differentiation between recurrent glioma and radiation change in two diagnostically difficult cases. Can J Neurol Sci 25 (1998) 13–22.
[17] Bueltmann, E., Ernemann, U., Schuele, R., Beschorner, R., Gharabaghi, A., Voigt, K., Naegele, T.: Diagnostische Wertigkeit der absolut quantifizierten, lokalisierten MR-Protonenspektroskopie beim dysplastischen zerebellären Gangliozytom (Lhermitte-Duclos). Klinische Neuroradiologie 15 (2005) 123–130.